



Virginia Commonwealth University  
**VCU Scholars Compass**

---

Theses and Dissertations

Graduate School

---

2012

# THE EFFECT OF A NAVIGATIONAL AID ON TRAINING OF A MINIMALLY INVASIVE SURGERY CAMERA TASK

Ketan Vidwans

*Virginia Commonwealth University*

Follow this and additional works at: <http://scholarscompass.vcu.edu/etd>

 Part of the [Biomedical Engineering and Bioengineering Commons](#)

© The Author

---

Downloaded from

<http://scholarscompass.vcu.edu/etd/2855>

This Thesis is brought to you for free and open access by the Graduate School at VCU Scholars Compass. It has been accepted for inclusion in Theses and Dissertations by an authorized administrator of VCU Scholars Compass. For more information, please contact [libcompass@vcu.edu](mailto:libcompass@vcu.edu).

© Ketan Vikas Vidwans 2012

All Rights Reserved

THE EFFECT OF A NAVIGATIONAL AID ON TRAINING OF A MINIMALLY INVASIVE  
SURGERY CAMERA TASK

A Thesis submitted in partial fulfillment of the requirements for the degree of Master of Science

at

Virginia Commonwealth University

by

Ketan Vikas Vidwans  
Bachelor of Engineering  
Mumbai University, India, 2005

Directors:

Dr. Dianne T.V. Pawluk, Ph.D.  
Associate Professor, Department of Biomedical Engineering

Dr. Peter E. Pidcoe, PT, DPT, Ph.D.  
Associate Professor, Department of Physical Therapy  
Virginia Commonwealth University  
Richmond, Virginia

August, 2012

## **Acknowledgements**

I dedicate this thesis to my family - my wonderful parents, Mr. Vikas Mahadeo Vidwans and Mrs. Vandana Vikas Vidwans, and my lovely wife – Gunjan. Baba, you are and have always been my hero and an inspiration in every aspect of life. Your ethics, energy, determination and intelligence are the pillars of strength that motivate me to achieve the best. Aai's silent yet strong support has kept me going through tough times. The happiness I have seen in her eyes for my achievements have made me strive for more success. I am most thankful to God to have given me parents like you, who have dreamed great achievements for me, shaped my personality and provided me with best of the resources I could have ever thought of.

I am extremely thankful for having Dr. Dianne T. V. Pawluk as my research advisor. Under her supervision, I have learnt to identify research problems, take all possible factors under consideration and address them in a comprehensible manner. She has been a constant source of inspiration and guidance. Her immense support helped me deal with all crests and troughs throughout this period positively. She definitely was the guiding beacon for me whenever I felt lost in the course of project development, and I thank her for sharing her knowledge and vision with me.

I am also extremely thankful to Dr. Peter E. Pidcoe to have been my secondary advisor and been a part of my committee. His innovative mindset, vast knowledge and prudent feedback have always helped and inspired me to have a methodical approach to the problems faced during this project. His words of appreciation, concern and criticism regarding my performance and my thought process have always been an encouraging force for improvement. I truly appreciate his honest and timely recommendations, which have benefitted me a lot, both personally and professionally.

I am also obliged to have Dr. Ou Bai as a part of my committee. Undertaking Digital Signal Processing course under him honed my Matlab programming skills. He has always been there whenever I faced difficulties in Matlab, and am extremely thankful to him for his unconditional support.

I owe many thanks to my friends and labmates – Devnath, David, Ravi, Patrick, Cristofer, Justin and Victoria for their moral support. Being with all of them was a great experience and all of them made the lab a lively place to work in. I am also thankful to all the participants of the study for all their support during the experiments. I also take this opportunity to thank my closest friends Nachiket, Mohit, Zulfiqar, Sasidhar and Aalok who have been through thick and thin of my life.

I wish to express my special thanks to my parents-in-laws, Mr. Nawal Saxena and Mrs. Preeti Saxena. Their encouragement, love and blessings have always been a powerful source of inspiration and energy. I also wish to express countless thanks to my brothers and sisters for their unconditional love and support.

Finally, the most important thanks here goes to my beloved wife, Gunjan. You have always provided me a ray of hope, peace of mind and warmth in the most difficult times. You have been there with me to absorb all my tensions like a sponge. You taught me to be patient, think about big long-term goals, and achieve them in small steps by smart thinking coupled with hard work. Living my life with you is something that I am utmost grateful for to God. You are a true companion and an unbiased critique. I express my sincerest gratitude to you, for all your love and bringing out the best in me.

## Table of Contents

Acknowledgements.....	iii
List of Tables .....	xi
List of Figures.....	xiii
List of Equations.....	xvi
Abbreviations.....	xvii
Abstract.....	xix
CHAPTER 1 INTRODUCTION.....	1
CHAPTER 2 BACKGROUND.....	7
2.1 Camera navigation using graphics .....	7
2.1.1 Need for understanding directions during MIS .....	7
2.1.2 Introduction to Simulator Training in MIS.....	9
2.1.2.1 Current training setups.....	9
2.1.2.2 Lessons Learnt.....	12
2.1.3 Camera navigation using current training setups.....	12
2.1.3.1 Endoscope and port location used for camera navigation task.....	12
2.1.3.2 Camera navigation tasks designed in VR systems .....	13
2.1.3.3 Camera navigation tasks designed for box trainers .....	14
2.1.4 Providing graphical feedback .....	15
2.1.4.1 Providing graphical feedback in MIS.....	15

2.1.4.2	Pilot navigation and learning from their results .....	16
2.1.4.3	Other design factors for graphical aids.....	16
2.1.4.3.1	Colors and placement of information on the graphical screen.....	17
2.1.4.3.2	Contrast .....	17
2.1.4.3.3	Color-blindness .....	17
2.2	Proximity sensing.....	18
2.2.1	Proximity Sensor.....	19
2.2.1.1	Capacitive sensors .....	19
2.2.1.2	Inductive sensors .....	19
2.2.1.3	Ultrasonic sensors.....	20
2.2.1.4	Photoelectric sensors .....	20
CHAPTER 3 MATERIALS AND METHODS .....		22
3.1	Design of graphics for camera navigation .....	22
3.1.1	Materials .....	22
3.1.1.1	Trainer box .....	22
3.1.1.2	Simulated Endoscope .....	24
3.1.1.3	The <i>MotionMonitor</i> ® .....	24
3.1.1.4	Collision detection system.....	27
3.1.2	Pilot testing phase for testing the graphics .....	29
3.1.2.1	Directional Markers graphic .....	30

3.1.2.2	Position circle with Line graphic.....	32
3.1.2.3	Position circle with Shading graphic .....	32
3.1.2.4	Position circle with Line + Shading graphic .....	33
3.1.2.5	Exploration of the use of color .....	33
3.1.2.6	Exploration of the placement of the video monitor and the graphics screen ..	34
3.1.2.7	Feedback about graphics developed .....	34
3.1.3	Methods.....	36
3.1.3.1	Matlab presentation of graphics .....	36
3.1.3.2	Training and testing phase task trees.....	38
3.1.3.3	Experiment Setup .....	40
3.1.3.4	Experimental Design .....	42
3.1.3.4.1	Participants .....	42
3.1.3.4.2	Training Phase.....	43
3.1.3.4.2.1	Duration of training phase.....	44
3.1.3.4.2.2	Training Instructions .....	44
3.1.3.4.2.3	Stopping Criteria .....	45
3.1.3.4.3	Testing Phase.....	45
3.1.3.4.3.1	Testing task .....	45
3.1.3.4.3.2	Duration of the testing phase.....	47
3.1.3.4.4	Data collection and analysis .....	47



3.1.3.4.4.1	Training phase data analysis .....	48
3.1.3.4.4.1.1	Root mean squared error of 3D mental map on paper .....	48
3.1.3.4.4.2	Testing phase data analysis .....	49
3.1.3.4.4.2.1	Collection of reference data for the testing tree .....	50
3.1.3.4.4.2.2	Collection and analysis of the accuracy of the movement data for all targets of the testing tree .....	51
3.1.3.4.4.2.3	Collection and analysis of the time taken to decide the direction of movement .....	54
3.1.4	Statistical Analysis.....	55
3.2	Proximity Sensing.....	57
3.2.1	Materials .....	58
3.2.1.1	Sharp IR sensor.....	58
3.2.1.2	HSDL 9100.....	59
3.2.2	Methods.....	60
3.2.2.1	Proximity measurement for solid standard color sheets .....	60
3.2.2.1.1	Divergence angle of the sensor .....	61
3.2.2.1.2	Proximity measurement for multiple solid standard color sheets .....	61
3.2.2.2	Multiple sensor assembly .....	62
3.2.2.2.1	Multiple emitters and single detector sensor assembly.....	62
3.2.2.3	Camera chip of endoscope and White Balance (WB) .....	64

3.2.2.4	SenTechAmerica STC-N63 camera chip .....	64
3.2.3	Proximity calculation with unknown grayscale value .....	65
3.2.4	Proximity calculation for an actual object placed within the trainer box with unknown grayscale value .....	68
CHAPTER 4	RESULTS.....	71
4.1	Camera navigation using graphics .....	71
4.1.1	Participant characteristics .....	71
4.1.2	Training characteristics.....	71
4.1.2.1	Average number of training task trees and average training time needed to achieve proficiency .....	71
4.1.2.2	Average number of targets found per tree during the training phase .....	73
4.1.2.3	RMS error of the mental map of targets found on paper during the training phase .....	74
4.1.3	Testing characteristics.....	76
4.1.3.1	Average number of instructions with the endpoint within 0° - 30° error margin .....	76
4.1.3.2	Average number of instructions within a 0° - 30° error margin, 250 msec after giving the instruction .....	77
4.1.3.3	Time taken for deciding the correct direction of movement .....	78
4.2	Proximity sensing using HSDL 9100 .....	80
4.2.1	Family of output voltage curves for solid standard color sheets .....	80

4.2.2	Distance measurement for multiple color sheets .....	81
4.2.3	Distance measurement for unknown grayscale value .....	81
4.2.3.1	Ambient lighting conditions for Neutral 8.0 card.....	82
4.2.3.2	Ambient lighting conditions for Neutral 5.0 card.....	82
4.2.3.3	LED-lit conditions within the trainer box for Neutral 8.0 card.....	83
4.2.3.4	LED-lit conditions within the trainer box for Neutral 5.0 card.....	83
4.2.4	Distance measurement for actual trainer box objects .....	83
4.2.4.1	LED-lit conditions within the trainer box for white target cylinder.....	84
4.2.4.2	LED-lit conditions within the trainer box for tree trunk .....	84
CHAPTER 5	DISCUSSION .....	85
5.1	Camera navigation using graphics .....	85
5.1.1	Training phase characteristics.....	85
5.1.2	Testing phase characteristics.....	87
5.2	Proximity Sensor.....	92
CHAPTER 6	CONCLUSION AND FUTURE WORK.....	94
LITERATURE CITED	.....	96
APPENDIX	.....	105

## List of Tables

<b>Table 3.1</b> Components used for generating graphics .....	22
<b>Table 3.2</b> Geometric metric parameters for defining the target difficulty .....	39
<b>Table 3.3</b> Classification of different groups according to their training condition .....	43
<b>Table 3.4</b> Instructions to guide participants to reach locations of targets on testing tree .....	45
<b>Table 3.5</b> Set of instructions given to participants for performing endoscope movements in testing phase.....	46
<b>Table 3.6</b> Dimensions of the trainer box and paper plot .....	49
<b>Table 3.7</b> Assignment of the "Instruction number" to all instructions for target 2 .....	51
<b>Table 3.8</b> Assignment of the unique three-digit code to different time slots for target 2 for "Down" instruction .....	51
<b>Table 3.9</b> Components used for providing proximity in the trainer box setup .....	65
<b>Table 4.1</b> Participant characteristics.....	71
<b>Table 4.2</b> Average number of training task trees needed to achieve proficiency .....	71
<b>Table 4.3</b> Average training time.....	72
<b>Table 4.4</b> Average number of targets found per tree in training task trees attempted .....	74
<b>Table 4.5</b> Error of mental map of targets found on paper during the training phase .....	75
<b>Table 4.6</b> Average number of instructions with endpoint within a 0° - 30° error margin .....	76
<b>Table 4.7</b> Average number of instructions within a 0° - 30° error margin, 250 msec after giving the instruction.....	77
<b>Table 4.8</b> Time taken for deciding the direction of movement for the instructions with an endpoint within a 0° - 30° error margin.....	79
<b>Table 4.9</b> Distance measurement for the Neutral 8.0 under ambient lighting conditions.....	82

**Table 4.10** Distance measurement for the Neutral 5.0 under ambient lighting conditions ..... 82

**Table 4.11** Distance measurement for the Neutral 8.0 under LED-lit conditions within the trainer box..... 83

**Table 4.12** Distance measurement for the Neutral 5.0 under LED-lit conditions within the trainer box..... 83

**Table 4.13** Distance measurement for white target cylinder with a 6 mm restricting ring ..... 84

**Table 4.14** Distance measurement for tree trunk with a 6 mm restricting ring..... 84

## List of Figures

<b>Figure 3.1</b> (a) Endoscopic Trainer box system; (b) Trainer box system (Vasudevan, 2012) .....	23
<b>Figure 3.2</b> (a) Slider arrangement (Vasudevan, 2012); (b) Simulated trocar (Vasudevan, 2012)	23
<b>Figure 3.3</b> (a) 30° Simscope ( <a href="http://www.3-dmed.com/SimScopes_Descriptions_(CAM07).html">http://www.3-dmed.com/SimScopes_Descriptions_(CAM07).html</a> retrieved May 18, 2012); (b) Endoscope after disabling both built-in port attachment and rotary mechanism .....	24
<b>Figure 3.4</b> (a) The <i>MotionMonitor</i> <sup>®</sup> system; (b) Sensor attached to endoscope handle .....	25
<b>Figure 3.5</b> (a) Side view of camera head; (b) Front view of camera head.....	25
<b>Figure 3.6</b> (a) Accelerometer ADXL 203; (b) Pinout diagram.....	28
<b>Figure 3.7</b> Front screen of LabView program.....	28
<b>Figure 3.8</b> Schematic of the entire data collection system.....	29
<b>Figure 3.9</b> Pilot phase task tree .....	29
<b>Figure 3.10</b> Directional markers with vertical height bar .....	31
<b>Figure 3.11</b> Attitude meter for an airplane.....	36
<b>Figure 3.12</b> Illustrations of the three different graphics provided to the participants. The lower rectangle in each graphic contained an annotated vertical bar. The white filling of this bar changed as a function of the endoscope tip height in the trainer box. The upper part of each display illustrated the different graphics. (a) Graphic 1 was a circle indicating the XY position of the endoscope tip with a line indicating direction of view of the endoscope; (b) Graphic 2 was a circle indicating the XY position of the endoscope tip with a shaded circle indicating orientation of the endoscope; (c) Graphic 3 was a combination of graphics 1 and 2. ....	37
<b>Figure 3.13</b> (a) Training task tree; (b) Target numbers at different depths .....	38
<b>Figure 3.14</b> Testing task tree.....	40

<b>Figure 3.15</b> Participant during training phase of experiment.....	41
<b>Figure 3.16</b> (a) Accelerometer placed at half height of trunk; (b) Location of transmitter with respect to trainer box.....	42
<b>Figure 3.17</b> Target number visible on TV monitor and directions with respect to TV monitor..	46
<b>Figure 3.18</b> Paper plot given to participants to draw 3D mental map .....	48
<b>Figure 3.19</b> Points marked as Down, Left, Right and Up for target 2 .....	50
<b>Figure 3.20</b> Plots for the "Up" instruction for target 2 in testing tree.....	55
<b>Figure 3.21</b> (a) Sensor assembly with IR LED turned on; (b) Sensor placed in front of Neutral 3.5 color card .....	61
<b>Figure 3.22</b> Left-right and right-left combination of White and Black color sheets .....	61
<b>Figure 3.23</b> (a) Circular array of 940 nm IR LEDs; (b) Concentrically reduced IR LED emitter array with HSDL 9100 detector in center .....	62
<b>Figure 3.24</b> (a) HSDL 9100 assembly on a Lego square block for sensing proximity; (b) IR fields of all four proximity sensors .....	63
<b>Figure 3.25</b> Four HSDL 9100 sensor assembly placed on endoscope camera tip.....	63
<b>Figure 3.26</b> Circuit diagram for the four sensor assembly.....	64
<b>Figure 3.27</b> (a) Side view of the restricting ring placed over sensor assembly attached on the endoscope tip; (b) Restricting ring from front; (c) All the three restricting rings (widths 4 mm, 5 mm and 6 mm).....	70
<b>Figure 4.1</b> Average number of training task trees attempted for all groups .....	72
<b>Figure 4.2</b> Average training time for all groups.....	73
<b>Figure 4.3</b> Average number of targets found per tree during training phase for all groups .....	74

**Figure 4.4** Average RMS error for mental map of targets found on paper during training phase for all groups ..... 75

**Figure 4.5** Instructions with endpoint within a 0°-30° error margin for all groups (Percentage) 76

**Figure 4.6** Average number of instructions within 0-30 deg error margin 250 msec after giving instructions for all groups ..... 78

**Figure 4.7** Average time for deciding direction of movement for all groups ..... 79

**Figure 4.8** Family of output voltage curves for single HSDL 9100 sensor for all six standard color sheets..... 80



## List of Equations

<b>Equation 3.1</b> Root Mean Square error for the targets marked on paper plots .....	49
<b>Equation 3.2</b> Bonferroni correction formula for $m$ number of dependent or independent comparisons being performed.....	56

## **Abbreviations**

A/D – Analog to Digital converter

AI – Analog input

ANOVA – Analysis of variance

AR – Augmented Reality

AWB – Auto White Balance

CDS – Collision detection system

DOF – Degrees of freedom

FOC – Fiber Optic Cable

FOV – Field of View

gF – Gram-force

GPS – Global Positioning System

Hz – Hertz

IR – Infrared

IST – Innovative Sports Training

LASTT – Laparoscopic skills testing and training

LED – Light Emitting Diode

MIS – Minimally Invasive Surgery

MITS – Minimally Invasive Training System

OR – Operating Room

PSD – Position Sensitive Detector

RGB – Red, Green and Blue

RMS – Root Mean Square

ROI – Region of Interest

SA – Situation Awareness

SRT – Standard Range Transmitter

TCP/IP – Transmission Control Protocol / Internet Protocol

TER – Transfer Efficiency Ratio

TMM – The MotionMonitor<sup>®</sup>

V – Voltage

$V_{p-p}$  – Peak-to-peak voltage

VR – Virtual Reality

VT – Video Trainer

WB – White Balance / White Balancing

## **Abstract**

### **THE EFFECT OF A NAVIGATIONAL AID ON TRAINING OF A MINIMALLY INVASIVE SURGERY CAMERA TASK**

By Ketan Vidwans

A Thesis submitted in partial fulfillment of the requirements for the degree of Master of Science  
at Virginia Commonwealth University

Virginia Commonwealth University, 2012

#### Directors:

Dr. Dianne T. V. Pawluk, Ph.D.,  
Associate Professor, Biomedical Engineering

Dr. Peter E. Pidcoe, PT, DPT, Ph.D.,  
Associate Professor, Physical Therapy

Minimally Invasive Surgery (MIS) differs from Open Surgery as surgeons view the surgical site indirectly on a monitor. The view shown is typically from an angled endoscope off to one side of the surgery (i.e., uncollocated with the view of the hands). This makes camera navigation a challenging ability to learn. MIS thus requires longer training periods, more practice and mental effort to achieve proficiency. Current training setups and Operating Room (OR) environments lack appropriate real-time visual cues for navigation and other perception related information that could help with learning and performance in the OR. The purpose of this research was to design and develop graphical aids for improving understanding of camera navigation and depth perception in a trainer box necessary for enhancing surgeon's skills to perform endoscopic surgery. For the former, two alternate training methods: 1) using no graphics

(control group) and 2) using three different types of graphics conveying different information, were considered for this study. The effectiveness of the training was evaluated by a comparative analysis of different performance measures across all the groups. It was observed that training using graphics did improve the performance of participants in performing a minimally invasive surgery training task. For the latter, the use of a proximity sensor was explored.

## CHAPTER 1 INTRODUCTION

Surgery is a branch of medicine that requires physical intervention and uses both manual and instrument techniques to diagnose and/or treat a pathological condition of affected tissues or organs. Surgeries can be broadly categorized based on purpose, degree of invasion, body part, equipment used, urgency and so on (Dušková et al., 2009). Traditional or open surgical procedures involve surgeon performing large incisions on patients' bodies to access the area of interest. The surgeon can then directly look at the surgical site and access it with his hands and/or instruments to perform the necessary actions. Minimally Invasive Surgery (MIS) on the other hand, is a specialized surgical technique that started evolving and gaining popularity since the 1930s (Wayand, 2004). MIS uses an endoscope (a telescopic rod lens system) that goes through natural body openings or small incisions made on patient's body. A camera is either attached on the tip of the endoscope (known as "chip-on-tip") or behind the endoscope using a lens coupler. Light from a light source unit is carried by a fiber optic cable to and through an endoscope to illuminate the surgical field inside body cavity. The video signal from the camera is processed by a video processing unit and is then displayed on a television or suitable monitor (Lomanto et al., 2004). The surgeon views the operating field on this monitor and manipulates thin, long instruments (with various different ends) inserted through other incisions to carry out surgical actions within the human body beneath.

Tool manipulation and the perception of depth are easy in an open surgery as the surgeon's visual and working planes are same. However, open surgeries typically result in higher blood loss, longer incisions and longer recuperating times. MIS, in contrast, provides several benefits to patients, some of them being - reduced exposure of internal organs due to small incisions, lesser pain and post-operative scarring, reduced hemorrhaging, with all of these

resulting in shorter hospital stay. These benefits have increased the popularity of MIS, with an estimated 4.4 million procedures being carried out in 2010 in the US alone (Lapore, 2011).

However, MIS imposes additional stress and requirements on surgeons, due to following -

1. Location of camera and other tools – Camera and other endoscopic tools are inserted through different ports present at different locations on the body cavity. The camera is held and manipulated by an assistant who stands beside the surgeon. To avoid the endoscope obstructing the movement of other instruments during surgery, it is inserted from another port in order to view the surgical space. Thus, the camera is not collocated with surgeon's use of tools, making him lose his sense of direction easily (Breedveld et al., 2001),
2. Indirect view of workspace – In an open surgery, surgeon's visual and working planes are present at the same location, and he can directly see the operative field and the instruments. Thus, it is easier for the surgeon to manipulate instruments as there are no discrepancies between his visuo-motor transformation and the surgical field. In MIS however, the surgeon's visual and working planes are different as he operates with instruments below while observing their movements on a monitor placed in front of him. This mislocation of the monitor and inability to see his hands in the operative field simultaneously introduces discrepancies in his visuo-motor transformation. It is thus imperative for him to develop new hand-eye coordination skills to achieve proficiency (Breedveld et al., 2001),
3. Poor depth perception – The 3D view of surgical site is displayed on a 2D monitor that the surgeon views it on. This transformation can result in poor depth perception that may lead to past-pointing errors resulting in tissue damage

(Nicolaou et al., 2006). Poor depth perception makes precise movements difficult, thus increasing complexity and thereby affecting surgeon's performance and increasing overall time and cost of procedure (Taffinder et al., 1999),

4. Fulcrum effect – Motion reversal of the tool tip with respect to surgeon's hands is caused by this effect at the port of entry. This can confuse the surgeon in terms of direction of a movement, thus reducing dexterity and making MIS a non-intuitive motor skill that is difficult to learn (Cavusoglu et al., 2003),
5. Reduced degrees of freedom (DOF) – Long instruments inserted through the trocar get restrained to only four DOF (three rotations and one in-out translation), affecting dexterity and inducing severe ergonomic limitations (Li et al., 2000),
6. Lack of force feedback – The surgeon uses long MIS tools to manipulate tissue within the body cavity rather than his own hands. This results in lack of force feedback, making it difficult for surgeon to feel the tissue and apply appropriate force as required (Keehner et al., 2004),
7. Image magnification and reduced field-of-view (FOV) – Image magnification and reduced FOV make it difficult for a surgeon to identify anatomic structures, even though it may display better details of the structure. Reduced FOV causes the surgeon to frequently manipulate the endoscope resulting in time consuming surgeries and also increase in the risk of accidental injury to anatomical structures not in sight (Breedveld, 1997).

Surgeons must be able to counter these inherent problems to perform a successful surgery. Earlier training methods were based on the traditional “Apprentice model” of teaching, with an expert surgeon teaching and demonstrating steps of a surgery to novice surgeons



(Gallagher et al., 2002). This model typically utilizes either cheaper training methods using box trainers or inanimate models or expensive training methods using patients or porcine models that are unstructured, and are also incapable of providing objective feedback on trainee's performance (Gallagher et al., 2004). These drawbacks have made it essential to develop alternate training methods outside OR environment such as Video Trainer (VT) systems and Virtual Reality (VR) simulators (Jones, 2007).

Training with box trainers and VT systems is economical and has shown improvements in both psychomotor and cognitive skills of surgeons that can ensure smoother transition to OR (Hiemstra, 2012). Training on such systems is risk-free, can be structured and offers an excellent opportunity for surgeons to practice wide range of skills along with objective feedback until mastery is achieved (Dunkin et al., 2007).

One of the most difficult yet fundamental problems faced by surgeons while performing MIS is to understand the conceptual relationship between the endoscope, the video scene on the monitor and the patient's anatomy. The endoscope inserted through a port uncollocated with the surgeon's position is manipulated by an assistant standing beside the surgeon. The surgeon's line-of-sight is thus different from the camera's line-of-sight. This rotated view (misorientation) seen on the monitor placed in front of him (mislocation) severely affects his hand-eye coordination (Breedveld et al., 2001). To worsen the situation, the fulcrum effect reverses the direction of movement of endoscope. The camera assistant manipulates the endoscope based on surgeon's instructions, which are with respect to the surgeon's frame of directions. As the endoscope is not collocated with the surgeon, the surgeon has to perform mental transformations in order to move the tools to the desired location in the surgical field. The projection of 3D surgical field on 2D monitor results in lack of binocular disparity, severely degrading the depth

perception (Tendick et al., 1993). Degraded depth perception also leads to reduced field of view, thereby affecting the capability of surgeon to spatially orient and build a cognitive model of the surgical environment (DeLucia et al., 2004).

It is necessary to provide real-time graphical presentation of fundamental information about handling an endoscope to improve the effectiveness and efficiency of learning camera navigation and proximity. From the various operational difficulties mentioned for MIS, this research concentrated mainly on two goals –

1. To develop a training method using graphics to help participants to more effectively and efficiently learn camera navigation based with a box trainer, and
2. To develop a sensory system with graphical feedback to improve proximity sensing so as to avoid tissue damage, which is critical for performing MIS.

Graphical aids were developed that would provide basic information about the location of the endoscope tip, direction of view and rotation of endoscope to teach camera navigation in Goal 1. For Goal 2, an array of proximity sensors were mounted on tip of the endoscope. Graphical information was intended to be provided based on the distances sensed.

Box trainers and VT systems can be used to train novice surgeons to a certain level of automation of psychomotor skills and spatial judgments in a risk-free environment. This would ensure a decrease in their extraneous cognitive load, freeing working-memory capacity to acknowledge and learn steps to handle complications, rather than wasting time in the OR to achieve proficiency of basic technical skills (Gallagher et al., 2005; Sweller et al., 1998).

One of the primary objectives of this research was to train participants to use an endoscope in a way that would enable them to transfer their knowledge to new problems within the same as well as different operational setups. Task trees with varying target locations were

presented to participants in an effort to teach camera navigation skills and workspace exploration. To facilitate training, a custom built box-trainer previously designed and built in our lab was used. This box-trainer simulates the surgical environment and is an accepted method of training MIS skills. Training effectiveness was assessed using a testing tree that would require participants to perform a new task in an environment that approximates the actual OR.

## CHAPTER 2 BACKGROUND

### 2.1 Camera navigation using graphics

#### 2.1.1 Need for understanding directions during MIS

Understanding the direction of movement of endoscopic tools is extremely important for the surgeon in order to avoid unexpected and grave complications during surgery. However, understanding of directions is complex in MIS, mainly due to -

1. Lack of collocation between the endoscope and the tools being manipulated,
2. Lack of visual cues present within the surgical field,
3. Difficulty in judging angle of rotation of endoscope when rotated,
4. Difficulty in judging depth as the 3D surgical field is projected on a 2D monitor, thus restricting visual feedback that is critical in performing dexterous movements (Taffinder et al., 1999),
5. The fulcrum effect caused at the incision or the port of entry of the endoscopic tool.

The endoscope is not collocated with the position of the surgeon and is manipulated by the camera assistant. Due to need of the surgery, the camera assistant may have to stand opposite to the surgeon, and still continue to manipulate the endoscope based on surgeon's instructions. This change of their relative positions introduces a variation in their respective frames of directions. The surgeon's left side becomes the camera assistant's right side. The surgeon may still continue to give instructions based on his reference frame of directions to the camera assistant. However, the camera assistant may correlate the two frames incorrectly as their sides and hence movement directions seen via the camera are now reversed (mirror-like). The assistant accordingly may manipulate the endoscope to undesired locations of the surgical field. This leads

to more confusion for the surgeon (Rivera et al., 2005; Korndorffer et al., 2005; Uecker et al., 1995), and can result in potential tissue damage and longer surgeries. To complicate things further, in most surgeries, an endoscope with an objective lens (at the end of the endoscope lens system) of 30° is used, and the camera assistant manipulating the endoscope may not be well trained for such a critical job (Nishikawa et al., 2010; Korndorffer et al., 2005). Rotation of this angled endoscope changes the axes of direction, increasing the possibility of incorrect manipulation of the endoscope (Omote et al., 1999).

Tools that are used to perform electrocautery, diathermy or the ones used for cutting of anatomical structures might be mishandled by the surgeon due to lack of depth perception, resulting in past-pointing errors, thereby damaging surrounding tissues (Nicolaou et al., 2006). To avoid such errors and mishaps, information regarding location, direction of view, rotation and depth of the endoscope seem to be critical to be provided to the surgeon.

Research conducted by Wentink et al. (2002) concluded that hand-eye coordination improved when an instrument shaft was visible in the video monitor. Presence of the instrument shafts in the video monitor helped in placing the visual and working fields of the surgeon in the same plane similar to an open surgery, thereby improving their hand-eye coordination. They also concluded that expert surgeons use the incision point as a point of reference while manipulating an endoscopic tool. However, the tool tip is not always visible on the monitor, and although surgeons can look down at their hands to understand the direction of the tool, they prefer not to glance away from the monitor. This necessitates the need of training the surgeons using graphical aids to describe the relationship between motion of tool handle, location and orientation of endoscope tip.

## **2.1.2 Introduction to Simulator Training in MIS**

Many recent research papers have highlighted similarities between surgical training and pilot training. Both fields are extremely dynamic and can give rise to grave and unexpected situations, thereby inducing stress, increasing the potential for error and so forth. To be successful, both surgeons and pilots have to perform complicated technical and intellectual tasks with little or no margin for error. Simulators can present a wide range of scenarios to impart skills in a risk-free, controlled environment at a pace that is subject to each trainee's inherent capabilities (Dunkin et al., 2007).

The classical method of teaching open surgery, such as the "Apprentice model" was used to teach the basics of MIS originally. This model involved novice surgeons observing and then mimicking steps performed by expert surgeons in the actual OR. This also required biological tissues, such as human or porcine models (live or cadaver) for endoscopic skill training (Guruswamy et al., 2009). But these tissues are costly, have limited availability and individual variations in them make standardizing of assessments difficult (Munz et al., 2004). The surgical community hence widely accepted that this model was inadequate for teaching basic skills required to perform MIS, and started to look towards, accept and use simulators for surgical training.

Simulator systems use computers for developing simulations, assess performance and provide feedback to trainees. Some of the current training setups will be discussed in detail in the following section.

### **2.1.2.1 Current training setups**

Fundamental skills of MIS are taught using the following models, namely –

1. Inanimate models – human anatomical parts made from moldable materials (Kolkman et al., 2008),
2. Box trainers and Video trainer (VT) systems – Tulane Trainer (Stefanidis et al., 2007),
3. Virtual Reality (VR) simulators – Endotower<sup>TM</sup> (Stefanidis et al., 2007), MIST-VR (Gallagher et al., 2004), the SIMENDO (Verdaasdonk et al., 2006), LapSim (Munz et al., 2004).

Inanimate models are low-cost alternatives to animal or human models and hence have gained popularity in recent times. They are easily reproducible with no variations and can be used for unlimited practice without the need of any expert's supervision (Anastakis et al., 1999). However, there are two major drawbacks with their usage -

1. They may not be as realistic as living tissue and may not exactly mimic human anatomy, and
2. There has been no concrete evidence suggesting that their usage helps in transfer of skills to actual OR (Scott et al., 2000).

Development of low-cost training systems such as box trainers coupled with recent advances in computer technology are helping resident surgeons practice and get trained outside the OR. Researchers have shown that training in vitro on box trainers, VT and VR systems can improve performance of novice surgeons in the OR (Fried et al., 1999; Munz et al., 2004; Debes et al., 2010). Researchers have also compared these three techniques and have concluded that there are no major advantages of one system over others (Munz et al., 2004; Stefanidis et al., 2007). Construct validity is defined as the degree to which assessment can discriminate between different ability or experience levels of participants. Similarly, face validity is defined as the

degree of resemblance between the real activity and the system under study (Maithel et al., 2006). Box trainers, VT and VR systems have also been found to have excellent construct validity and good face validity (Carter et al., 2005; Stefanidis et al., 2007), especially for novice surgeons (Munz et al., 2004).

However, some practical advantages make developing a box trainer a better alternative to VR systems. These include –

1. Haptic feedback – Actual endoscopic instruments are used while training surgeons on box trainers. Physically handling these instruments provides natural haptic feedback to the surgeons (Hiemstra, 2012). VR simulators such as LapSim and SIMENDO do not provide haptic feedback, which is crucial for a surgeon while performing a MIS (Munz et al., 2004; Verdaasdonk et al., 2006). Recent VR simulators such as MIST-VR have started providing haptic feedback, but it is not particularly realistic,
2. Cost and mobility – Developing a VR system’s software, hardware and their interface, along with its validation requires a lot of time. Designing of more realistic models increases the complexity of the VR system. This also tends to make the systems costly and relatively less mobile, thereby reducing their accessibility, affordability and availability (Verdaasdonk et al., 2006). Furthermore, there is no concrete evidence about the “Transfer Efficiency Ratio (TER)” for any type of surgical simulator that can help measure their effectiveness in terms of cost (Munz et al., 2004),
3. Real-time objective assessment – The major disadvantage of box trainers compared to VT and VR systems was that they did not provide automatic



performance assessment. However, the development of endoscopic instruments mounted with miniature sensors such as TrEndo that can be used in a box trainer environment has now alleviated this drawback (Chmarra et al., 2006).

### **2.1.2.2 Lessons Learnt**

Research has shown that providing training in multiple short sessions instead of one long session allows cognitive consolidation of the psychomotor and procedural skills learnt (Gallagher et al., 2005; Verdaasdonk et al., 2007). It has also been concluded that one-hour training on a box trainer per week, for seven weeks in total is sufficient for developing skills that are not only better acquired and retained for a longer time, but also better transferred to be applied to new problems or tasks. Retention of skills has been found to be effective when trained on box trainers even for testing performed 11 months after training (Hiemstra, 2012; Moulton et al., 2006).

### **2.1.3 Camera navigation using current training setups**

Various studies and researchers have developed custom navigation tasks for teaching the basic skills required for performing MIS in box trainers, VT and VR systems. This section describes various tasks in detail that have been designed to teach camera navigation.

#### **2.1.3.1 Endoscope and port location used for camera navigation task**

Endoscopes come with different angles of objective lens, one of which is  $0^\circ$  that is the simplest to use and provides a straight view (view that is directly in front of endoscope). However, angled endoscopes such as  $30^\circ$  and  $45^\circ$  are useful as they expand the range of viewing aspect, thereby being more versatile and more widely used (Eyal et al., 2001; Lansdowne et al., 2012). Furthermore,  $30^\circ$  endoscopes cause less disorientation in comparison to their  $45^\circ$

counterparts, and hence, are more preferred by surgeons for most of the endoscopic procedures (Fried et al., 2002). Therefore, a 30° endoscope was used for training and testing participants.

In terms of port location, the typical “Baseball diamond” arrangement of incisions is used to perform most endoscopic surgeries, so that no repositioning of the patient is required to access the entire surgical field using endoscopic instruments (Eun et al., 2007). It is desirable to place the endoscope in middle of the other ports used for inserting other instruments. This helps surgeons in terms of better depth perception using shadows, linear and motion parallax, relative sizes and aerial gradients of anatomical structures inside. However, in a general endoscopic surgery setup, the camera assistant stands beside the surgeon to manipulate the endoscope, obstructing the surgeon’s hand movements. It can also be obstructive inside the body cavity as well. To alleviate this problem, surgeons use the ipsilateral port position for the camera. This places the camera away from the operative field, avoiding interference with the surgery, but making camera navigation more difficult. (<http://www.laparoscopyhospital.com/Port%20Position%20in%20Minimal%20Access%20Surgery.html> retrieved Apr 05, 2012). Although this placement of endoscope requires the surgeon to perform additional mental transformations between what he sees and what he manipulates, research has shown that ipsilateral placement of the endoscope to the left of the periumbilical region gives best cosmetic results and provides better ergonomics for surgeons (Ng et al., 2003). Therefore, the left port of trainer box was used for both training and testing participants.

### **2.1.3.2 Camera navigation tasks designed in VR systems**

Endotower<sup>TM</sup> was one the first VR systems to teach endoscopic camera navigation, thereby enhancing and testing the visuospatial skills of participants (Haluck et al., 2001; Maithel et al., 2006). The simulation consisted of a 3D virtual tower that housed seven holes, six of

which were randomly oriented arrows as targets. Participants were expected to find and maintain a specific view of these targets through exploration using a 30° virtual endoscope. Navigating the angled endoscope through positioning and rotation in order to observe and orient the arrows required use of spatial cognizance, thereby testing the visuospatial skills of participant. Eyal and Tendick too utilized a similar task to test spatial abilities of participants, except that they used a 45° virtual endoscope and the targets were in form of alphabets instead of arrows.

Another study that evaluated transfer of basic endoscopic skills taught by VR simulator LapSim to OR implemented a similar design of experiments. Participants were asked to navigate a 30° endoscope in order to find and focus on certain number of balls that appeared randomly in a virtual environment (Hyltander et al., 2002). A coordination module employing a simple pick-and-transfer task for a number of balls was also present in LapSim VR simulator. An enhanced product of the LapSim family, LapSim Gyn, simulated the sterilization process, which required manipulation of camera with one hand while the other hand required for dissecting the fallopian tube, thus testing the coordination of hands of the participant.

Such tasks were used to demarcate novice and expert surgeons based on parameters such as path length, total time taken for the task, angular path, number of errors committed etc.

### **2.1.3.3 Camera navigation tasks designed for box trainers**

Korndorffer and his colleagues (2005) also developed a task similar to Eyal and Tendick, which taught camera navigation but in box trainers. A Laparoscopic Skills Testing and Training (LASTT) model was developed to test camera navigation and other typical endoscopic tasks using a box trainer by Molinas et al., (2008). In this model, the camera navigation task required participants to identify targets which were mounted on different modules by using all movements of endoscope, namely, rotation, lateral along axis and zoom-in, zoom-out movements. In this

study, the targets had a large symbol (either number or alphabet) that could be identified from a distance, and a small symbol, which could be identified only from a close-up view. The task thus trained and tested a participant for his camera navigation skills.

#### **2.1.4 Providing graphical feedback**

The adage “A picture is worth a thousand words” can be suitably used to describe the importance of graphics. Providing graphics makes understanding of large amounts of data and a complex idea quick and easy. Graphics have a quick impact as they get directly absorbed in the human visual information-processing system, which is still being explored (Kosslyn, 1985). For example, it is easier to interpret “Danger / Stop / Restricted” just by looking at the color red even from a long distance, and a suitable action can be taken beforehand. Research suggests that graphical feedback takes less time for interpretation if displayed in the simple forms. Providing graphical feedback has been extremely useful in many fields like use of Global Positioning System (GPS) for navigation, in aviation industry and most recently, in MIS.

##### **2.1.4.1 Providing graphical feedback in MIS**

Some researchers have concluded that providing graphical aids as a means of feedback to the surgeon improved their performance in MIS. Superimposing of computer-generated graphical aids on the video of and/or on the actual surgical field is known as Augmented Reality (AR). As mentioned before, use of long instruments instead of hands result in lack of haptic feedback for the surgeon. Due to this, it is difficult for the surgeon to estimate the amount of force that should be applied while handling anatomical structures or performing surgical tasks like suturing within the operative field. Application of forces higher than required can result in rupture of the structure or the suture, leading to medical emergencies.

A research conducted in Johns Hopkins provided force overlays in the form of dynamically color changing circles superimposed on the normal video stream of a da Vinci<sup>®</sup> Surgical System. Forces applied using the endoscopic tool were sensed using strain gages and were divided into three ranges – nominal, ideal and excessive. A green colored circle indicated nominal, yellow indicated ideal and red indicated application of excessive force on the tissue. A concept of providing information about pitch, yaw and axial forces using similar circular overlays, changing size of the circle to provide forces applied and color of the circle to indicate the oxygenated levels of tissue was also proposed in this study (Akinbiyi, 2005).

#### **2.1.4.2 Pilot navigation and learning from their results**

Graphics have been extensively used in the aviation industry, especially for both the pilots and the Air Traffic Controllers. Simulators for the aviation industry progressed rapidly in the last 75 years and have become an effective and mandatory tool for the training and skill verification of pilots. Pilots need to know lot of information while in-flight and need to address emergencies with little or no room for error. Graphical presentation of all this information is the quickest method to help them easily understand and make quick corrective decisions. Research has shown that tactical situation awareness (SA) improved with usage of color-coded displays in simulator training (Derefeldt et al., 1999). Presentation of graphics as a feedback can thus be used to alert and generate faster response times from the participant, thereby decreasing errors and improving overall understanding of the environment.

#### **2.1.4.3 Other design factors for graphical aids**

Various factors in a graphic can be used to impart clarity or additional information. Colors, placement of information and contrast are some of the important factors that can affect performance of the participants, and shall be discussed in this section.

#### **2.1.4.3.1 Colors and placement of information on the graphical screen**

Colors can be used to represent information of various types. Any color produced on a LCD screen is an additive color space combination of the three primary colors, red, green and blue (RGB). A pixel can be defined as “White” if RGB values for that pixel are [255, 255, 255]; while a pixel can be defined as “Black” if RGB values for that pixel are [0, 0, 0]. Different colors can thus be generated for each pixel using various combinations of these RGB values. The human visual system is trichromatic (similar to the RGB color space), and hence it is a suitable color model for generating graphics on a computer (Salvendy, 2006).

Research has shown that the cones and rods of the eye perceive different colors or color combinations and that their perception corresponds to different regions of the visual field. For example, red and green are easily identified by cones in the eye as compared to rods. It is hence recommended that red and green colors should not be used in the periphery, but in the center of the visual field (Helander et al., 1997). Similarly, colors such as black, blue, white and yellow should be used near the periphery of visual field, as the retina is more sensitive to these colors in the peripheral regions (Helander et al., 1997).

#### **2.1.4.3.2 Contrast**

Legibility of any graphic is highly dependent on the background of the graphic. The higher the contrast, the better is the legibility, which in turn is necessary for faster reaction times and better understanding of information being imparted (Proctor et al, 2004).

#### **2.1.4.3.3 Color-blindness**

Color-blindness was also a problem that should be considered when designing graphical aids. A participant having these deficiencies would not be able to differentiate between red and green, yellow and blue, thereby subduing the purpose of graphics (Wogalter et al., 1999). To

counter this problem, pure white graphics on a black background were generated and used as final graphic screens. As this combination produces the greatest clarity due to the highest difference possible in their RGB values, they produce an effect of precision, alertness and objectivity (Feisner, 2006).

Another research study highlighted the fact that participants preferred color displays in comparison to black and white, however, there was no evidence that color improved aesthetics, legibility and reduced eye-strain of participants (Pastoor, 1990). From this, it was concluded that providing graphics in black and white colors would not affect performance of participants as compared to graphics with colors.

## **2.2 Proximity sensing**

The visual ability to perceive the world space in 3D and the distance of an object in it is known as depth perception. Depth perception can be judged using both monocular (require visual input only from one eye) and binocular (require visual input from both eyes) cues. Some examples of monocular cues are motion parallax, relative size, texture gradient, accommodation, lighting and shading (shadows) and so on; while stereopsis, shadow stereopsis and convergence are examples of binocular cues (Gibson, 1974; Kelsey, 1993). In MIS, the 3D surgical field is projected on a 2D video monitor, resulting in lack of some of these cues, hampering the judgment of depth of the surgeon (Nicolaou et al., 2005). Similarly, an apparent shadowless operative field that results due to the coaxial arrangement of light source and camera optics leads to loss of the important visual cue of shadow. This can result in past-pointing errors with instruments that are used for cutting and diathermy among others, which might result in grave mishaps and complications during surgery (Nicolaou et al., 2006). Providing an estimation of proximity hence, is of great importance.

### **2.2.1 Proximity Sensor**

A sensor that is able to detect the presence or is able to provide the distance of an object without any physical contact is defined as a proximity sensor. A proximity sensor can be of various types - capacitive, inductive, infrared, magnetic, photoelectric, ultrasonic and so on.

#### **2.2.1.1 Capacitive sensors**

Capacitive sensors use the technology of capacitive coupling, and can detect any object (especially plastic) that is conductive or has a dielectric different than air (Wimmer et al., 2007). They produce an electrostatic field instead of an electromagnetic field. A change in the field occurs when a target approaches within the nominal range, thereby detecting presence of an object.

As all the objects within the trainer box were made of plastic, capacitive sensors could be used for detection and sensing proximity of the objects. However, they would be inefficient in OR environment as there are no plastic objects or anatomical structures made of plastic present within the human body. Also, the physical sizes of capacitive sensors available were much bigger than what could be mounted on the tip of endoscope, and hence, were not considered for implementation in this system.

#### **2.2.1.2 Inductive sensors**

An electric sensor that can detect the presence of metallic objects without touching them is known as an inductive proximity sensor (Johnstone, 2005). The principle works on creating a magnetic field that is generated through the passage of electric current through an induction loop.

However, this type of sensor could not be used with this system for following reasons -

1. The magnetic field generated could interfere with the electromagnetic field generated by the Ascension miniBIRD's transmitter,



2. Physical size of these sensors was too large for placing them on tip of endoscope,
3. There were no metallic objects present in the simulation system and are restricted to endoscopic tools in the OR.

#### **2.2.1.3 Ultrasonic sensors**

High frequency sound waves (typically above 18,000 Hz), generated through the usage of a transducer, are sent and the echo is received back by the receiver module. The distance of an object is determined by calculating the time interval between transmission and reception of the sound signal (Escolà et al., 2011).

However, this type of sensor could not be used for two reasons with this system, namely -

1. The blind zone (the smallest permissible range of detection) (Hernández et al., 2007) for the sensors found were in the range of 60-800 mm, which were too large to be considered in the box trainer setup,
2. Physical size of these sensors was too large for placing them on the tip of the endoscope.

#### **2.2.1.4 Photoelectric sensors**

Photoelectric sensors are an electronic device that can detect the presence / absence and the distance of an object using a light transmitter, typically using an infrared transmitter and a photoelectric receiver (Heaton et al., 2008).

This type of sensor had the mechanism to detect distances in the range of 0-150 mm which are typically encountered in the box trainer setup. Sizes of some sensors of this type were small enough to be easily mounted on endoscope tip. Hence, a photoelectric sensor was selected for giving information regarding proximity from any object placed within the trainer box.

IR sensors typically emit an infrared light, or an electromagnetic radiation whose wavelengths (780 nm – 1 mm) are longer than those of visible light (400 nm - 780 nm) (Castro, 2008). Any type of visible light used for detecting proximity, such as a laser, would distract the participant if visible within the visual field. On the other hand, infrared light being invisible to human eye can be used to measure proximity of objects within the trainer box without distracting the user.

## CHAPTER 3 MATERIALS AND METHODS

### 3.1 Design of graphics for camera navigation

A surgeon can perform efficient navigation of an endoscope and other endoscopic tools if he understands the spatial relationships between multiple factors that exist in the OR. The relationships between the port of entry of the endoscope, the video present on monitor and the surgeon's own location are critical for effective and timely surgical performance. The surgeons get confused with directions thereby producing surgical errors and take longer time to navigate endoscope (Shanafelt et al., 2010; Wetzel et al., 2006; Arora et al., 2010). These surgical errors might be reduced if surgeons are trained in the presence of visual cues. A set of different graphics were developed to impart various real-time information related to endoscope to enable better camera navigation. They then were investigated in pilot work and modified appropriately.

#### 3.1.1 Materials

The main components used for generating the graphics are mentioned in Table 3.1.

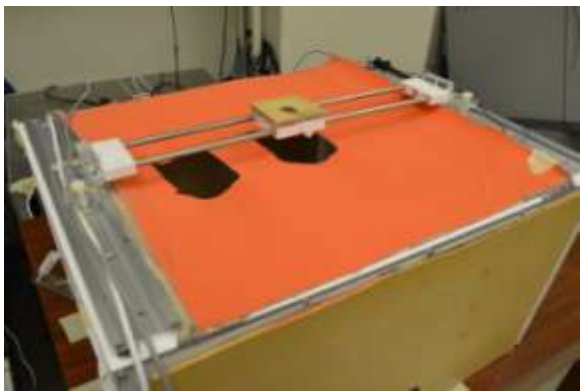
**Table 3.1** Components used for generating graphics

<b>Component</b>	<b>Source</b>
<b>Trainer box</b>	Human Performance Lab, VCU
<b>Simulated Endoscope</b>	3-DMEd SimScope™
<b>The <i>MotionMonitor</i>® (TMM)</b>	Innovative Sports Training with Ascension miniBIRDS

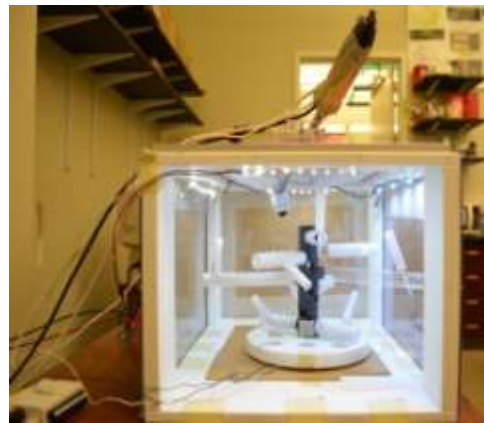
##### 3.1.1.1 Trainer box

The trainer box (Figure 3.1a and 3.1b) was designed and developed earlier in our lab to represent the human anatomical space (Vasudevan, 2012). Sides of the rectangular box were made opaque using rubber sheets (Rubbercal) to prevent direct viewing of objects placed inside the box. The top of the box was covered with an opaque cloth to simulate the opacity of human body through which an endoscope was inserted to reach the simulated body cavity.

Four 15V-200 mA white-colored LED strips (<http://www.ttelectronics.com/home/> retrieved May 02, 2012) were fixed on the inner faces of the four edges of the top of box to illuminate its internal space. A 12 mm diameter by 20 mm deep simulated trocar, designed and developed earlier using Velcro-attached plastic and a rubber sheet, was used to simulate the port through which the simulated endoscope was inserted (Figures 3.1b and 3.2b). The purpose of the rubber sheet was to simulate the resistance of human body to that of inserted endoscope.

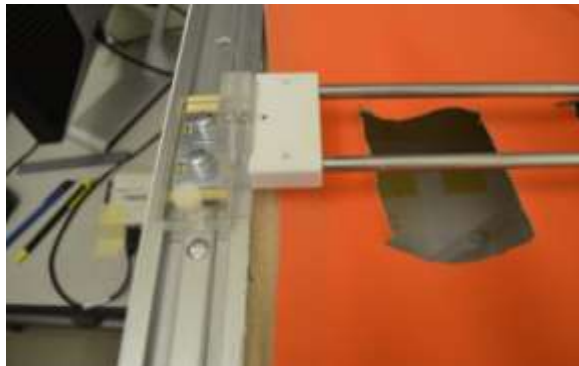


(a)



(b)

**Figure 3.1** (a) Endoscopic Trainer box system; (b) Trainer box system (Vasudevan, 2012)



(a)



(b)

**Figure 3.2** (a) Slider arrangement (Vasudevan, 2012); (b) Simulated trocar (Vasudevan, 2012)

A slider arrangement (Figures 3.2a and 3.2b) was designed that could move the trocar to any desired location over the width of the trainer box. The location of simulated trocar could be altered and then locked using a locking screw along the length of trainer box to act as either center, left or right ports (Figure 3.2b).

### 3.1.1.2 Simulated Endoscope

A 362 mm length, 10 mm diameter, fixed focus 3-DMED SimScope™ was used to simulate an endoscope (Figure 3.3a). The shaft had a camera attached at the tip at a fixed angle of 30°, which was powered using a standard 9V DC, 0.8A adaptor. The standard 1Vp-p video signal was viewed on a TV monitor placed at eye level in front of the participant, as shown in Figure 3.15. The camera had a built-in rotary mechanism that could rotate the camera head by 360° along the shaft axis. This was disabled using Loctite® for this series of experiments, to mimic an actual endoscope with an objective lens of 30°. The endoscope also had a built-in port attachment that could be used to snap this endoscope in some Minimally Invasive Training Systems (MITS) available from 3-DMED. This port attachment was also dismantled to allow the endoscope to fit into the trainer box system (Figure 3.3b).

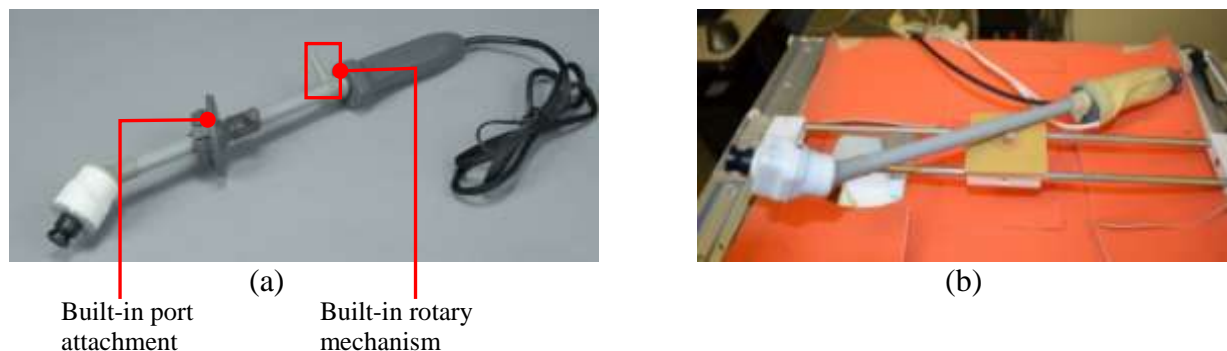


**Figure 3.3** (a) 30° Simscope ([http://www.3-dmed.com/SimScopes\\_Descriptions\\_\(CAM07\).html](http://www.3-dmed.com/SimScopes_Descriptions_(CAM07).html) retrieved May 18, 2012); (b) Endoscope after disabling both built-in port attachment and rotary mechanism

### 3.1.1.3 The MotionMonitor®

Innovative Sports Training The *MotionMonitor*® (TMM) system (Figure 3.4a) was used to collect all the data regarding movement of endoscope within the trainer box. The system consisted of electromagnetic tracking devices, Ascension Technology Corporation's miniBIRDS, consisting of a Standard Range Transmitter (SRT) and four 8mm sensors. One of the sensors

(Sensor #3) was attached to the endoscope handle (Figure 3.4b) and was used to track and record XYZ coordinates from four static points marked on the endoscope.

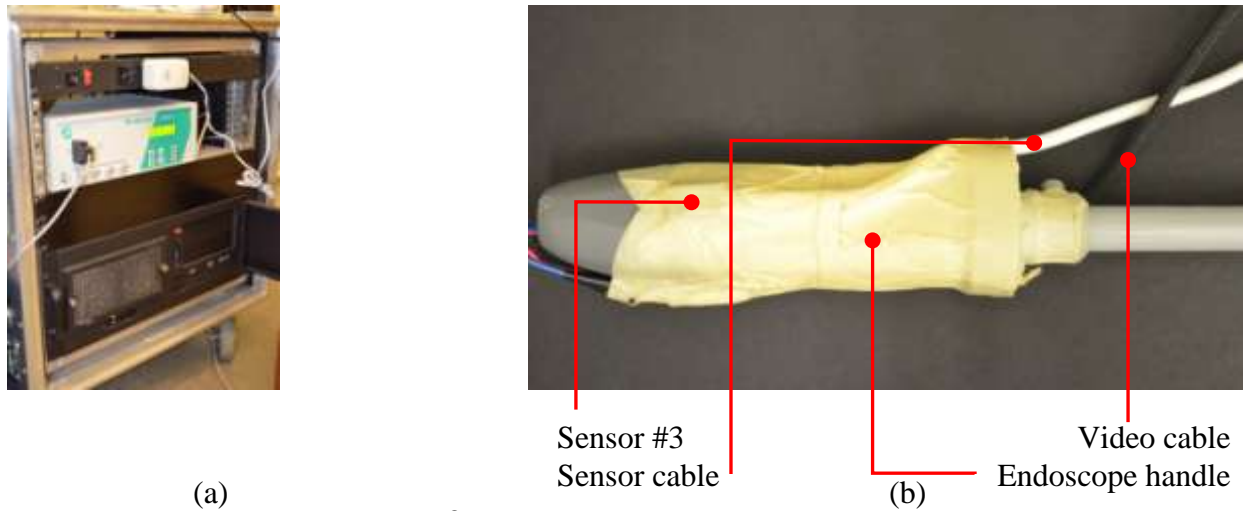


**Figure 3.4** (a) The *MotionMonitor*<sup>®</sup> system; (b) Sensor attached to endoscope handle

Locations of all four points tracked, known as “Landmarks” are shown in Figures 3.5a and 3.5b.

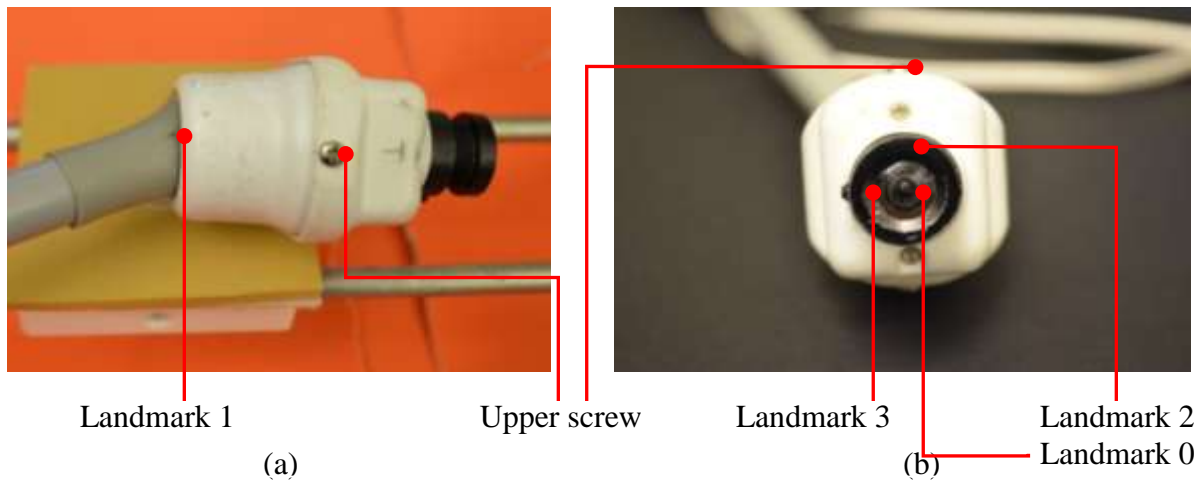


**Figure 3.5** (a) Side view of camera head; (b) Front view of camera head

Landmark #0 was set at the center of camera lens, while landmark #1 was set at the joint of the endoscope shaft and camera head. Landmark #2 was set at the 12 o’clock position and landmark #3 was set at the 9 o’clock position with respect to landmark #0 respectively. XYZ data for all four landmarks was reported relative to sensor #3 attached to endoscope handle.

Real-time XYZ data from all four landmarks was used to generate and manipulate the three real-time graphics developed in Matlab. Marking of these four landmarks is independent of the angle of the objective lens, and hence, all the graphics can be easily generated for an endoscope with any angle of objective lens that is used in this setup.

Sensor #3 was set at a sampling rate of 20 Hz. A trigger button connected to analog-to-digital converter (A/D) Board #0, channel #0 of the TMM and sampled at 100 Hz was used to mark time points at which targets were found during the training phase, and to differentiate time slots for endoscope movements during the testing phase. The static resolution of the TMM sensors for position and orientation were 0.5 mm and 0.1° respectively, both at 30.5 cms. Accuracy of the TMM for position and orientation were 1.4 mm and 0.5° respectively, both at 30.5 cms (<ftp://ftp.ascension-tech.com/> retrieved March 28, 2011).

Special care was taken to keep power sources and computer screens away from the TMM transmitter to reduce electrical noise being induced in the data collected. Both AC and DC field technologies are susceptible to presence of ferrous materials in their tracking area. The transmitted magnetic fields induce a flow of eddy currents within the surfaces of the metal objects. These eddy currents produce magnetic flux within the metal object, whose intensity is dependent on proximity, size, shape and orientation of the metal object. This magnetic flux can interfere with the TMM electromagnetic field, and thus can distort values obtained and recorded by the TMM. A similar study that used a similar motion tracking setup concluded that accuracy of the system is not compromised if the distance between metal items and the transmitter and sensors is at least 33 cms (Schendel et al., 1990). To avoid this distortion, ferrous and non-ferrous metal items were kept at more than 2 feet of distance from both the transmitter and

sensors. Similarly, all objects used within the trainer box setup were made from plastic or other non-metallic materials.

#### **3.1.1.4 Collision detection system**

A collision detection system (CDS), designed and developed earlier in our lab, was used for detecting collisions with the task setup in the trainer box (Vasudevan, 2012). Collisions could occur between the endoscope and any of the objects placed within trainer box, such as branches, target cylinders or central trunk of task trees. Rubbercal sheets placed beneath the task tree and on exterior sides of trainer box (in order to make it opaque) prevented external collisions such as “knocking on the box” to be recorded, thus increasing the reliability of the CDS.

The system consisted of a dual-axis accelerometer ADXL-203, the schematic and pinout diagrams of which are as shown in Figures 3.6a and 3.6b respectively. It has a precision range of  $\pm 1.7g$ , with a typical bandwidth of 2.5 kHz, sensitivity of 1000 mV/g and noise density of 110  $\mu g/\sqrt{Hz}$ . The accelerometer detects changes in dynamic acceleration, for example, vibrations. When fixed to the trainer task, it detects vibrations associated with collisions of the endoscope with objects of the trainer task. Data from the accelerometer was recorded using a LabView program via a National Instruments Data Acquisition Card (NI-DAQ) NI USB-6008 connected to a desktop computer, as shown in Figure 3.7.



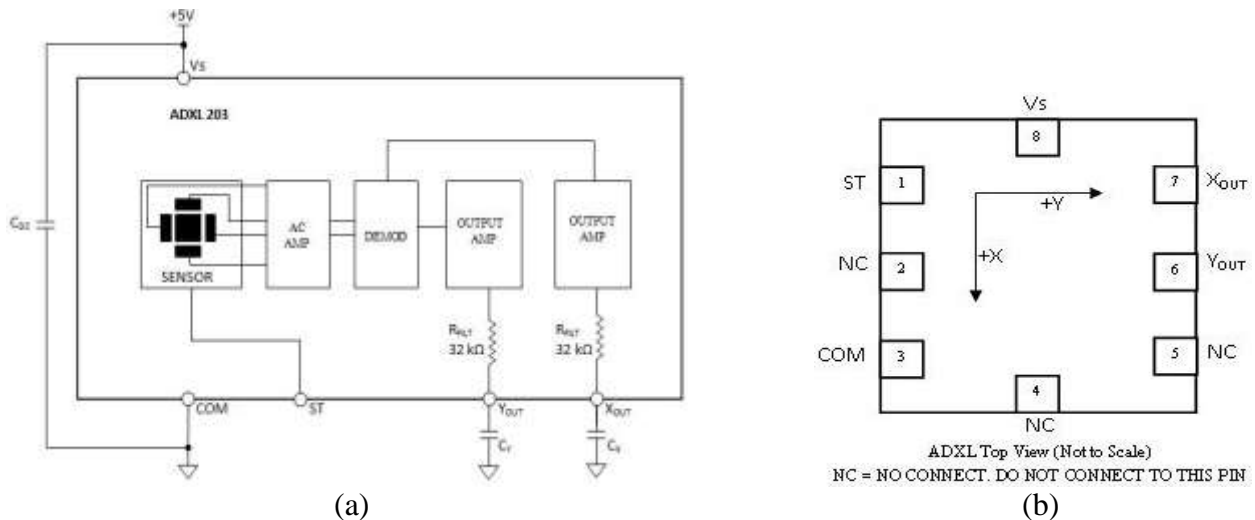


**Figure 3.6** (a) Accelerometer ADXL 203; (b) Pinout diagram  
 (Redrawn from [http://www.analog.com/static/imported-files/data\\_sheets/ADXL103\\_203.pdf](http://www.analog.com/static/imported-files/data_sheets/ADXL103_203.pdf)  
 retrieved May 23, 2012)

The NI USB-6008 has 8 single-ended (or 4 differential) analog inputs (12-bit resolution, 10 kS/s sampling rate), from which analog-input channel #4 (AI4) was used to record vibrations from the accelerometer. The +5V power supply and ground for the accelerometer were provided through the NI USB-6008 by connecting the +5V and GND of NI-6008 to pin #8 and #3 respectively. A LabView program was written to record and differentiate collisions as “Minor” (5-25 gF) and “Major” (>25 gF) based on intensity. The front screen of this LabView program is shown in Figure 3.7.

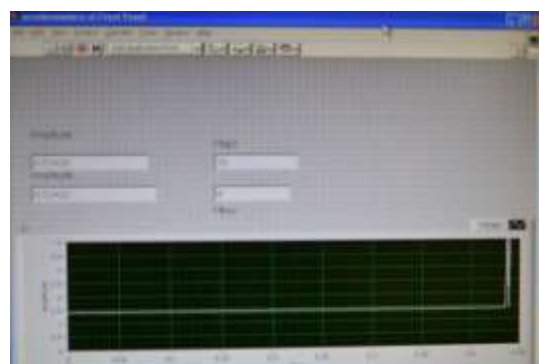


**Figure 3.7** Front screen of LabView program

A schematic diagram of the complete system used for this study has been shown in

Figure 3.8.

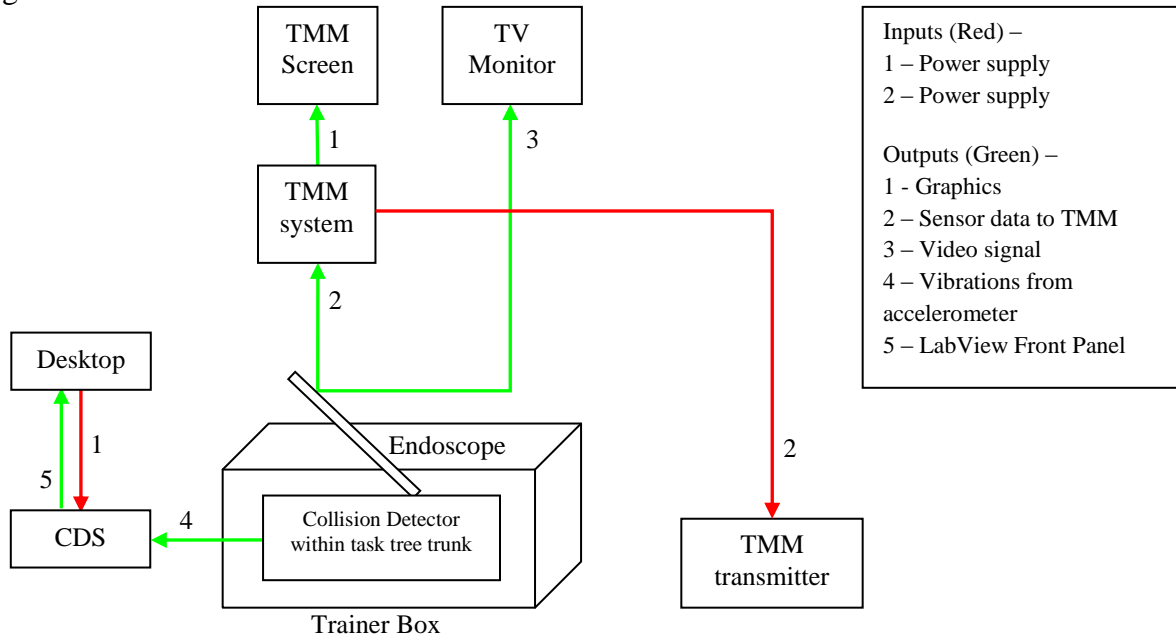


**Figure 3.8** Schematic of the entire data collection system

### 3.1.2 Pilot testing phase for testing the graphics

The pilot testing phase was used to explore the potential of different types of graphical aids to assist in learning a camera navigation task. For the task, four task trees similar to the task trees built by Eyal and Tendick (2001) were used. Each tree had transparent hollow tubes called “branches” at various heights, angles and of various lengths (Figure 3.9).

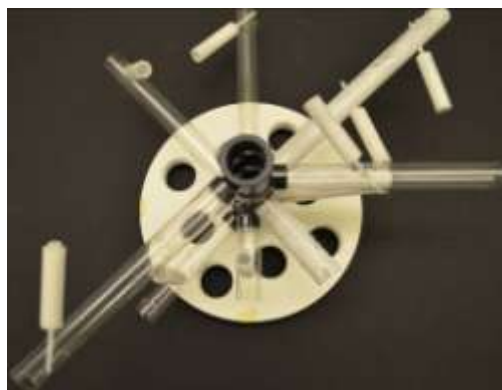


**Figure 3.9** Pilot phase task tree

The central trunk had holes in a radial manner at specific intervals to which branches were attached using black colored plastic knobs. Each tree had eight white cylinders attached to the branches each of which contained a unique target number from 0 to 9. All target cylinders were at different positions, heights and orientations and contained the target number at different depths within the target cylinder.

A total of ten participants were tested in this phase. Four different graphics programmed using Matlab were provided to participants. Graphics were designed to impart real-time information about the location, direction and rotation of endoscope tip. Participants were asked to identify the targets placed in the task tree and draw their approximate position and orientation on paper using the various graphics created. A brief description of these graphics follows:

#### **3.1.2.1 Directional Markers graphic**

One of the graphics used for training camera navigation to participants is as shown in Figure 3.10. Real-time video was displayed in the center of this graphical window, while four directional markers indicated the X-Y location of the endoscope tip along the sides of the video. For this graphic, the center of the trainer box along the X-Y plane was taken as the origin, and appropriate direction markers were proportionately filled based on the coordinates of the endoscope tip obtained from the TMM. A vertical height bar was also provided to give an estimate about the height of endoscope tip within the trainer box.



**Figure 3.10** Directional markers with vertical height bar

Although this was a simple and easy-to-understand design, pilot studies revealed certain disadvantages of this graphic, which were -

1. The process of taking a snapshot of video, placing it in the center of graphical screen and other calculations for changing the graphics took too long: a noticeable lag existed between the actual endoscope movement and the video shown, thus not making the display real-time,
2. Direction markers indicated only the coordinates of the location, but no information was provided regarding the direction of view and rotation,
3. Most participants did not bother to look at the vertical height bar present in lower right corner, as they were more focused on the central real-time video to search and find targets

This graphic lacked information regarding location, direction and rotation of endoscope tip. Participants were not able to understand the change in directions on rotation of endoscope, and marked the targets incorrectly on paper. Feedback received from participants of pilot study made it necessary to design graphics that would be simple, self-explanatory and imparted

information of endoscope to the participant. Wentink et al., (2002) concluded that displaying the endoscopic tool in the video had improved the hand-eye coordination of the surgeon. Conclusions from this study were used as a reference to impart knowledge of position, direction and rotation of endoscope to the participant.

### **3.1.2.2 Position circle with Line graphic**

The tip of the 30° endoscope is at a fixed angle with respect to its longitudinal shaft; hence, knowing the location of its tip and the direction of camera head becomes essential for the surgeon to have better idea of directions.

A real-time graphic with a circle indicating position of the endoscope tip (landmark #0) in the trainer box and a line indicating the direction of the camera head was developed, as shown in Figure 3.12a. To this position circle, a line was generated using the real-time XYZ coordinates of landmarks #0 and #1. This line was the projection of distance on to the XY plane between landmarks #0 and #1. Being the projection, if the endoscope pointed straight downwards, the length of the line would reduce to a “dot” or “point” in the center of the position circle.

This graphic imparted information relating to position and direction of view of the endoscope tip to the participant in real-time.

### **3.1.2.3 Position circle with Shading graphic**

For this real-time graphic design, the position circle described in 3.1.2.2 was filled or shaded to indicate the rotation of 30° endoscope. The slope of the line between landmarks #0 and #3 was calculated using their XYZ coordinates in real-time. Based on the XYZ coordinates of landmark #2 with respect to landmark #0, the particular half of a square matrix was filled or shaded. A “bitwise (logical) AND” was then performed with an image of a filled circle. Following this, a “bitwise (logical) OR” was performed with the image of the position circle.

The result of these operations was to achieve real-time shading of the circle, to indicate rotation of the endoscope. The “base” (or upright) orientation was indicated when the upper half of position circle was “black” and the lower half was “white”. This meant that the directions of the XY axes of the trainer box and those of the endoscope were the same. Based on the rotation of the “shading”, a participant could rotate their mental frame of axes in that direction for that angle of rotation to understand the new frame of axes.

#### **3.1.2.4 Position circle with Line + Shading graphic**

This real-time graphic was a combination of both the added line and shading of the position circle. This graphic gave complete information about position, direction of view and rotation of the endoscope tip to the participants.

#### **3.1.2.5 Exploration of the use of color**

An attempt with using a colored display was also made during this pilot study. The direction line and the filling of the position circle were programmed to change colors as either red or green, depending on the height of the endoscope tip within the trainer box. If the endoscope tip was below half the height of the trainer box, the line or filling would be red in color, otherwise, it would be green in color; this indicated the height of the endoscope tip in center of the visual field. To give a better estimate of height, filling of the vertical height bar was made yellow so as to indicate height of the endoscope tip within the trainer box. Yellow as chosen as the height bar was placed in the periphery of the visual field on the TMM screen near the side of the video.

However, color combinations such as red/green, blue/yellow, green/blue and red/blue create illusions of shadows or vibrations (Helander et al., 1997): effects that were not desirable

for an aid. Hence, the red/green coloring of the position circle along with its shading and direction line was not incorporated in the final design of the aids.

### **3.1.2.6 Exploration of the placement of the video monitor and the graphics screen**

An attempt was made to combine the video and graphics together on one screen during the initial stages of this exploration phase. However, based on subjective feedback received from participants during pilot trials, the video and graphics were split on two separate screens so as to have real-time video as seen in an actual OR environment.

It was also tested if placement of both the video and graphics screens with respect to each other caused any variations in the performance of the participants. Maintaining both screens at the participant's eye-level, the left-right positions of both screens were alternated through the task. In terms of the number of targets found in each of the task tree, there was no difference in performance for the two different conditions, thereby indicating that left-right placement of the video and graphic screens did not affect the performance of the participants.

A top-down arrangement of both the screens was also tested as a possible method of placing screens together. Ergonomically, the video monitor should be placed 15° - 40° below the surgeon's eye level for maximum comfort in actual OR environment (Whelan et al., 2006). The top-down arrangement of monitors placed the upper screen much above the participant's eye level. The participants complained of neck pain due to the stress induced by inappropriate ergonomic positions. Hence, this arrangement was not considered for this series of experiments.

### **3.1.2.7 Feedback about graphics developed**

The pilot studies conducted gave subjective feedback from the participants about the position circle + line graphic, position circle + shading graphic and the position circle + line + shading graphic. Participants accepted and liked the information content provided by each of the

three graphics. Participants who were provided with the direction line affirmed the graphic made it easier for them to understand the direction where the camera was looking at. Some participants provided with shading of the position circle took a longer time than others to understand the graphic, but were able to rotate their mental frame of axes. Participants provided with both line and shading affirmed that the information content provided was helpful for understanding all motion aspects of the endoscope.

Of the ten participants that participated in this pilot study, all agreed that the radius of position circle of 10 units was appropriate. When radius was reduced to 5 and 7.5 units, participants felt strain on their eyes when viewing the position circle on the monitor that was placed at a distance of 4 ft from the participant. This distance was in accordance with a typical OR setup, where the monitor is placed in the range of 3 ft to 10 ft from the surgeon (Shallaly et al., 2006). Similarly, all participants were comfortable with the height and location of the vertical height bar. Based on the recommendations of seven participants, a legend indicating height (in percentage) of the endoscope tip within the trainer box was added along with horizontal lines to indicate the level.

One participant recommended replacing the white-black filling of the circle with a blue-brown filling, a combination corresponding to the artificial horizon in a flight attitude meter as shown in Figure 3.11. A change of filling of the circle indicated the direction of rotation of the endoscope, thus alerting participant to rotate his mental frame of axes accordingly in that direction. A flight attitude meter also serves a similar purpose, indicating banking of an aircraft to the pilot ([http://en.wikipedia.org/wiki/File:VMS\\_Artificial\\_Horizon.jpg](http://en.wikipedia.org/wiki/File:VMS_Artificial_Horizon.jpg) retrieved January 8, 2009).





**Figure 3.11** Attitude meter for an airplane

However, since the sensitivity of retina for blue is less in the center of visual field (Helander et al., 1997), the blue-brown combination was not selected for filling the position circle. Thus, considering all design aspects such as colors and their placement in visual field, contrast, color-vision deficiencies (if any) of participants etc., the white-black combination of colors was finalized for all the graphics including filling of the position circle to be used during the training phase of the experiment.

### **3.1.3 Methods**

Three different graphic aids (position circle + line, position circle + shading, position circle + line + shading) were chosen to examine their effects on learning a camera navigation task. All information displayed on the graphic screens corresponded to the endoscope in real-time. The aids were used during the training phase. During the testing phase, no aids were used. Although fading is recommended for any type of assistive aids, the simplest experimental design was chosen as it would transfer most easily to actual training.

#### **3.1.3.1 Matlab presentation of graphics**

Three different graphical aids were used. White colored graphics were provided on a black background to achieve the best contrast and in accordance with suggestions from the pilot studies.

All graphics used the height bar and legend to display the height of the endoscope tip on the lower right corner of the screen. It consisted of a vertical bar that indicated the Z-coordinate of landmark #0, i.e., the center of the lens. In addition, a map depicting the top view of the trainer box was placed in the upper right corner of all three graphic screens. A position circle (as described in 3.1.2.2) was used that indicated XY coordinates of the center of endoscope tip (landmark #0). In addition to these two features, additional information was given in each of the graphics. Graphic 1 was the position circle + line indicating direction of the camera head of the endoscope (as described in 3.1.2.2). Graphic 2 was the position circle + shading indicating the direction of rotation of endoscope (as described in 3.1.2.3). Graphic 3 was a combination of position circle + line + shading, providing complete information about position, direction of view and rotation of the endoscope to the participants (as described in 3.1.2.4). All the three graphics are shown in Figures 3.12a, 3.12b and 3.12c.

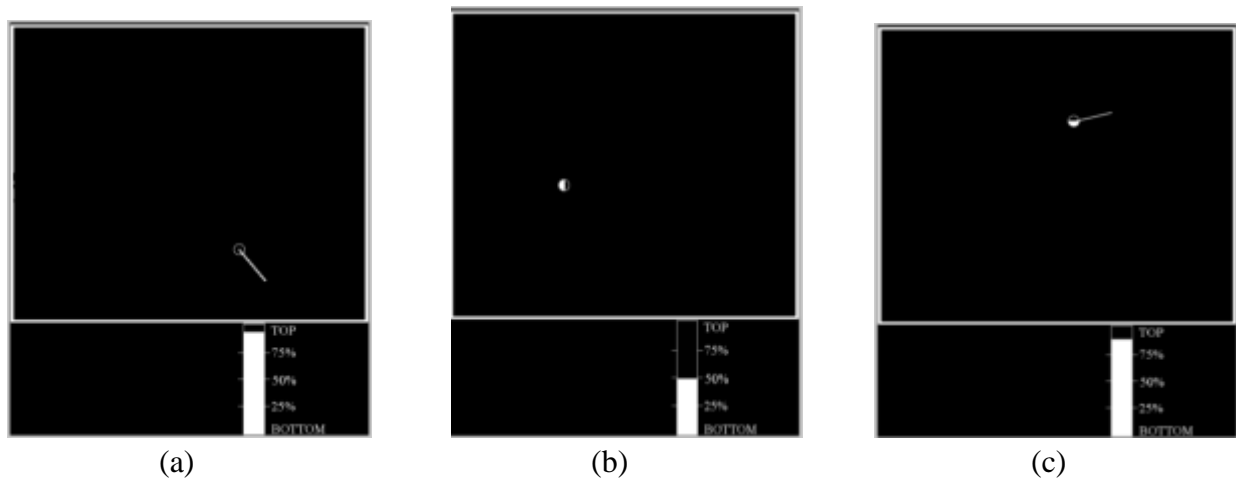


**Figure 3.12** Illustrations of the three different graphics provided to the participants. The lower rectangle in each graphic contained an annotated vertical bar. The white filling of this bar changed as a function of the endoscope tip height in the trainer box. The upper part of each display illustrated the different graphics. (a) Graphic 1 was a circle indicating the XY position of the endoscope tip with a line indicating direction of view of the endoscope; (b) Graphic 2 was a circle indicating the XY position of the endoscope tip with a shaded circle indicating orientation of the endoscope; (c) Graphic 3 was a combination of graphics 1 and 2.

### 3.1.3.2 Training and testing phase task trees

In order to train and test camera navigation, a set of task trees similar to Eyal and Tendick (2001) as described in 3.1.2 were used. A total of seven training task trees containing eight targets each were constructed and these were different from the ones used for the pilot testing phase of the experiment. As mentioned in 3.1.2, the target cylinders were placed at different positions, heights and orientations, with the target number positioned at different depths within the target cylinders (Figure 3.13). This impacted the ability to see the number from different viewing angles. For example, a target number mounted deep in the target cylinder could only be viewed when the endoscope looked directly down in the target cylinder. If the viewing angle deviated off-axis by a few degrees, the target number would become obscured, and hence, unidentifiable. Targets were rated as “Easy”, “Medium” and “Hard” using a geometric metric to describe their required viewing position. This method was previously developed in our lab (Vasudevan, 2012). Certain branches present on the task tree were installed to act as obstacles to restrict either the endoscope movement or restrict the field of view of the endoscope. This helped to make some of the targets “Medium” and “Hard”, in order to mimic situations when a surgeon has to navigate the endoscope to view an anatomical structure hidden behind another anatomical structure.

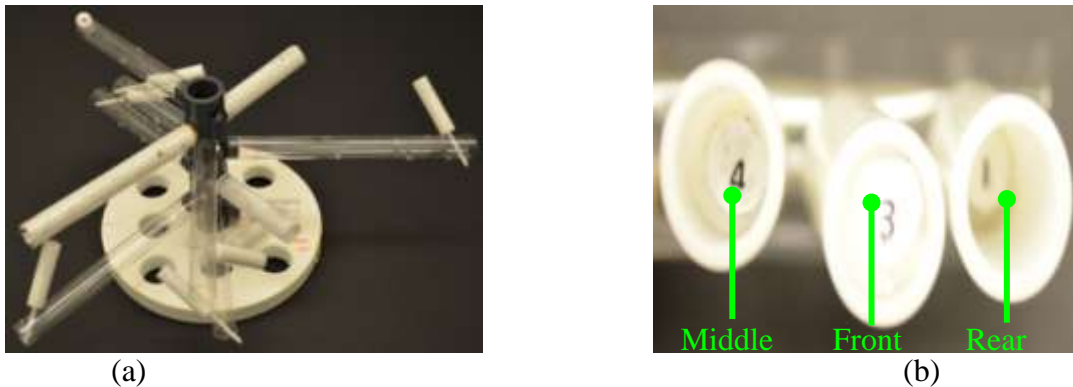


**Figure 3.13** (a) Training task tree; (b) Target numbers at different depths

The geometric metric used is shown in Table 3.2. The geometric score for each cylinder was the sum of scores given for each of the six parameters.

**Table 3.2** Geometric metric parameters for defining the target difficulty

Parameters	Geometric Metric Scores		
	Easy (1)	Medium (2)	Hard (3)
Letter Position (in target cylinder)	Front	Middle	Rear
Cylinder location (cm)	0 - 10	10 - 20	> 20
Depth (cm)	0 - 5	5 - 10	>10
Letter Proximity (cm)	< 0.5	1 - 2	>2
Number of Obstacles	0 - 1	2 - 3	>3
Angle (°)	0 - 5	5 - 25	25 - 45

Target numbers present within each training tree were unique and randomly numbered from 0 to 9. Care was taken by providing target number 9 with a bar above it ( $\bar{9}$ ) so that participants would not confuse it with the number 6 in any of the training trees.

The testing phase required moving endoscope to align with a cylinder and then to move in six directions relative to that alignment (Up, Down, Left, Right, In and Out). Only one testing task tree was constructed as shown in Figure 3.14. Due to the different nature of the testing phase, in contrast to the training task trees, the testing tree contained only seven targets and no extra branches were present to act as obstacles. Target cylinders of the testing tree were located at different positions and orientations, ensuring that the target numbers could be viewed in their upright orientation on rotation of the endoscope. The seven targets were numbered 1, 2, 3, 4, 5, 7 and  $\bar{9}$ , and were placed at different depths within their respective target cylinders. Symmetrical target numbers such as 0, 6 and 8 were not included in the testing tree to avoid confusion in identification of their upright orientation.

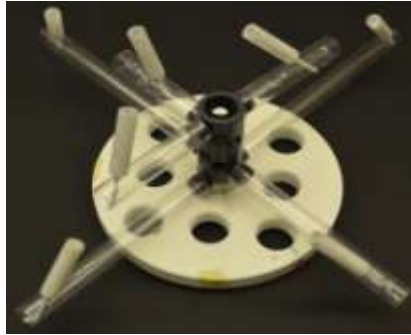


**Figure 3.14** Testing task tree

The task tree setup was designed to reduce any position bias of the targets that could have affected task difficulty. All targets were randomly placed throughout the trainer box, within the constraint that target numbers were visible using the same left port and 30° endoscope as used in the training phase. Targets were not placed too close together to avoid participants using another target visible on TV monitor as a reference. Targets were hence, uniformly distributed throughout the trainer box and were not clustered in a single area.

### **3.1.3.3 Experiment Setup**

The experiment setup is shown in Figure 3.15. The trainer box was placed at a height of 2.5 feet from the ground. This enabled participants to hold the endoscope at an ergonomic angle (angle between upper and lower arm was in range of 90° and 120°). Both the TV screen and the TMM screen displaying the graphics were placed at a height of 4 ft 2 inches beside each other at a distance of 4 feet from the participant, directly in front of the participant and at eye-level (Whelan et al., 2006). Pilot studies suggested that a left-right or right-left placement of the TMM screen and TV monitor did not affect performance of participants in finding targets in a task tree, as long as the graphics displayed on the TMM screen were placed on the side closer to the TV monitor. For this experiment, the TMM screen was placed on the left side of the TV monitor and the graphics were placed on the right side of the TMM screen, so as to be closer to TV screen.

The task trees were placed from the open left side of the box on to a rubber mat in the center of the trainer box. The accelerometer PCB was placed inside the task tree trunk at half the height of the trunk as shown in Figure 3.16a. The front panel of LabView program displayed both major and minor collisions in real-time on a desktop screen during the entire data collection period, but was not visible to the participant. The transmitter for the position sensors was placed on the right side of the trainer box as shown in Figure 3.16b.

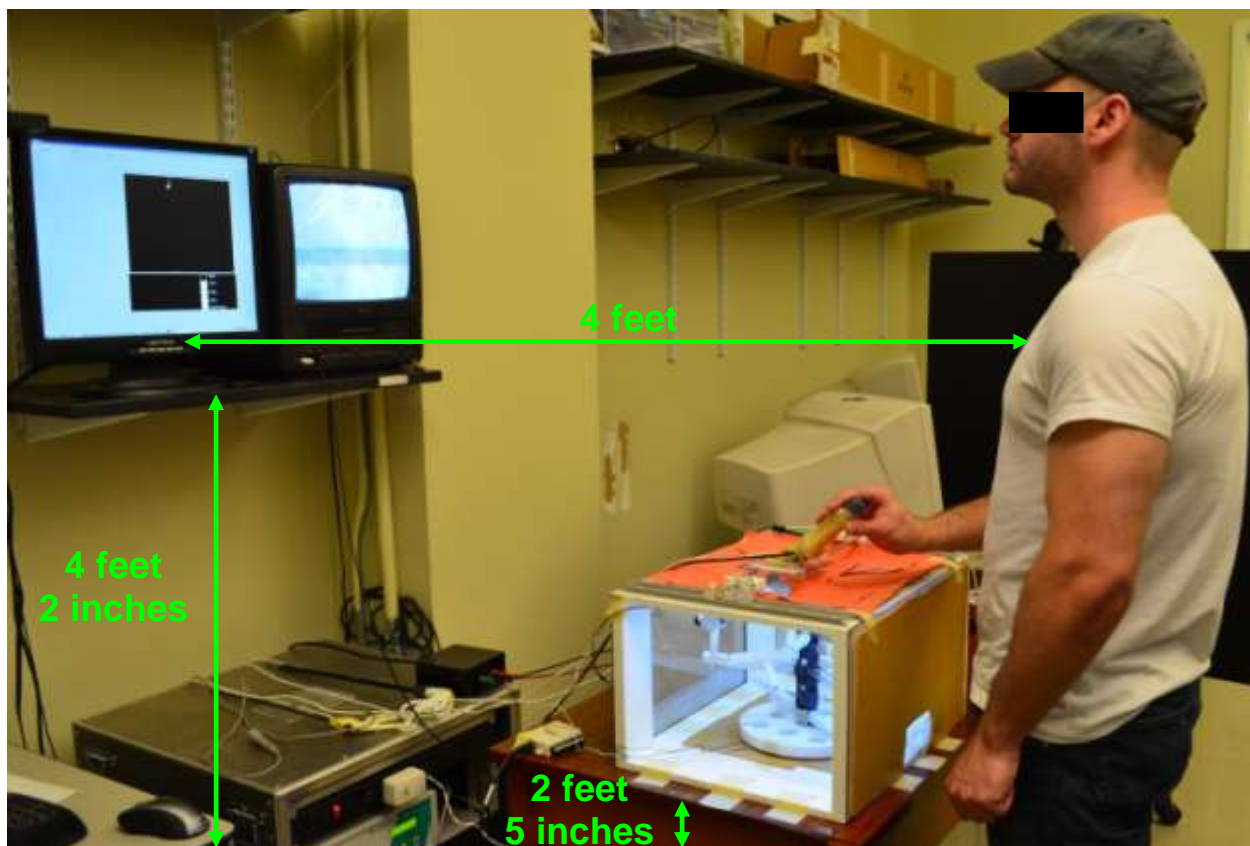
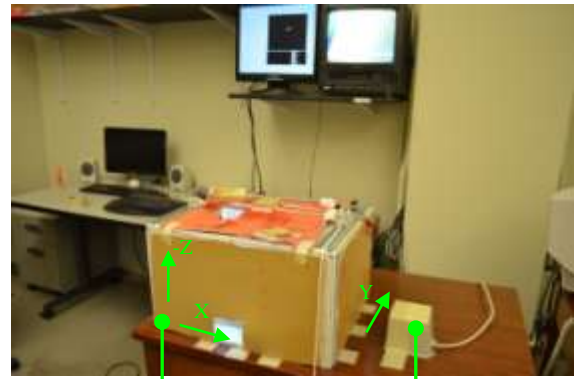


**Figure 3.15** Participant during training phase of experiment



(a)



Origin

Transmitter

(b)

**Figure 3.16** (a) Accelerometer placed at half height of trunk; (b) Location of transmitter with respect to trainer box

Only the left port was used for the entire experiment (both the training and testing phases). The coordinates of the world axes were set to “Hardware axes” of the TMM, with the origin at the front left-bottom corner of the trainer box. The axes setup was as shown in Figure 3.16b. The raw values of the XYZ coordinates of landmark #0 were then processed by an in-built specialized software integrated with the TMM system. These values were then exported in real-time to a Matlab program using the TCP/IP protocol installed on the TMM itself for real-time manipulation of graphics, and were also recorded separately for further analysis described later in this section.

### 3.1.3.4 Experimental Design

#### 3.1.3.4.1 Participants

A total of 36 individuals (14 females and 22 males) participated in the study. Before the experiment began, participants were asked which was their dominant hand (left or right) and if they had previous endoscopic experience. The sex of the participant was also recorded. All the participants either worked or studied at Virginia Commonwealth University and were recruited via posted advertisement and emails. This process was approved by the VCU IRB.

### 3.1.3.4.2 Training Phase

All participants were randomly assigned to one of the four groups (n = 9 per group) as summarized in Table 3.3.

**Table 3.3** Classification of different groups according to their training condition

<b>Classification</b>	<b>Group Name</b>	<b>Description</b>
<b>Group 1</b>	No Graphics (NG)	Participants trained with “No Graphics” during the training phase
<b>Group 2</b>	Line (L)	Participants trained with the “Line (showing direction of the view of endoscope)” during the training phase
<b>Group 3</b>	Shading (S)	Participants trained with “Shading (filling of the position circle to indicate rotation of endoscope)” during the training phase
<b>Group 4</b>	Line + Shading (L + S)	Participants trained with both “Line and Shading” during the training phase

Groups 2, 3 and 4 also used a position circle to indicate the tip position of the endoscope and the height bar.

The basic learning task considered for this study required participants to learn the use of a 30° endoscope from the left port of entry within the operating field. The primary task for participants was to find and identify the number placed inside the target cylinders in a sequence of task trees until they reached the stopping condition described later. The secondary task for participants trained under Groups 2, 3 and 4 was to concentrate and use the information presented through the respective graphics on the TMM screen while performing the primary task. The training phase used a maximum of eight task trees. Seven different task trees were constructed for this training phase. These trees were presented in a random order, and, if all seven trees were used by a participant, a randomly selected tree from the previously presented six trees would be presented as the eighth training tree.



#### **3.1.3.4.2.1 Duration of training phase**

Each participant was trained for a maximum of two consecutive days to learn the task and assimilate all information given by the graphics (in case of Groups 2, 3 and 4 only) until the stopping criteria described later was met. Each training task tree was presented for a maximum of 25 minutes, and training lasted for a maximum of 3.5 hours spread over two days (1.75 hrs on each day) to avoid fatigue.

#### **3.1.3.4.2.2 Training Instructions**

On the first day, participants were introduced to the basics of endoscopic surgery and were shown how to use the endoscope, namely, to manipulate its position, direction and rotation. They were also shown the way to stand, view the monitor and a combination of power-grip and pen-grip holding methods to have a stable movement of the endoscope. Participants in the Line, Shading and (L + S) groups were familiarized with graphics (presented on the TMM screen) by giving them a real-time demonstration and interpretation of the information. Each participant was then given hands on practice time using a dummy task tree (which was not part of the set of seven training task trees) placed inside the trainer box to get familiar with different locations, heights, orientations of target cylinders and depths of target numbers within each target cylinder.

Participants were also told that they would have to make a map of the task tree targets they found on paper. They then were described the process of marking the targets on the outline map given, which should be done one target at a time when the target is found. All 36 participants were given 10 minutes each to find all the targets present on dummy tree and mark 3D locations of its targets.

Participants were also instructed to avoid making any major collisions defined as when the force of contact was greater than 25gF as measured by the accelerometer.

### 3.1.3.4.2.3 Stopping Criteria

The training phase continued until the participant could locate at least 85% (7 out of 8) targets in two consecutive task trees. However, the training was also stopped after a maximum of eight task trees were used, which corresponded to approximately 3.5 hours, to allow the training phase to be tractable.

### 3.1.3.4.3 Testing Phase

To help the participant cognitively consolidate knowledge assimilated during the training phase, the testing phase was scheduled 24 hours after the end of the training phase (Gallagher et al., 2005). For the testing phase, each of the seven targets on the testing tree were oriented at different positions and rotations, thus having a different coordinate axes system with respect to the trainer box coordinate system. The main objective of this phase was to compare the effect of training on performance of different groups.

#### 3.1.3.4.3.1 Testing task

The testing phase included only real-time video on the TV monitor. The TMM screen which displayed graphics during the training phase was removed. Participants were guided to the locations of seven targets present on the testing tree one at a time with instructions as shown in Table 3.4.

**Table 3.4** Instructions to guide participants to reach locations of targets on testing tree

Target Number	Instruction to search and reach target
1	Target 1 lies in the Rear Left-upper corner of the trainer box, near the central trunk
2	Target 2 lies in the Rear Right-bottom corner of the trainer box
3	Target 3 lies in the Rear Left-bottom corner of the trainer box
4	Target 4 lies in the Rear Right-upper corner of the trainer box, near the central trunk
5	Target 5 lies in the Front Right-bottom corner of the trainer box
7	Target 7 lies in the Front Left-bottom corner of the trainer box
9	Target 9 lies in the Front Left-upper corner of the trainer box, near the central trunk

On finding the target, participants were asked to manipulate the endoscope to view the target number in an upright orientation on the TV screen, in order to test their understanding of endoscope navigation, as shown in Figure 3.17. This was intended to rotate the base orientation of endoscope to align with the axes of the target, resulting in a change of directions.

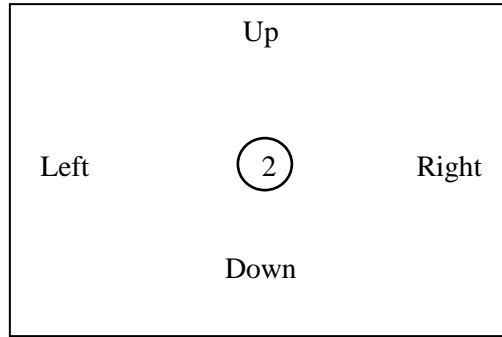


**Figure 3.17** Target number visible on TV monitor and directions with respect to TV monitor

After aligning and holding the endoscope steady for 5 seconds, participants were given the instructions shown in Table 3.5 in a random order, one at a time: these are commonly used instructions in the actual OR.

**Table 3.5** Set of instructions given to participants for performing endoscope movements in testing phase

<b>Instruction</b>	<b>Description of instruction and visual effect on TV monitor</b>
<b>Show Down</b>	Move the endoscope tip such that the target number moved upwards on the TV screen, thus showing the area of the trainer box lying “Down” of the target cylinder
<b>Show Left</b>	Move the endoscope tip such that the target number moved rightwards on the TV screen, thus showing the area of the trainer box lying “Left” of the target cylinder
<b>Show Right</b>	Move the endoscope tip such that the target number moved leftwards on the TV screen, thus showing the area of the trainer box lying “Right” of the target cylinder
<b>Show Up</b>	Move the endoscope tip such that the target number moved downwards on the TV screen, thus showing the area of the trainer box lying “Up” of the target cylinder
<b>Move In</b>	Move the endoscope tip towards the target number while keeping it in focus on the TV screen, thus “moving In” closer to the target cylinder
<b>Move Out</b>	Move the endoscope tip away from the target number while keeping it in focus on the TV screen, thus “moves Out” from the target cylinder

All instructions were with respect to the upright target number visible on the TV screen, and participants had to move the endoscope tip as per the instruction. These six instructions were arranged in random order for each of the targets for each participant. Instructions with movements in opposite directions, such as “Right-Left”, “Up-Down” and “In-Out” never followed one another. Participants were instructed to continue moving in the direction they decided and not to change it even if they realized they had started moving in the wrong direction. On reaching their extreme position of movement, they were told to hold the endoscope steady for 5 seconds, following which, they returned back to the target. In case they rotated the endoscope while coming back, they were given time to realign and view the target number in its upright orientation before the next instruction. The next instruction for that particular target followed after the endoscope was held steady for 5 seconds. This process was repeated for all other targets once all six instructions for the first target were completed. Thus, for all the seven targets present, each participant performed a total of 42 movements. Instructions and target numbers were counterbalanced across participants to reduce the influence of order of instructions and order of target numbers on the results obtained (Coolican, 2010).

#### **3.1.3.4.3.2 Duration of the testing phase**

Participants were given a set of instructions described later regarding performance. On an average, a maximum of 35 minutes were needed to complete the testing phase.

#### **3.1.3.4.4 Data collection and analysis**

Movement data collected during the training and testing phases was used for further analysis to identify performance variations across participants, groups and trials. The TMM position sensor was sampled at 20 Hz, while the Data Acquisition Board #0, which received the button clicks to mark the start and stop of trials, was sampled at 100 Hz. Data collected was

aligned to the Data Acquisition Board #0, thereby spreading the data received from the position sensor, at 20 frames per second, to 100 frames per second. Linear interpolation was used to obtain the data for 4 frames between the 2 consecutive data frames obtained from the position sensor.

#### 3.1.3.4.4.1 Training phase data analysis

Analysis of data collected during the training phase included calculating the average number of task trees required to achieve proficiency, the average training time, the average number of targets found per tree and the root mean square error of 3D mental map of each task tree attempted on paper for all groups.

##### 3.1.3.4.4.1.1 Root mean squared error of 3D mental map on paper

Paper plot given to participants to draw the 3D mental map is shown in Figure 3.18.

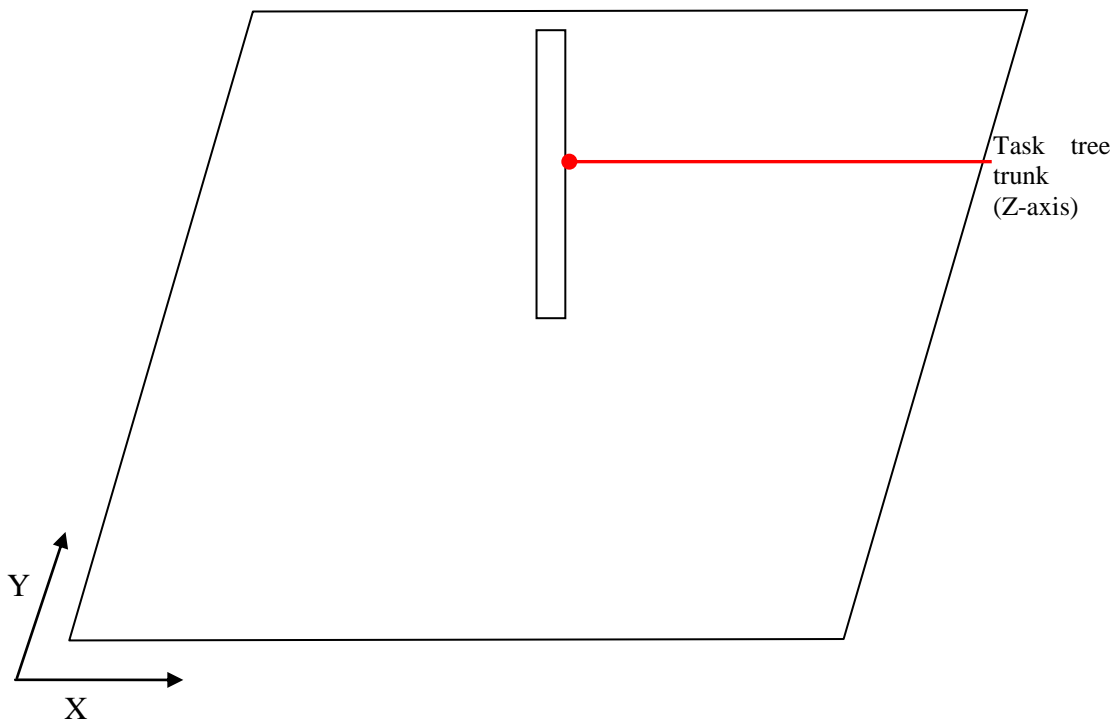


**Figure 3.18** Paper plot given to participants to draw 3D mental map

Dimensions of the trainer box and paper plot are summarized in Table 3.6.

**Table 3.6** Dimensions of the trainer box and paper plot

Axes	Box dimension (cms)	Paper dimension (cms)	Unit Ratio
<b>X</b>	45.5	10.3	4.42
<b>Y</b>	38.7	8.8	4.40
<b>Z</b>	15	3.9	3.85

Actual XYZ coordinates of all targets were obtained using the “Test sensors” option from the TMM. Lines parallel to both X and Y axes were drawn from endpoints of the targets marked on paper plot. As the mental map on paper was 2D, the only way to estimate error in Z coordinate was to calculate the distance of the branch containing the target from the base of the trunk shown in Figure 3.18. The error was calculated as the Root Mean Square (RMS) of differences between ( $X_{actual}$ ,  $Y_{actual}$ ,  $Z_{actual}$ ) and ( $X_{marked}$ ,  $Y_{marked}$ ,  $Z_{marked}$ ) as per the equation given below –

$$Error = \sqrt{((X_{actual} - X_{marked})^2 + (Y_{actual} - Y_{marked})^2 + (Z_{actual} - Z_{marked})^2)}$$

**Equation 3.1** Root Mean Square error for the targets marked on paper plots

#### 3.1.3.4.4.2 Testing phase data analysis

Data collected during the testing phase included the real-time XYZ coordinates of all four landmarks. For the testing phase, only the four direction instructions, “Show Down”, “Show Left”, “Show Right” and “Show Up” were used for analysis, as these required the endoscope to be moved in a way surgeons typically ask the camera assistant to move an endoscope in an actual OR environment (Korndorffer et al., 2005; Groeger et al., 2008; Schuller et al., 2008). The other two instructions, “Move In and Move Out” required moving endoscope along –Z axis of trainer box while keeping target number in focus (Korndorffer et al., 2005; Groeger et al., 2008). Hence, they would not serve as indicators of understanding of directions and were not considered for

analysis. Velocity, error in the movements for the four instructions for different time points, and the time taken by participants to decide the direction of movement for the above mentioned instructions for all groups were calculated and analyzed. Analysis was hence done for a total of 28 instructions, four instructions for each of the seven targets present on the testing task tree.

#### 3.1.3.4.4.2.1 Collection of reference data for the testing tree

To determine the correct direction of movement (i.e., the reference data), first, the target face location and orientation, and three random points were selected on the rim of every target and digitized using the TMM. From this data, the center for each target was calculated mathematically. Depending on the orientation of the target number within the target cylinder, four diametrically opposite points were marked at right angles to each other. These four points marked the Down, Left, Right and Up directions for that particular target, as shown in Figure 3.19.

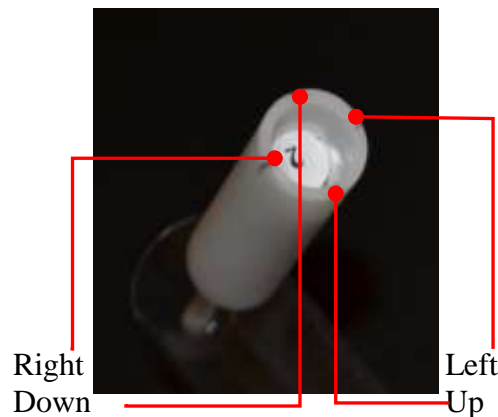


**Figure 3.19** Points marked as Down, Left, Right and Up for target 2

The XYZ coordinates of each of those four points were obtained using the “Test Sensors” option of the TMM. The origin of the coordinate system of the trainer box was then shifted to the center of each target by subtracting the XYZ coordinates of the target center from the corresponding XYZ coordinates of the Down, Left, Right and Up points of that target. The Cartesian vectors obtained above were then converted to spherical coordinates to obtain the

angles of the Down, Left, Right and Up points with respect to the center of each target. These angles were taken as reference angles for the correct direction of movement and a unit vector was obtained in all four directions.

**3.1.3.4.4.2 Collection and analysis of the accuracy of the movement data for all targets of the testing tree**

Movement for all instructions including stable periods was collected using the TMM with the data aligned to Data Acquisition Board #0 (i.e., the trigger time points). Individual stable periods and movements were marked using the trigger connected to the TMM and were assigned a unique three-digit code, with the first digit corresponding to the target number, the second digit corresponding to the instruction number, and the third digit corresponding to the stable and movement periods. Assignment of "Instruction number" to each of the six instructions is shown in Table 3.7, while assignment of unique codes to different time slots is shown in Table 3.8.

**Table 3.7** Assignment of the "Instruction number" to all instructions for target 2

<b>Target Number</b>	<b>Instruction</b>	<b>Instruction number</b>	<b>First two digits of unique three-digit code</b>
<b>2</b>	Down	1	21
	In	2	22
	Left	3	23
	Out	4	24
	Right	5	25
	Up	6	26

**Table 3.8** Assignment of the unique three-digit code to different time slots for target 2 for "Down" instruction

<b>Target Number</b>	<b>Instruction</b>	<b>Unique three-digit time slot code</b>
<b>2</b>	Hold stable	211
	Show Down	212
	Hold stable (at end of movement)	213
	Come back to target	214
	Align if necessary	216
	Hold stable (at target after realignment)	215



For all calculations and analysis, the XYZ coordinates of only landmark #0 were used as it corresponded to center of the endoscope lens, which did not change even on rotation of the endoscope. After the assignment of the unique-three digit codes to all time slots, the velocity was calculated for all time slots using a 5-point central difference formula as used by the TMM (to calculate velocity data) for all instructions. The velocity data was then filtered using a 5<sup>th</sup> order low-pass Butterworth filter with a 10 Hz cutoff frequency.

To analyze the accuracy of movements for instructions given in testing phase, the planes of the target and the endoscope needed to be matched. Plane of each target cylinder mouth and the orientation of the target number inside that cylinder differed with the trainer box coordinate system. Conventionally, “Up” direction on a 2D plot corresponds to +Y axis or the 12 o’clock position, while “Right” corresponds to +X axis or the 3 o’clock position. To maintain this uniformity of directions across targets in spite of their orientation with respect to the trainer box for the instructions given for movement, the trainer box coordinate system was transformed to the plane of each target cylinder at its center, using a rotation matrix. To obtain a rotation matrix in order to generate an orthonormal coordinate system at the target center, extremes of the new axes system need to be provided. Thus, rotation matrices were calculated for each target, by assigning “Right” and “Up” points of targets mentioned earlier as extremes of X-axis and Y-axis respectively.

The starting point of movement was considered to be the first time frame after the end of the trigger that was pressed for giving the instruction. Different time points such as the end point and 250 msec from the time of instruction given were considered for analysis of movement with respect to start point for that instruction. Average reaction time for humans is between 200-300 msec (<http://www.higher-faster-sports.com/reactiontime.html> retrieved February 06, 2012).

Hence, 250 msec after giving the instruction was taken as another time point in addition to the endpoint for analysis of performance for all participants.

The end point of movement was considered to be the last time frame before the start of the trigger which was pressed when the participant reached the extreme location of endoscope movement for that instruction. As participants were instructed to move only in the direction they started to move and not change it later, the endpoint of movement should be the best indicator of movement accuracy, and hence, their understanding of directions. The trigger or Data Acquisition Board #0 was sampled at a rate of 100 Hz, thereby providing 100 frames of position data per second.

The 25th frame of data after the last time frame of the trigger pressed for giving instruction corresponded to the 250 msec time point of analysis. Performing time-motion analysis helps in analyzing the effect of different training methods on camera navigation task performance (Geryane et al., 2004; den Boer et al., 1999). Time-motion analysis has shown that expert participants require less time, have lesser path length and more smoothness in their motion as compared to novice participants. Thus, time-motion analysis can be used to demarcate novice and expert participants (Stefanidis et al, 2009; Ritter et al., 2007).

The XYZ coordinates for these time points were obtained from the velocity plots and the rotation matrices calculated above were multiplied with them. Direction vectors for these XYZ coordinates were then calculated by subtracting the start point of endoscope. Cartesian vectors obtained above were then converted to spherical coordinates to obtain the angles of these time points for Down, Left, Right and Up points with respect to the start point of endoscope for the given target. These angles were taken as movement angles. The differences between the reference angle and movement angle for respective instructions were calculated to determine the

accuracy of movement. On the basis of pilot experiments conducted, a movement was considered to be accurate if the endpoint was within  $\pm 30^\circ$  of reference direction.

#### **3.1.3.4.4.2.3 Collection and analysis of the time taken to decide the direction of movement**

Motion data was collected for all 42 instructions for all participants. It was hypothesized that training with graphics could reduce the time for deciding the correct direction of movement for given instructions. If the participant moved the endoscope in the wrong direction, the primary objective of the task was not fulfilled. Hence, analyzing the time taken for deciding the direction of this movement, would not have contributed in determining the effectiveness of graphical training, in terms of time taken to decide the correct direction of movement. Thus, only the instructions whose endpoints were accurate were considered for calculating the time taken by participants to decide the direction of movement.

To calculate the time taken, the start point of endoscope and each point of movement were multiplied by the rotation matrix obtained before for that target. A unit vector was then obtained for the direction between the starting point and each point of movement of the endoscope. Radial differences between unit vectors of the reference for that command and movement directions indicated the error of the path taken by participant. The time point beyond which the radial difference between the two unit vectors was consistently less than  $30^\circ$  (or the distance between endpoints of both vectors was consistently less than 0.52 units) was considered to be the time taken by participants to decide the direction of the endoscope movement.

The physical movement of the endoscope tip in the trainer box, the radial difference between the reference and each movement vector, the distance between end points of both those vectors and the direction of physical movement along with movement after being multiplied by rotation matrix were generated for all participants for all instructions for all targets as shown in

Figure 3.20. A green circle marked the start point of the endoscope, while a red circle marked the end point of movement. A black star marked in both “Error plots” showed the time point at which participant had decided the direction in which he wanted to move the endoscope. The X-axis shown in both “Error plots” represented the TMM trigger frame number and hence, a value of 135 corresponds to 1.35 seconds for participant’s data shown in Figure 3.20.

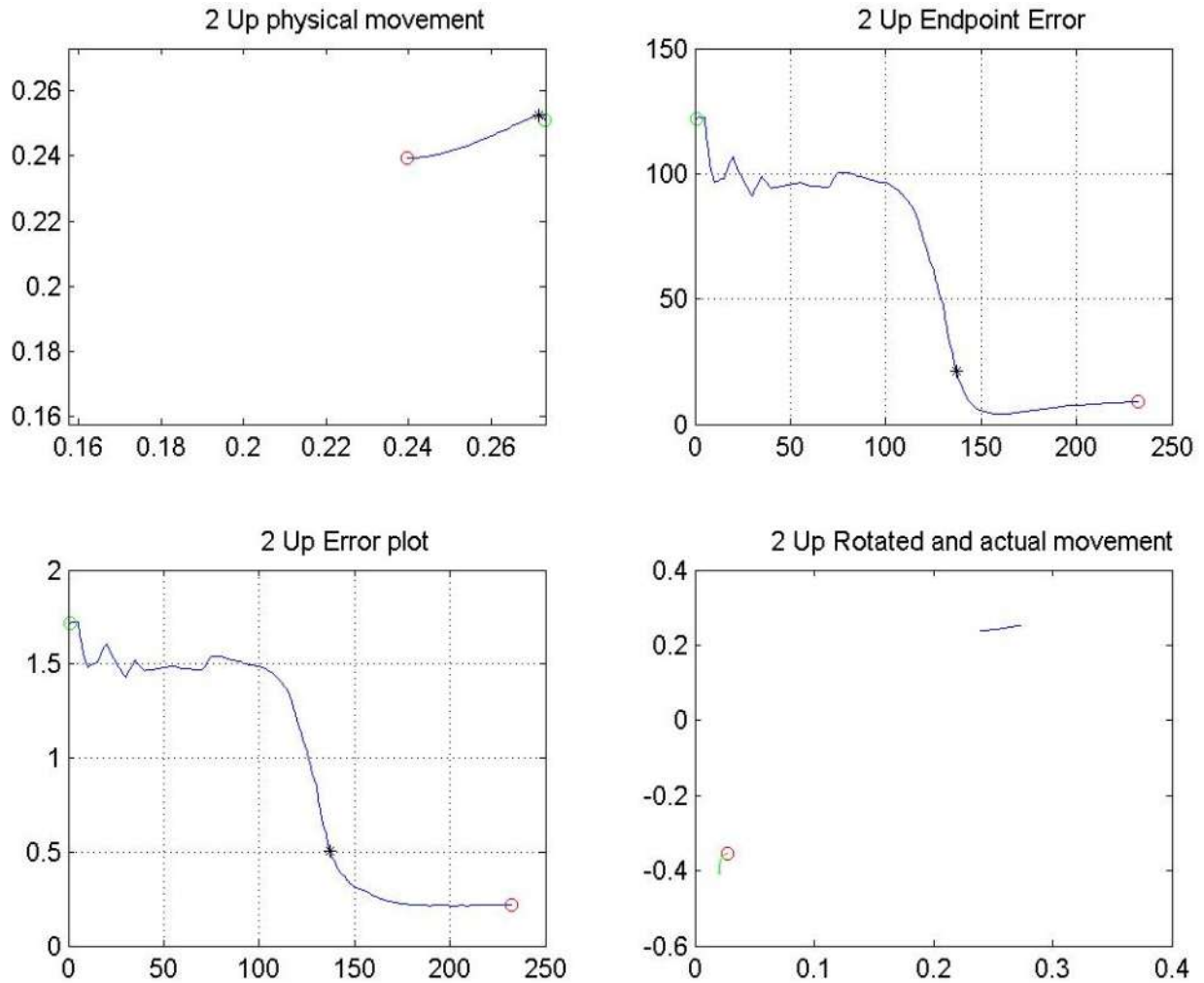


**Figure 3.20** Plots for the "Up" instruction for target 2 in testing tree

### 3.1.4 Statistical Analysis

Data obtained for the various training and testing phase parameters was not normally-distributed. Hence, non-parametric statistical methods such as Kruskal-Wallis one-way analysis

of variance and Mann-Whitney tests were used to determine the effectiveness of training methods, as they are robust when data is not normally-distributed data and can account for unequal group sizes too (Lowry, 2000).

For all variables, a Kruskal-Wallis one-way analysis of variance (ANOVA) was performed to compare the performance of all groups. Then, Mann-Whitney U-tests were performed to compare the groups pairwise. The performance variables were compared with a significance level of  $\alpha = 0.05$ , corresponding to 95% confidence. To avoid the occurrence of spurious positives due to multiple comparisons, a Bonferroni correction was applied (Jones et al., 2008) for performance variables of both the training and testing phases. The Bonferroni correction was calculated using Equation 3.2 as shown below -

$$p_{\text{new}} = 1 - (1 - \alpha)^{\frac{1}{m}}$$

**Equation 3.2** Bonferroni correction formula for  $m$  number of dependent or independent comparisons being performed

For the training phase, there were six comparisons amongst the four groups, and hence, the number of tests ( $m$ ) was taken as 6. After the Bonferroni adjustment, the overall significance level  $\alpha$  dropped to 0.008. Thus, if the p-value was less than 0.008 (signifying 99.2% confidence), the null hypothesis could be rejected, implying there was a difference in performance of participants which was dependent on their training method.

In the testing phase, the variable of number of instructions in the accurate direction had six comparisons for two time points, while the variable of time taken for deciding the direction of movement had only six comparisons amongst the four groups. Hence, the number of tests ( $m$ ) for number of instructions in accurate direction and time taken to decide the direction of movement were taken as 12 and 6 respectively. After the Bonferroni adjustment, the overall

significance level  $\alpha$  dropped to 0.004 for the number of instructions in the accurate direction, and to 0.008 for the time taken to decide the direction of movement.

Thus, if the p-value was less than 0.004 (signifying 99.6% confidence), the null hypothesis could be rejected, implying there was a difference in performance of participants in terms of moving the endoscope in accurate direction, which was dependent on their training method. Similarly, if the p-value was less than 0.008 (signifying 99.2% confidence), the null hypothesis could be rejected, implying there was a difference in the time participants took to decide the direction of movement of endoscope.

### **3.2 Proximity Sensing**

Projection of 3D surgical field on a 2D monitor results in lack of binocular disparity, leading to loss of depth perception. This leads to collisions, which can result in complications in a surgical scenario. Hence, providing proximity of the object directly in front of the endoscope to the participant is necessary. Proximity sensor works typically on generation of an electromagnetic field or transmission of an electromagnetic beam (typically infrared), and looks for changes in the field or awaits the return of the beam. Depending on the intensity of the change in field or the strength of the reflected beam, the distance is calculated based on time or other factors.

Color, surface properties such as texture and material of construction, shape and temperature (to a certain extent) of the object do not affect the results of a proximity sensor detecting change in electromagnetic field. But, they do affect the sensors which work with the detection of the reflected light. As a photoelectric sensor emitting and receiving an infrared beam was selected for detecting proximity for this trainer box setup, it was necessary to take these factors into consideration for calculating distance of objects from the tip of the endoscope. A

white colored object reflects most of the incident light falling on it, while a black object absorbs most of the incident light, reflecting less light. Various shades of grey reflect light depending on their white-black composition. Thus, lighter the grey, the reflectance pattern would be closer to that of white, and darker grey would be closer to that of black.

The trainer box setup consisted mainly of three objects, the white target cylinders and the base of the task tree, the transparent hollow tubes or the branches, and the dark grey central trunk. Since the branches were transparent, reflection of light would be minimal, and hence, they were painted with white spray paint. As these objects had different colors, the strength of the reflected IR beam would differ for the same proximity of the endoscope tip with them. Hence, in order to identify the color of the object being sensed, the real-time video from the camera was used.

### **3.2.1 Materials**

The different sensors considered were -

#### **3.2.1.1 Sharp IR sensor**

The Sharp GP2Y0A02YK0F IR sensor was considered for use as a proximity sensor. The sensor houses an IR transmitter and position-sensitive detector (PSD) pair. It uses a triangulation method to calculate distance (Günther et al., 2009), resulting in consistent and reliable readings, which are insensitive to both temperature variations and object's reflectivity. The analog output voltage of the sensor depended on the distance of object, thus functioning as a proximity sensor. The supply voltage for this sensor was 4.5 - 5.5V, while the distance measuring range was between 200 - 1500 mm. This detection range was much higher than desired in the trainer box setup. Furthermore, the size of this sensor was too large, making it difficult to be mounted on an endoscope tip. Even if placed on an endoscope tip, the size would make maneuvering of

endoscope tip difficult as it would collide with other objects in the trainer box, thereby increasing the number of collisions. Due to the range and mechanical limitations, this sensor was not used in this study.

### **3.2.1.2 HSDL 9100**

The Avago Technologies HSDL-9100 surface-mount proximity sensor was then considered for both proving the concept and sensing proximity of objects within the trainer box in this study. This sensor is a retroreflective infrared sensor, whose peak wavelength is 940 nm and a forward voltage of 1.5V. Some of the prominent features of this sensor are as follows –

1. It is an analog-output reflective sensor, housing both a high efficiency IR emitter and a photodiode in a small SMD package,
2. The presence of a metal-shield for excellent optical isolation, resulting in low optical cross-talk.

This sensor was also low-cost and could detect objects from 0-60 mm. The sensor's output voltage is dependent on the amount of IR light reflected back by the object in front of sensor. This reflected light is indirectly proportional to the distance of the object, signifying that the amount of IR light reflected back to the sensor detector would increase if the distance decreases, and vice versa. The amount of light reflected back depended also on the color of object. For example, a white object would reflect most of the incident light, while black would absorb most of the light, thereby reflecting a lesser amount of IR light. Furthermore, being a surface-mount device, it was small in size, and could be mounted on front face of endoscope camera tip. Hence, HSDL-9100 was selected to be used for proximity sensing in this study.



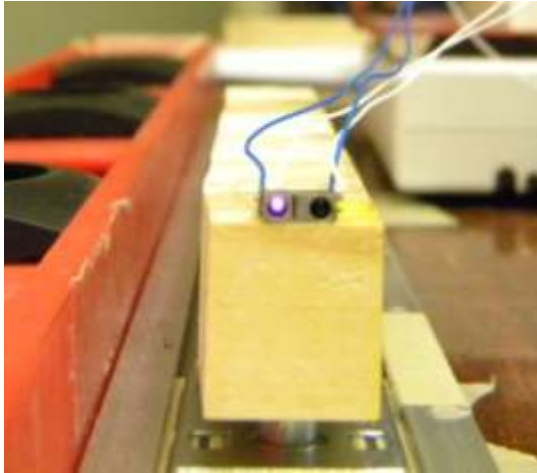
## **3.2.2 Methods**

### **3.2.2.1 Proximity measurement for solid standard color sheets**

As mentioned before, output of HSDL 9100 was dependent on both color and distance of the object from the sensor. The property of color-dependent reflection of IR light was used to check the accuracy of the sensor in detecting distance for various standard solid colors.

The assembly used to measure distances for standard color cards consisted of a single HSDL 9100 sensor fixed horizontally atop a rectangular parallelepiped wooden block. The wooden block was attached to a slider mechanism for smooth and accurate analog movement of the assembly for various distances. An engineer's scale was attached vertically beside the slider to manually place the sensor assembly at fixed distances from the colored sheets as shown in Figure 3.21a. X-Rite ColorChecker® Color Rendition Chart containing different solid colors was clamped vertically in front of the sensor assembly. A forward voltage of 3V was applied and a current of 100 mA was passed through the sensor. Output voltage of sensor was obtained across a 100 k $\Omega$  load resistor. This voltage was recorded using the NI USB-6211 (16 single-ended (or 8 differential) analog inputs (16-bit resolution, 250 kS/s sampling rate) DAQ card.

After a color from the Color Rendition Chart was placed in front of the sensor as shown in Figure 3.21b, the sensor was placed at a distance of 1 mm. Output voltage was recorded as an average of 25 values obtained. Output voltages were recorded till a distance of 60 mm, with 1 mm interval from 0-6 mm, and 2 mm intervals from 6-60 mm. The same process was repeated for six standard colors - White, Neutral 8.0, Neutral 6.5, Neutral 5.0, Neutral 3.5 and Black.



(a)



(b)

**Figure 3.21** (a) Sensor assembly with IR LED turned on; (b) Sensor placed in front of Neutral 3.5 color card

### 3.2.2.1.1 Divergence angle of the sensor

The datasheet provided by the manufacturer of HSDL 9100 does not state the divergence angle of the beam. The divergence angle was calculated using similar procedure as used by Castro (2008).

### 3.2.2.1.2 Proximity measurement for multiple solid standard color sheets

As mentioned before, the trainer box consisted of different colored objects which could be simultaneously sensed by the sensor. A color card with a left-right and right-left combination of the two colors, White and Black was constructed as shown in Figure 3.22.



**Figure 3.22** Left-right and right-left combination of White and Black color sheets

The same assembly discussed above was tested for random distances ranging between 0 - 60 mm for this combination.

### 3.2.2.2 Multiple sensor assembly

After testing single sensor, different combinations of multiple sensors were tested for six standard solid colors – White, Neutral 8.0, Neutral 6.5, Neutral 5.0, Neutral 3.5, Black and the combination color cards for distances 0 - 60 mm, with 1 mm interval from 0-6 mm, and 2 mm intervals from 6-60 mm as discussed below.

#### 3.2.2.2.1 Multiple emitters and single detector sensor assembly

A concept of uniform distribution of IR light around the detector was tested. For this, a HSDL-9100 sensor was placed in center of a larger concentric array of 36 high power IR LED emitters, each emitting IR of 940 nm wavelength, as shown in Figure 3.23a. The array required a power supply of 13.2V DC, and had a viewing angle of 50°. Only the detector in HSDL-9100 was enabled, while the circular LED array was used as the emitter.



(a)



(b)

**Figure 3.23** (a) Circular array of 940 nm IR LEDs; (b) Concentric array of IR LED emitter array with HSDL 9100 detector in center

Another set of experiment was conducted to measure proximity with concentrically reduced number of emitter LEDs as shown in Figure 3.23b. As this emitter array could not be placed on the endoscope, another assembly of four HSDL 9100 sensors was built in the shape of a '+' (plus) formation on a Lego block. Emitters of the four sensors were placed on the outside, while the detectors were placed on the inside, as shown in Figure 3.24a. The IR fields of the four sensors are shown in Figure 3.24b.

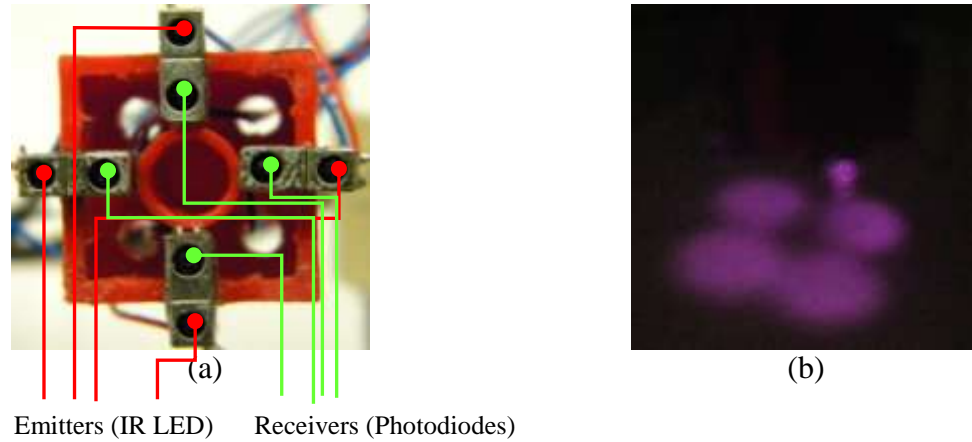


**Figure 3.24** (a) HSDL 9100 assembly on a Lego square block for sensing proximity; (b) IR fields of all four proximity sensors

A similar assembly using the circuit diagram shown in Figure 3.26 was then built and mounted on endoscope tip for measuring proximity of objects present within the trainer box, as shown in Figure 3.25. As shown in the circuit diagram, 100 mA current was passed through each HSDL-9100 sensor. Each IR LED was forward biased, while the photodetectors were reverse-biased. The output voltage across the load resistor  $R_L = 100 \text{ k}\Omega$  is proportional to the IR light reflected from an object in front of the sensor. This output voltage for each sensor was obtained using four differential analog input channels of a NI USB-6211 (16 single-ended (or 8 differential) analog inputs (16-bit resolution, 250 kS/s sampling rate)). They were then stored using a LabView program. An average of 25 output voltage values of each sensor for that distance was used as the final measurement, which was later converted to a logarithmic value.

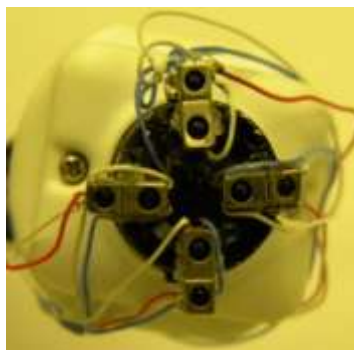


**Figure 3.25** Four HSDL 9100 sensor assembly placed on endoscope camera tip

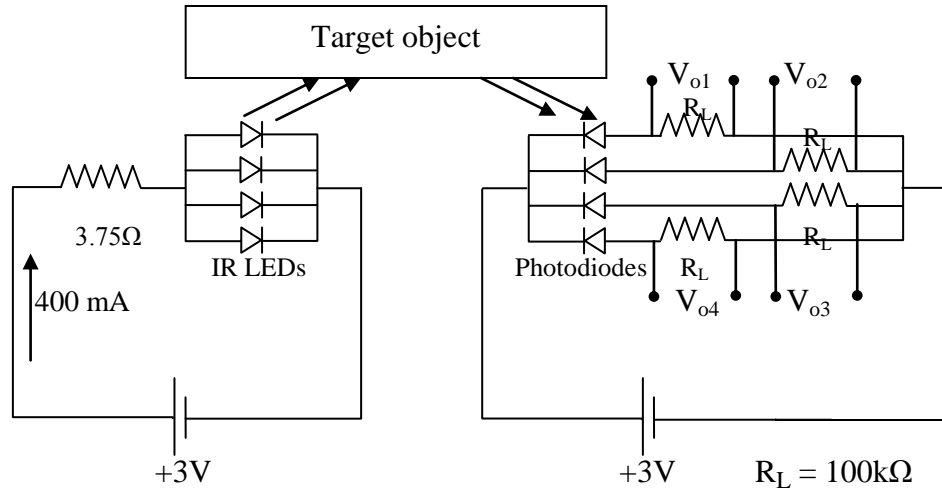


**Figure 3.26** Circuit diagram for the four sensor assembly

### 3.2.2.3 Camera chip of endoscope and White Balance (WB)

Proximity of object directly in front of endoscope was to be provided to the participant so as to avoid collisions. As objects of various materials and colors were present within the trainer box, it was essential to identify the color of the object which was directly in front of the endoscope. For this purpose, the video signal from the camera was used.

One potential problem was that the camera used, a fixed focus 3-Dmed SimScope with an OmniVision OV7949 camera chip had automatic white balancing (WB), which was difficult to override. White balancing is normally used to adjust the lighting in order to make white objects appear white in an image. However, this white balancing is not performed for the proximity sensors. Unfortunately, it would be necessary to redesign the camera board to manually turn the white balance off. Hence, to test the concept of proximity sensing, an alternative and a more advanced camera chip STC-N63 from SenTechAmerica was used.

### 3.2.2.4 SenTechAmerica STC-N63 camera chip

The STC-N63 is a high resolution 1/3" color CCD, NTSC board-based remote-head camera that offers 480 TV lines, and has a 10-bit DSP. This camera has Auto, Manual and Push-to-Set white balancing modes. The camera requires 12V DC power supply, while the output is a

standard 1Vp-p / 75Ω video signal that can be connected directly to a TV monitor. This output was connected to a video capture device, Diamond One Touch Video Capture VC500 to be sent to Matlab Image Acquisition Toolbox.

This camera operates in AWB mode by default. To manually set White Balance, the “WB-Lock” and “GND” pins of this camera need to be shorted together. A commonly available switch was used to short / open the connection between these two pins to achieve WB locking. By placing the X-Rite ColorChecker® White Balance card in front of this camera, white balance could be locked manually to achieve consistency of colors for objects seen by this camera.

The main components used for proximity sensing were as mentioned in Table 3.9.

**Table 3.9** Components used for providing proximity in the trainer box setup

<b>Component</b>	<b>Source</b>
<b>Proximity Sensor HSDL 9100 array</b>	Avago Technologies National Instruments Data Acquisition Card USB 6211
<b>Camera chip STC-N63</b>	Sensor Technologies America Inc. (SenTech America) Matlab Image Acquisition Toolbox version 3.0
<b>Simulated Endoscope</b>	3-DMEd SimScope™

### 3.2.3 Proximity calculation with unknown grayscale value

To determine the grayscale value to use to determine the proximity of an object, the image obtained from STC-N63 camera was used. The STC-N63 was connected via Diamond One Touch Video Capture VC500 device to the computer. The largest video format possible in Matlab Image Acquisition Toolbox used for the camera was UYVY\_720x576. By accessing settings of the video object in Matlab, the ‘ReturnedColorSpace’ was changed to RGB, and the Region of Interest (ROI) was fixed at 720x480, as that was the largest possible format available. White balance was locked 10 seconds after the White sheet was placed in front of the camera.

Images obtained from the camera were converted from RGB to grayscale using Matlab, for easy calculations of pixel averages.

For detecting the proximity of an object in front of the camera, it was necessary to confirm both the camera and the sensor assembly were looking at the same object. For this, the field-of-views of both the camera and sensor assembly were plotted. Since the sensor's output was available only between 0 – 60 mm from the object, it was necessary to determine the field-of-view (FOV) for the entire range of 60 mm at intervals of 10 mm. As the thickness of the sensors was 2.75 mm and they were mounted on front end of the camera. The camera was mounted at a distance of 63 mm from a white sheet of paper, and the FOV was marked by marking corner points of the video available on the TV monitor. Similarly, to determine the FOV of the sensor assembly, the standard color Black sheet was moved across on the white paper, 1 mm at a time, while observing a change in output readings of the sensors. As long as the black sheet was outside the FOV of sensors, the output corresponded to the white sheet. As soon as the black sheet entered the FOV, a change in voltage was observed. This position of the black sheet corresponded to an edge of the sensor FOV.

After marking all four edges of the sensor and camera FOVs for various distances, it was observed that the ratio of both the FOVs (width of FOV divided by height of FOV for both camera and sensors) was constant at 1:1.

$$C_W / C_H = S_W / S_H = 1.2 / 1.2 = 1:1$$

where  $C_W$  was the Camera FOV width,  $C_H$  was the Camera FOV height,  $S_W$  was the Sensor FOV width and  $S_H$  was the Sensor FOV height. The 1:1 ratio meant that the camera and sensor were both looking over almost the same area.

With the FOV ratio being constant for various distances, an average of grayscale values of all pixels of the image was calculated. A family of curves or database was already built for the six standard color cards present in the lab. To test and verify the sensing of proximity, standard colors Neutral 8.0 and Neutral 5.0 were selected as test sheets, while the other four colors, White, Neutral 6.5, Neutral 3.5 and Black were taken as reference database colors. Each test sheet was placed one at a time at a random distance between 0 – 60 mm from the sensors, and log values of voltages for all four sensors were obtained. Grayscale values were obtained from the image of the test colors (Neutral 8.0 and Neutral 5.0), and normalized with images of White (RGB [238, 238, 238]) and Black (RGB [5, 5, 5]) colors as the positive and negative extremes. The normalized value was used as the grayscale for which interpolated log values of voltages for all four sensors were calculated. 2D spline interpolation in Matlab (the ‘interp2’ function) was used with log values of voltages of all four sensors for all distances for the four color reference as the look up table. These log values obtained were searched for in the interpolated columns of log values for all four sensors, and the corresponding distances were recorded.

To verify the robustness of algorithm, different lighting conditions such as ambient and LED-lit environment within the trainer box were tested. The grayscale values obtained for each of the six colors were different as the camera white balance was locked in the LED lit-environment. A new database for all six colors was generated by placing them inside the trainer box, and this database was again used for testing the test color sheets, Neutral 8.0 and Neutral 5.0 in the same process described above. Creating the new database containing voltage values for all six colors was necessary because even though the sensor output signal would not be affected by the LED-lit environment, the grayscale calculated would be different due to higher



illumination present within the trainer box. Log values obtained for all six colors under LED lighting conditions were checked for repeatability and hysteresis.

### **3.2.4 Proximity calculation for an actual object placed within the trainer box with unknown grayscale value**

After having tested the robustness of both the sensor assembly and algorithm to calculate proximity of standard color sheets, objects actually present within the trainer box were used for testing. These objects included the white base of the task trees, the task tree trunk, branches and the white-colored target cylinders. Branches used in the training trees were transparent, and would have not have reflected IR light back to the sensors, thus affecting the output of the sensors. To counter this problem, all the branches in the training trees were painted with white spray paint.

A task tree was placed in the trainer box LED-lit environment, with the sensor assembly placed perpendicular at a random distance between 0 – 60 mm from it. The WB locked image was taken from the camera (STC-N63). The same process of converting the image to grayscale, normalizing the grayscale value obtained, and then obtaining interpolation values of voltages was repeated. The corresponding distances for a white target cylinder and a central gray trunk were checked for accuracy; however, the results were significantly different.

To rectify this error, two solutions were implemented. One solution was to avoid shadows in the visual field due to overhead lighting conditions of the trainer box, as all LED strips were placed on the inner side of the upper edges. The hypothesis was that the presence of shadows in the image was altering the overall grayscale value, thus leading to a different set of interpolated voltage values. To avoid shadows, different lighting conditions such as vertical

lighting from the corners of the trainer box and lighting of the trainer box from the bottom were tested. However, these did not improve the accuracy of proximity sensing.

The other solution was to apply a restricting ring that shall in a way collimate the IR light received back from the object. The initial idea was to place a collimator encompassing the detectors forming the inner circle of the sensor assembly. However, this placement would have restricted the incident IR light to go straight, and not illuminate the area in front of the camera. Therefore, a restricting ring, enclosing both the emitters and detectors was placed on the endoscope tip. Three different rings of widths 4 mm, 5 mm and 6 mm (or 1 mm, 2 mm and 3 mm ahead of the sensor's front surface, as the sensor was 2.75 mm in width) were tested in front of the assembly. The reason for selecting these small sizes for the restriction ring was to maintain the easy maneuverability of the endoscope. If the restriction ring would have been longer, it would have resulted in more collisions, and would have restricted the endoscope tip going too close to a target. The restricted ring assembly was placed as shown in Figure 3.27 (a) and (b), while (c) shows all three restricting rings.

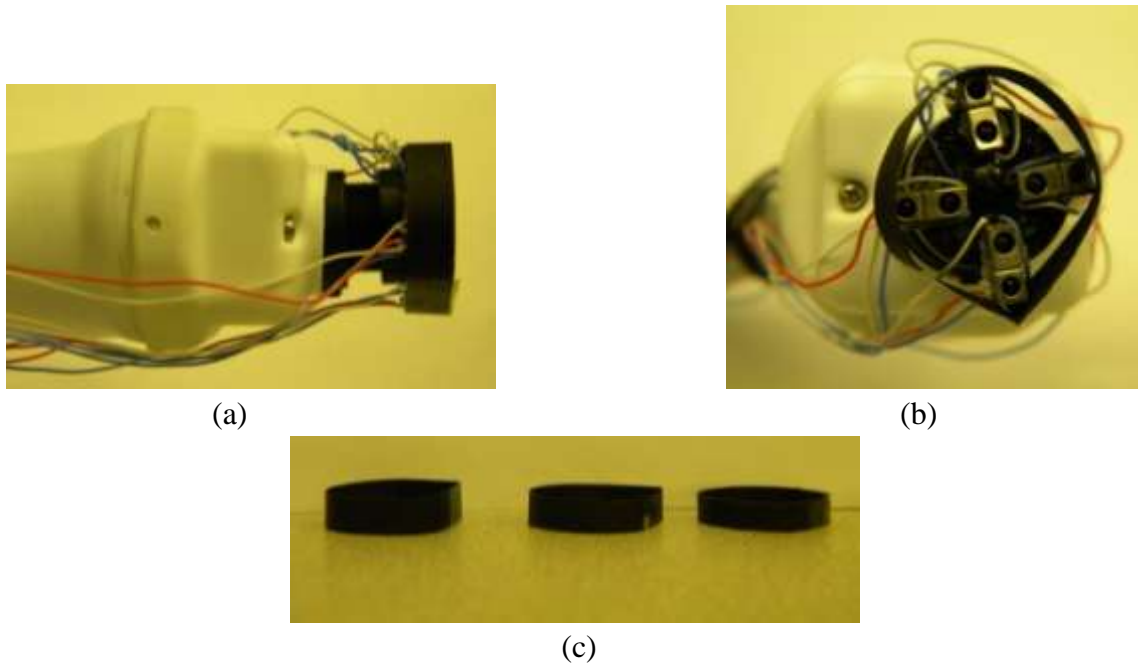


**Figure 3.27** (a) Side view of the restricting ring placed over sensor assembly attached on the endoscope tip; (b) Restricting ring from front; (c) All the three restricting rings (widths 4 mm, 5 mm and 6 mm)

To avoid the restricting ring having an undue influence on the output voltages, a black colored ring was chosen instead of white. The presence of a white ring close to the sensor would have unnecessarily increased the output voltage as compared to a black one. Voltage values were measured without placing any object in front of the sensor assembly attached with the restricting ring. Logarithmic values of these voltages were then subtracted from all log values obtained for various distances for all six standard colors. A new database for all six calibration colors was thus generated with each of the three restricting rings, and the same testing method was repeated for the actual task tree placed in the LED-lit trainer box space. 4 mm and 5 mm restricting rings did not make significant change in output voltage when compared with the ones without the restricting ring. These rings failed to provide any collimation of the reflected IR light and hence, only 6 mm restricting ring was used for further testing.

## CHAPTER 4 RESULTS

### 4.1 Camera navigation using graphics

#### 4.1.1 Participant characteristics

Participant characteristics for the 36 participants are summarized in Table 4.1. The sample had dissimilar numbers of 22 males (61.11%) and 14 females (38.89%), participants were primarily right handed (94.44%) and none of them had any previous endoscopy experience.

**Table 4.1** Participant characteristics

<b>Participant Characteristics</b>		<b>Count</b>	<b>Percent</b>
<b>Sex</b>	Male	22	61.11
	Female	14	38.89
<b>Dominant Hand</b>	Right	34	94.44
	Left	02	5.56
<b>Endoscopy Experience</b>	Yes	00	0.00
	No	36	100.00

#### 4.1.2 Training characteristics

##### 4.1.2.1 Average number of training task trees and average training time needed to achieve proficiency

The average number of task trees required to achieve proficiency by all groups during training phase are shown in Table 4.2 and graphically represented in Figure 4.1.

**Table 4.2** Average number of training task trees needed to achieve proficiency

<b>Groups</b>	<b>Average number of training task trees needed to achieve proficiency</b>	
	Mean	SD
<b>NG</b>	4.33	1.66
<b>Line</b>	2.44	1.33
<b>Shading</b>	2.44	0.88
<b>(L + S)</b>	2.22	0.44

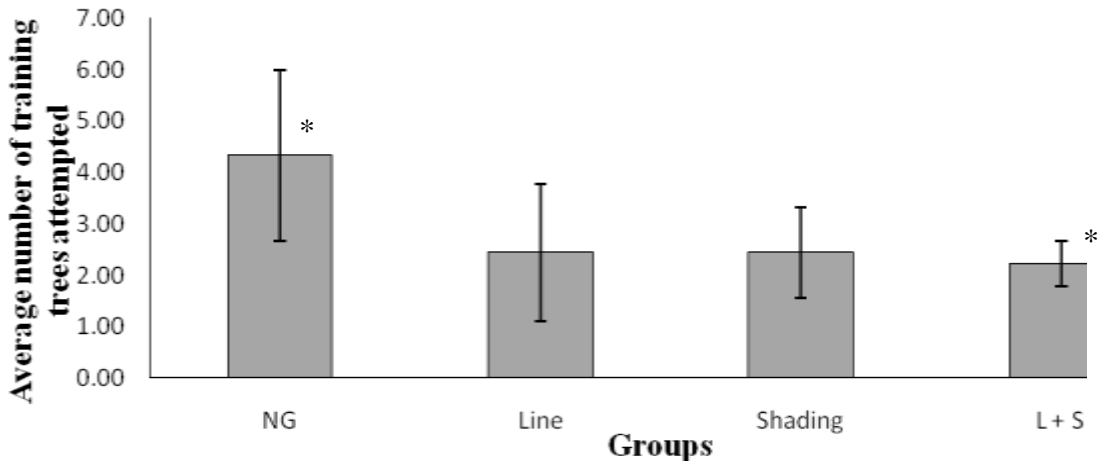


**Figure 4.1** Average number of training task trees attempted for all groups

\* Significant difference for NG vs. (L + S) at  $p < 0.008$

A statistically significant ( $p \leq 0.008$ ) difference was observed in the average number of training trees attempted by NG as compared to (L + S) ( $p = 0.008$ ), but not when compared to both Line as well as Shading ( $p > 0.008$ ). Similarly, there was no statistically significant difference between the average number of training task trees attempted by the Line, Shading and (L + S) groups ( $p > 0.008$ ).

Similarly, the average training time taken by all groups during training phase are shown in Table 4.3 and graphically represented in Figure 4.2.

**Table 4.3** Average training time

Groups	Average training time (minutes)	
	Mean	SD
NG	97.30	35.67
Line	48.28	39.11
Shading	50.31	22.47
(L + S)	40.41	17.63

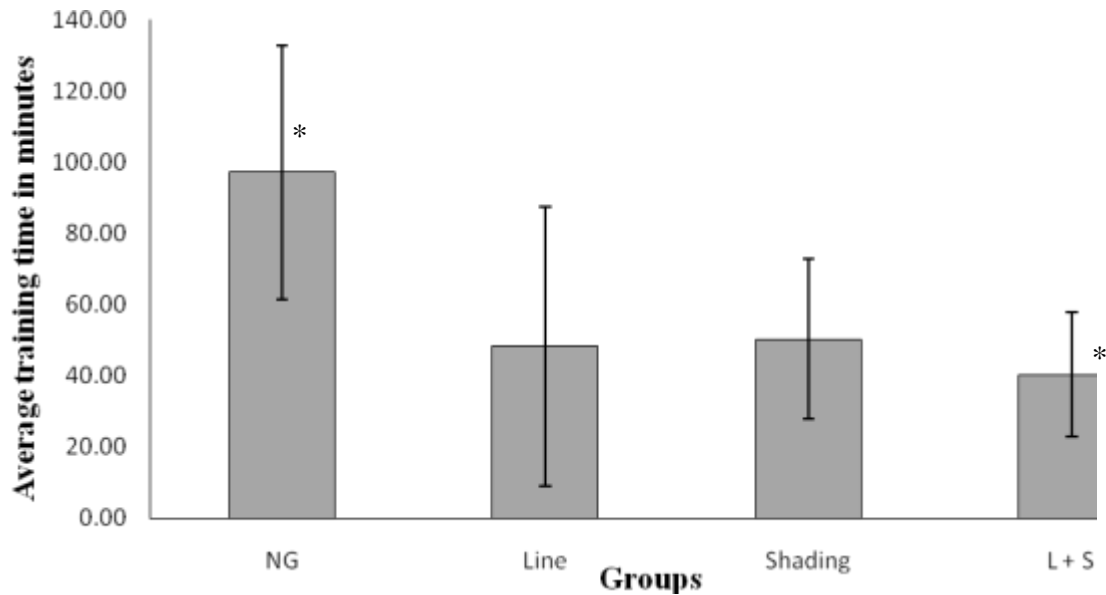


**Figure 4.2** Average training time for all groups  
 \* Significant difference for NG vs. (L + S) at  $p < 0.008$

Thus, the average time per training phase tree for NG group was  $22.62 \pm 2.22$  minutes, while participants of Line, Shading and (L + S) groups took an average of  $18.60 \pm 5.27$ ,  $20.31 \pm 3.12$  and  $17.74 \pm 5.37$  minutes per training phase tree respectively.

A statistically significant ( $p < 0.008$ ) difference was observed in the average training time for NG as compared to the (L + S), but not when compared to both Line as well as Shading ( $p > 0.008$ ). Similarly, there was no statistically significant difference between the average training times of the Line, Shading and (L + S) groups ( $p > 0.008$ ).

#### 4.1.2.2 Average number of targets found per tree during the training phase

The average number of targets found per tree during the training phase by all groups are shown in Table 4.4 and graphically represented in Figure 4.3.

**Table 4.4** Average number of targets found per tree in training task trees attempted

Groups	Average number of targets found per tree during training phase	
	Mean	SD
NG	5.96	1.26
Line	7.44	1.16
Shading	7.39	0.86
(L + S)	7.72	0.47

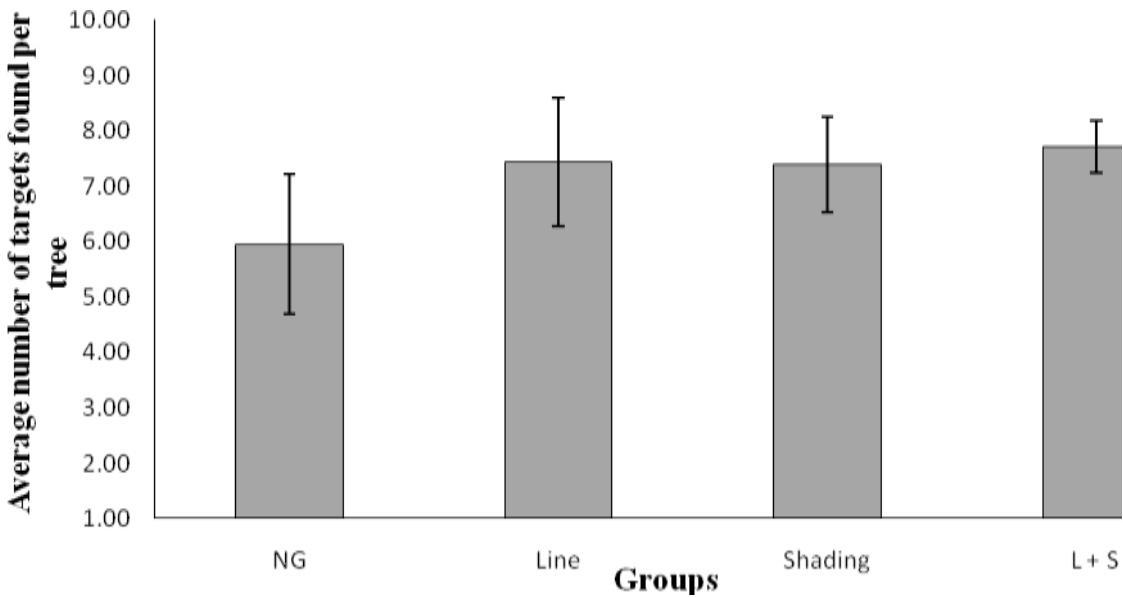


**Figure 4.3** Average number of targets found per tree during training phase for all groups

No statistically significant difference was observed in the average number of targets found per tree for the NG group as compared to the other three groups ( $p > 0.008$ ). Similarly, there was no statistically significant difference between the average number of targets found per tree attempted by the Line, Shading and (L + S) groups ( $p > 0.008$ ).

#### **4.1.2.3 RMS error of the mental map of targets found on paper during the training phase**

The average RMS error of the mental map of targets found on paper during the training phase for all groups were are shown in Table 4.5 and graphically represented in Figure 4.4.

**Table 4.5** Error of mental map of targets found on paper during the training phase

Groups	Average RMS error for mental map of targets found on paper during the training phase (cms)	
	Mean	SD
NG	14.47	5.45
Line	8.76	1.59
Shading	9.36	1.11
(L + S)	8.69	1.36

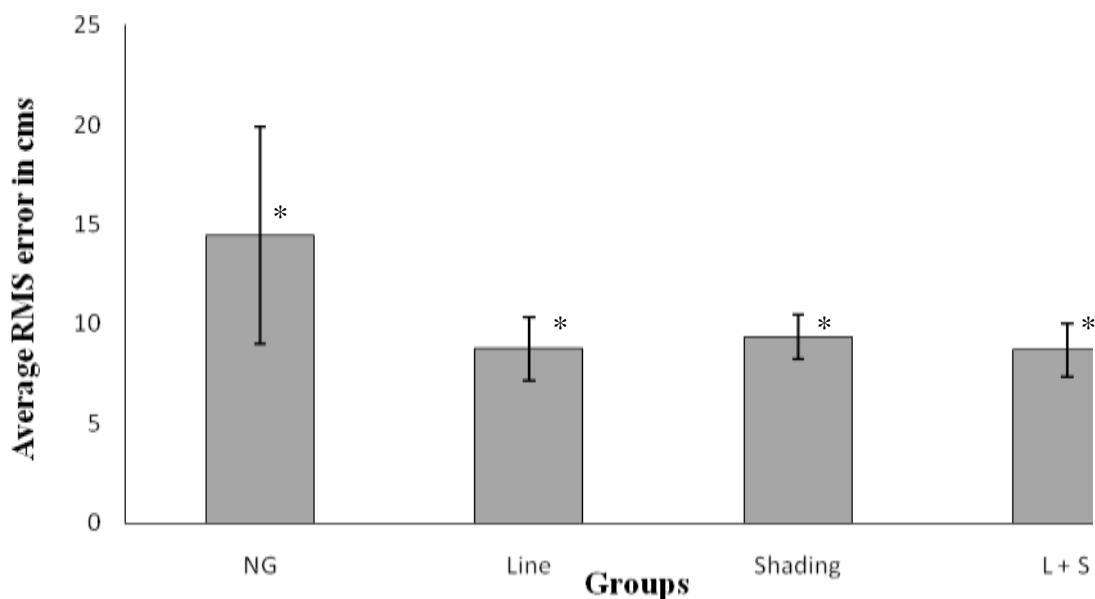


**Figure 4.4** Average RMS error for mental map of targets found on paper during training phase for all groups

\* Significant difference for NG vs. Line, Shading and (L + S) groups at  $p < 0.008$

A statistically significant ( $p < 0.008$ ) difference was observed in the average error for the NG as compared to all the three groups. However, there was no statistically significant difference between the average RMS error for mental map of targets found on paper during the training phase of the Line, Shading and (L + S) groups ( $p > 0.008$ ).



### 4.1.3 Testing characteristics

#### 4.1.3.1 Average number of instructions with the endpoint within 0° - 30° error margin

The average number of instructions with the endpoint within a 0° - 30° error margin out of 28 instructions during the testing phase for all four groups are shown in Table 4.6. Figure 4.5 graphically represents the percentage of instructions with the endpoint within a 0° - 30° error margin for all the four groups.

**Table 4.6** Average number of instructions with endpoint within a 0° - 30° error margin

Groups	Average number of instructions with the endpoint within a 0°-30° error margin		Percentage of instructions with endpoint within a 0°-30° error margin	
	Mean	SD	Mean	SD
NG	5.78	1.09	20.63	3.90
Line	21.11	4.68	75.40	16.70
Shading	21.22	3.67	75.79	17.59
(L + S)	22.33	4.92	79.76	17.59

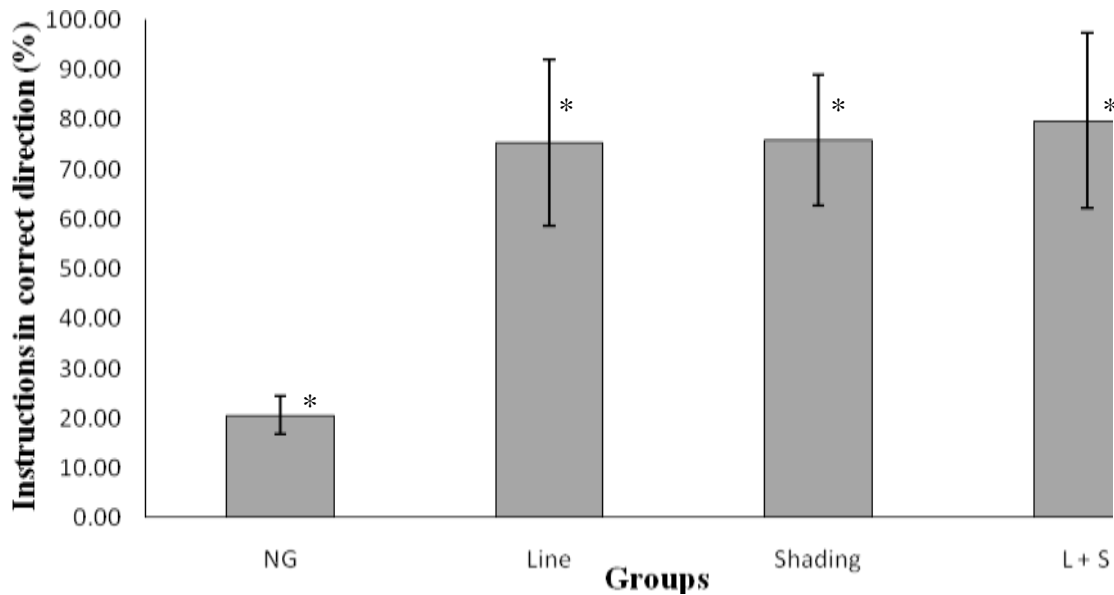


**Figure 4.5** Instructions with endpoint within a 0°-30° error margin for all groups (Percentage)

\* Significant difference for NG vs. Line, Shading and (L + S) groups at  $p < 0.004$

A statistically significant ( $p < 0.004$ ) difference was observed in the number of instructions for the NG as compared to all three graphic groups. However, there was no statistically significant difference between the number of instructions for the Line, Shading and (L + S) groups ( $p > 0.004$ ).

**4.1.3.2 Average number of instructions within a 0° - 30° error margin, 250 msec after giving the instruction**

The average number of instructions with the XYZ location of landmark #0, 250 msec after giving instruction within a 0° - 30° error margin with respect to the starting point out of 28 instructions during the testing phase for all four groups are shown in Table 4.7 and graphically represented in Figure 4.6.

**Table 4.7** Average number of instructions within a 0° - 30° error margin, 250 msec after giving the instruction

Groups	Average number of instructions within a 0° - 30° error margin, 250 msec after giving the instruction	
	Mean	SD
NG	4.11	1.62
Line	4.11	1.45
Shading	5.56	1.74
(L + S)	5.22	1.56

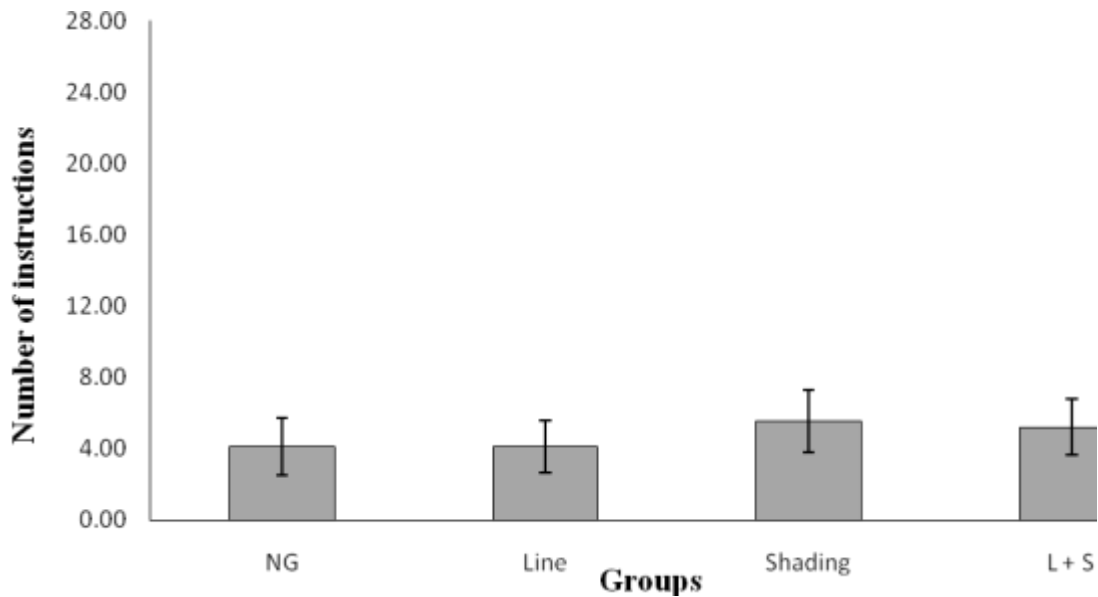


**Figure 4.6** Average number of instructions within 0-30 deg error margin 250 msec after giving instructions for all groups

No statistically significant difference was observed in the number of instructions for the NG as compared to all three graphic groups ( $p > 0.004$ ). Similarly, there was no statistically significant difference between the number of instructions for the Line, Shading and (L + S) groups ( $p > 0.004$ ).

#### 4.1.3.3 Time taken for deciding the correct direction of movement

The average time taken for deciding the direction of movement for the instructions with an endpoint within a  $0^\circ - 30^\circ$  error margin during the testing phase for all four groups are shown in Table 4.8 and graphically represented in Figure 4.7.

**Table 4.8** Time taken for deciding the direction of movement for the instructions with an endpoint within a 0° - 30° error margin

Groups	Average time taken for deciding the direction of movement for the instructions with an endpoint within a 0° - 30° error margin (seconds)	
	Mean	SD
NG	2.87	0.51
Line	2.94	0.98
Shading	2.78	0.82
(L + S)	2.47	0.73

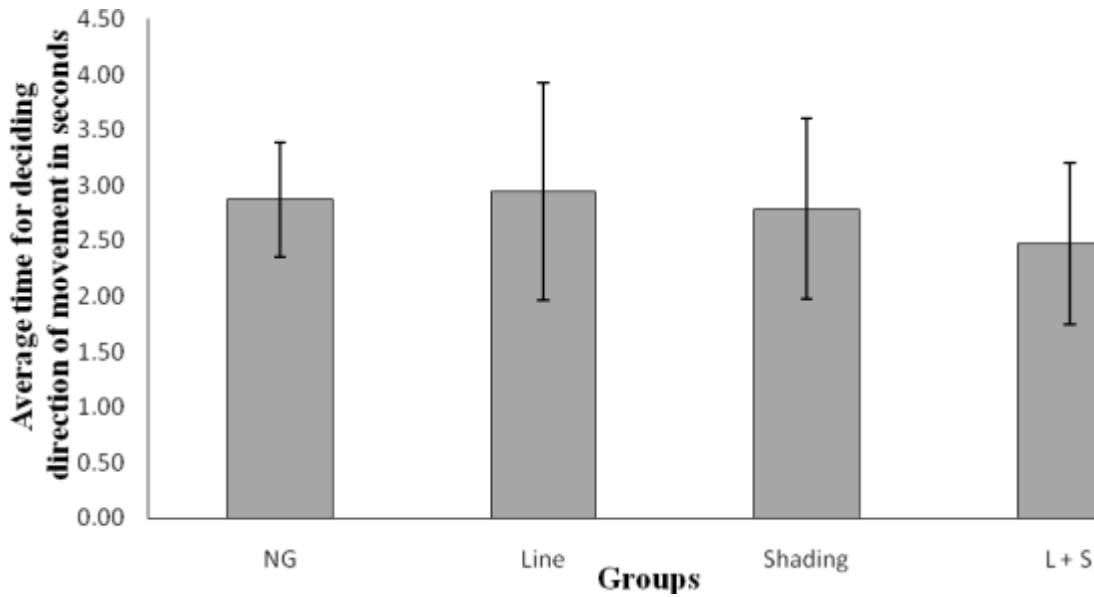


**Figure 4.7** Average time for deciding direction of movement for all groups

No statistically significant difference was observed between the average time taken by the NG as compared to all three graphic groups ( $p > 0.008$ ). Similarly, no statistically significant difference was observed between the average time taken by participants in the Line, Shading and (L + S) groups ( $p > 0.008$ ).

## 4.2 Proximity sensing using HSDL 9100

### 4.2.1 Family of output voltage curves for solid standard color sheets

A single HSDL 9100 was used to obtain output voltages for six standard solid color sheets – White, Neutral 8.0, Neutral 6.5, Neutral 5.0, Neutral 3.5 and Black for a range of 0 - 60 mm distance, with 1 mm interval from 0-6 mm, and 2 mm intervals from 6-60 mm. A family of curves on a logarithmic scale was obtained as shown in Figure 4.8.

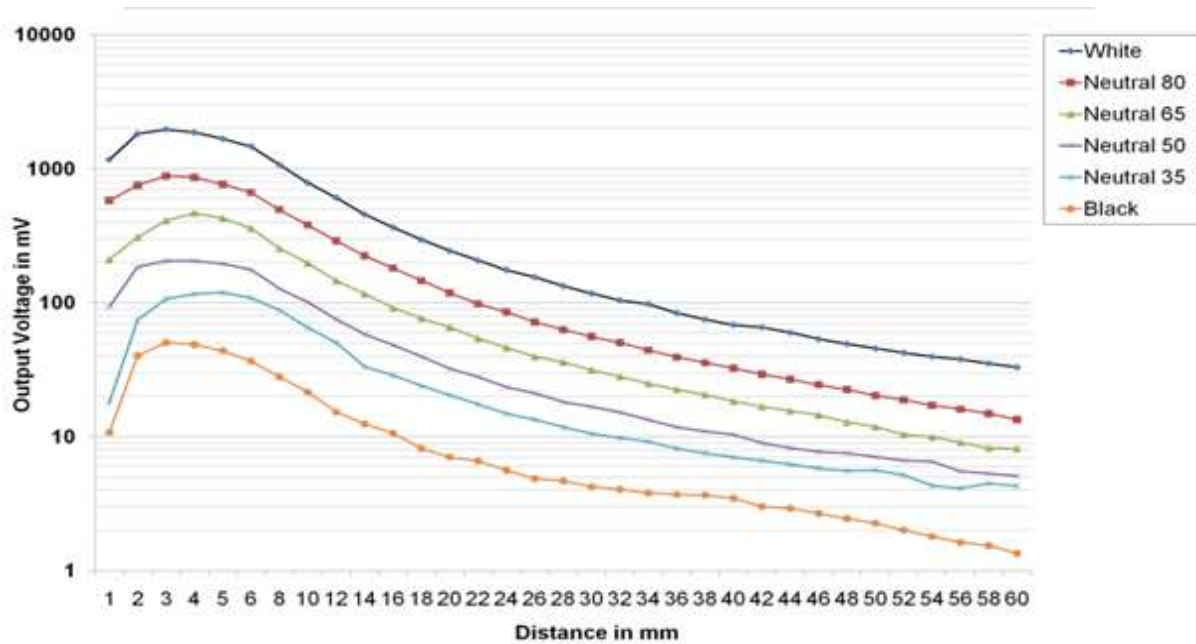


**Figure 4.8** Family of output voltage curves for single HSDL 9100 sensor for all six standard color sheets

Reflectance of IR light was highest for the White sheet and lowest for the Black sheet. Reflectance decreased for the four Neutral colors in the order of Neutral 8.0, Neutral 6.5, Neutral 5.0 and Neutral 3.5, with Neutral 8.0 closest to White, while Neutral 3.5 closest to Black. This database of logarithmic values of output voltages for various distances was used ahead to calculate the proximity of an object.

The color sheets used were 8.5 x 11 inches (21.6 x 27.9 cm) in size with a black border. To check if the black border was influencing the results at the full range of 60 mm, the IR beam

divergence angle of the sensor was calculated. It was found to be  $26^\circ$  and that at the full scale range, the border was not being illuminated at all. Thus, there was no influence of the black border on the output voltages.

#### **4.2.2 Distance measurement for multiple color sheets**

A left-right and a right-left placement of the White and Black color sheets were tested for random distances in the range of 0 – 60 mm with a single sensor. For the same distance, the output voltages obtained for the left-right combination were different than the right-left combination. It was observed that the output voltage generated by the sensor for the combination, was closer to the voltage generated by color directly in front of the detector when tested alone at the same distance. Thus it was necessary to have a uniform illumination around the detector. To test this hypothesis, the circular LED array was implemented with the detector placed in center of the LED array. Output voltages were obtained for random distances between 0 – 60 mm with an error of  $\pm 2$  mm. As the LED array was large in size, it was necessary to determine the minimum illumination required around the detector. It was found that reducing the number of emitter LEDs concentrically did not affect the distance measurement of multiple colors present at the same distance. Thus, the ‘+’ (plus) formation of four sensors on the Lego block was constructed.

#### **4.2.3 Distance measurement for unknown grayscale value**

Distance measurements were performed on the two test cards, Neutral 8.0 and Neutral 5.0 under different lighting conditions, both inside and outside the trainer box. Distance measurement of actual objects used within the trainer box, such as central tree trunk and the white target cylinders were also conducted with the 6 mm restricting ring. The distances at which the cards or the trainer box objects were mounted from the sensor assembly are mentioned in

column 5 of all the following tables. Similarly, column 6 of all the tables gives the distances indicated by the sensor assembly based on the calculated interpolation values of the log of voltages for that color.

#### 4.2.3.1 Ambient lighting conditions for Neutral 8.0 card

Three random distances were measured for the Neutral 8.0 ColorChecker<sup>®</sup> Card with HSDL-9100 assembly under ambient lighting conditions as mentioned in Table 4.9. Results indicated the distance with an error of  $\pm 1$  mm.

**Table 4.9** Distance measurement for the Neutral 8.0 under ambient lighting conditions

Log values of voltages for sensors (mV)				Actual distance in mm	Distances obtained from interpolated results in mm
Sensor at 12 o'clock	Sensor at 3 o'clock	Sensor at 6 o'clock	Sensor at 9 o'clock		
1.63	1.63	1.58	1.58	58	58 to 60
1.88	1.91	1.87	1.86	40	38 to 40
2.40	2.47	2.47	2.46	15	14 to 16

#### 4.2.3.2 Ambient lighting conditions for Neutral 5.0 card

Neutral 5.0 ColorChecker<sup>®</sup> Card was used to measure three random distances under ambient lighting conditions as mentioned in Table 4.10. Results indicated the distance with an error of  $\pm 1$  mm.

**Table 4.10** Distance measurement for the Neutral 5.0 under ambient lighting conditions

Log values of voltages for sensors (mV)				Actual distance in mm	Distances obtained from interpolated results in mm
Sensor at 12 o'clock	Sensor at 3 o'clock	Sensor at 6 o'clock	Sensor at 9 o'clock		
1.43	1.37	1.32	1.34	58	56 to 58
1.63	1.63	1.59	1.59	40	38 to 40
2.14	2.22	2.22	2.20	15	14 to 16

#### 4.2.3.3 LED-lit conditions within the trainer box for Neutral 8.0 card

The trainer box space was illuminated using white LED strips and random distances were measured using the Neutral 8.0 ColorChecker® Card as mentioned in Table 4.11. Results indicated the distance with an error of  $\pm 1$  mm.

**Table 4.11** Distance measurement for the Neutral 8.0 under LED-lit conditions within the trainer box

Log values of voltages for sensors (mV)				Actual distance in mm	Distances obtained from interpolated results in mm
Sensor at 12 o'clock	Sensor at 3 o'clock	Sensor at 6 o'clock	Sensor at 9 o'clock		
1.55	1.36	1.27	1.42	58	58
1.84	1.71	1.63	1.75	39	38
2.18	2.07	2.00	2.12	22	22 to 24

#### 4.2.3.4 LED-lit conditions within the trainer box for Neutral 5.0 card

The Neutral 5.0 ColorChecker® Card was used to measure three random distances under white LED-lit space of the trainer box, as mentioned in Table 4.12. Results indicated the distance with an error of  $\pm 1$  mm.

**Table 4.12** Distance measurement for the Neutral 5.0 under LED-lit conditions within the trainer box

Log values of voltages for sensors (mV)				Actual distance in mm	Distances obtained from interpolated results in mm
Sensor at 12 o'clock	Sensor at 3 o'clock	Sensor at 6 o'clock	Sensor at 9 o'clock		
0.68	0.56	0.58	0.62	55	56
1.67	1.51	1.42	1.54	22	21 to 23
2.23	2.09	1.95	2.11	5	4 to 6

#### 4.2.4 Distance measurement for actual trainer box objects

Distance measurement of actual trainer box objects such as the white target cylinder and the central gray trunk showed significant difference, and thus, a 6 mm black restricting ring was placed over the sensor assembly for further testing.



#### 4.2.4.1 LED-lit conditions within the trainer box for white target cylinder

A 6 mm black colored restricting was fixed around the sensor assembly. Random distances were measured for white target cylinder under white LED-lit space of the trainer box. Due to the shape of the target cylinder, the distances measured by each sensor in the assembly varied due to the reflection of IR back from the curved surface, thus giving multiple results as mentioned in Table 4.13.

**Table 4.13** Distance measurement for white target cylinder with a 6 mm restricting ring

Log values of voltages for sensors (mV)				Actual distance in mm	Distances obtained from interpolated results in mm
Sensor at 12 o'clock	Sensor at 3 o'clock	Sensor at 6 o'clock	Sensor at 9 o'clock		
1.47	1.49	1.38	1.43	52	60, 46 to 52
1.74	1.88	1.76	1.80	28	32, 26 to 28
2.07	2.14	2.02	2.05	14	24 to 26, 10 to 18

#### 4.2.4.2 LED-lit conditions within the trainer box for tree trunk

Random distances were measured for tree trunk in white LED-lit trainer box space with a 6 mm black restricting ring fixed around the sensor assembly. Due to the cylindrical shape of the task tree trunk and the perforations for attaching branches, the distances measured by each sensor in the assembly varied due to the reflection of IR back from the curved surfaces (both external and internal), thus giving multiple results as mentioned in Table 4.14.

**Table 4.14** Distance measurement for tree trunk with a 6 mm restricting ring

Log values of voltages for sensors (mV)				Actual distance in mm	Distances obtained from interpolated results in mm
Sensor at 12 o'clock	Sensor at 3 o'clock	Sensor at 6 o'clock	Sensor at 9 o'clock		
1.29	1.25	1.11	1.16	52	> 60
1.52	1.63	1.50	1.54	28	46 to 48, 34 to 38
1.62	1.88	1.76	1.78	14	36 to 38, 22 to 26

## CHAPTER 5 DISCUSSION

### 5.1 Camera navigation using graphics

The primary objective of this study was to evaluate the effect of navigational aids on the training of a MIS camera navigation task. The navigational tool consisted of different graphics that were developed using Matlab. Two training methods were compared: (1) training with no graphical aids (control group) and (2) training with graphical aids. Under training with graphical aids, three different graphics were designed, (1) a position circle with a line indicating the direction of view of endoscope, (2) a position circle with filling (shading) of circle indicating the rotation of endoscope, (3) a position circle with both line and filling of the circle. A vertical bar was provided with each of the three graphics mentioned above to help participants develop an estimate of height.

The performance variables during the training phase that were analyzed to evaluate effectiveness of the training methods in performing MIS camera navigation task were: (1) the average number of task trees required to achieve proficiency, (2) the average training time, (3) the average number of targets found per tree during the training phase and (4) the average RMS error of the mental-map of the training trees on paper. Performance variables evaluated for the testing phase were: (1) the average number of instructions in the correct direction (difference between the reference direction of movement and the actual direction of movement in the range of  $0^\circ - 30^\circ$ ) for two time points, namely the endpoint and 250 msec after the instruction was given, and (2) the average time for deciding the direction of movement.

#### 5.1.1 Training phase characteristics

The training phase results indicated that training with graphics enhanced the competency of participants to reach the same proficiency level at a faster rate (more so in the case of the

better designed graphic (L + S)), as they had better idea of manipulating the endoscope in a MIS camera navigation task. All the three graphics imparted different critical information regarding the endoscope tip, which helped participants manipulate the endoscope in a correct manner and explore the trainer box space. Information imparted by the graphics also saved time for these participants as their mental picture of the task tree and directions was better. Comparing the three graphics amongst themselves, no significant statistical difference ( $p > 0.008$ ) was observed. This suggests that there are not large differences amongst the three graphic displays. However, more participants are needed if one was to more precisely compare the three graphics (the needed sample size approaches 100 participants).

It is hypothesized that the difference between the NG group and the groups that used the graphical aids was that the graphical aids helped to guide participants that used them. This is supported by the observation that, in contrast to the other groups, participants in the NG group repeatedly explored already identified targets suggesting a poor understanding of the space. This resulted in loss of time to explore and identify the remaining targets of the 25 minute trials. This increased their exasperation, affecting their state of mind which deteriorated their performance. On the other hand, participants trained with graphics were given an understanding of the position of endoscope tip, direction of view of endoscope (Line and (L + S) groups) and rotation of endoscope (Shading and (L + S) groups). This might have helped them remember and recollect the explored targets and thus reduced re-exploration of the already found targets, leaving them with ample time to explore the remaining targets, thereby increasing their probability of reaching the stopping criteria sooner.

Poor understanding of the trainer box space was evident from the paper plots marked by the participants of NG group. They marked the locations of the targets solely based on the

direction of the branch seen in the real-time video. A majority of them eventually rotated the entire tree on paper by an angle approximately equivalent to the rotation of endoscope. On the other hand, participants trained with graphics had better understanding of the trainer box space and were able to mark the locations of the targets more accurately. For the participants of Line group, the graphic might have served as a self-explanatory map. Using the direction line, they were able to recognize the respective section of the box in real-time video irrespective of the rotation of the endoscope. For the participants of Shading group, the filling of position circle might have helped them understand rotation of endoscope. It was observed that participants of this group came back to the base orientation (orientation of endoscope when axes of both the trainer box and of the endoscope were same) in case they felt they were lost while exploring targets. They were able to integrate the information presented by graphics and real-time video, thus identifying the direction of branches and targets more accurately. Participants of the (Line + Shading) group were given complete information regarding position, direction of view and rotation of endoscope. This might have helped them generate better understanding of the trainer box space, thus requiring least number of task trees, training time and the least error of mental map on paper amongst all the groups.

### **5.1.2 Testing phase characteristics**

The testing phase results indicated that the participants trained with graphics were able to successfully transfer their knowledge acquired during the training phase to a different, but related camera navigation task. Although all the participants took nearly the same time to decide the correct direction of movement, the endpoint analysis of participants trained with graphics showed a much higher accuracy to move the endoscope in a desired direction as compared to the NG group. As participants were instructed to continue in the direction they decided to move and

not change it later during movement, endpoint would be the most reliable indicator of participants' understanding of directions. For 250 msec time point, no statistically significant difference in accuracy was observed across all the groups. This highlights the fact that these graphics only enhanced navigation abilities of endoscope of participants, but not the reaction or response times for endoscope navigation.

Rotation of endoscope to see target number in upright orientation changed the relationship of coordinate system of the trainer box with coordinate system of the target itself. Participants of NG group failed to understand this complicated relation that changed with each target of the testing tree. Unable to visualize this transformation, it was observed that these participants continued to assume and apply coordinate system of the trainer box to each target of the testing tree, irrespective of the target's orientation within the trainer box. Radial differences calculated between correct direction and direction of movement (based on endpoint with respect to starting point of endoscope) does support their lack of understanding of directions on rotation of the endoscope.

Participants of Line group, being trained with line indicating direction, were aware of the relation of endoscope handle with respect to all sections of the trainer box and hence, its sides and corners. When instructed to reach a particular target of testing tree, it seems they were able to relate sides of the trainer box with the orientation of the target number. Upon rotating the endoscope to view the target number in upright orientation, they were able to rotate their mental frame of axes and assign sides in view of the trainer box to four directions of the target number.

Participants of Shading and (L + S) groups were able to rotate their mental frame of axes based on the direction of rotation (clockwise or counterclockwise) of the endoscope. Overall results suggested that providing complete information regarding direction and rotation helped

and strengthened the understanding of directions of participants more than that in case of providing individual information.

Another explanation for the difference in performance of these four groups lies in the way humans perform arm movements. Arm movements are longer in duration as compared to eye movements like saccades, and hence, sensory feedback plays an important role in control of their movements (Shadmehr et al., 2010). The cerebellum region of the human brain is critical to perform coordinated, precise and accurate movements. Sensory inputs from spinal cord and other parts of brain are integrated by cerebellum to fine-tune motor activity. Damage to the cerebellum results in fine movement disorders, motor learning disorders etc., thereby resulting in degradation of smoothness and accuracy of movements (Fine et al., 2002). The cerebellum thus acts as a “forward model”, which basically can predict the consequences of a motor command (Pasalar et al., 2006; Shadmehr et al., 2008). Cerebellum, being the forward model, processes a motor command to predict its consequences before a sensory feedback (for example from an arm) is available. A study conducted by Miall et al. (2007) concluded that cerebellum performs two functions in terms of motor control –

1. It processes the history of motor commands to predict the state of the limb, and
2. Generates a cerebellar output (a “motion update” signal of the limb), which when combined with the delayed sensory feedback elsewhere in the brain, is used to generate a real-time state estimate for motor control, and hence, movement of limb.

Research conducted by Tseng et al. (2007) concluded that sensory errors (visual errors in their experiments) were the key factor of learning for cerebellum to adapt to visuomotor perturbations. Sensory errors occur when an initial motor command is generated, but the

predicted sensory consequences do not match the observed values. However, the crucial requirement for this learning to occur is to have accurate predictions, which in turn are dependent on the information provided. If a participant can construct an accurate forward model, the participant would be able to predict the motion that will occur for a certain motor command (Shadmehr et al., 2010).

Participants trained with no graphics during training phase performed movements of endoscope based solely on the real-time video. Thus, they would have generated a specific set of motor commands for manipulation of endoscope, thereby training their cerebellum only for exploration. However, their forward model was not provided with additional information regarding rotation and direction of view of endoscope to strengthen and generate accurate predictions for such different movements of endoscope. It seems participants of NG group were not able to predict the motion of endoscope required for instructions presented during testing phase. Due to lack of forward models generated with information about rotation and direction of endoscope, participants of NG group went in wrong directions for most of the instructions.

Participants of all the three graphic groups, on the other hand, had an additional visual cue in the form of graphics during training phase, which may have helped them cognitively to generate more robust forward models that included predictions for direction of view and rotation of endoscope. It seems participants of the three graphic groups created these forward models, learnt navigation of endoscope through sensory errors during the training phase and applied them to move endoscope in correct directions for most of the instructions. Thus, participants of the three graphic groups were trained to apply knowledge of the training task effectively to the new problem given to them in the testing phase.

The experimental study performed by Zheng et al. (2003) to compare mean reaction times for movements of a grasper, used a 0° endoscope that was rotated by 45° clockwise to create and simulate misalignment of video with respect to the trainer box. Their experiment involved reaching a specific point indicated by a light-emitting diode (LED) in trainer box environment from another specific start point. Thus, their experiment had a definite direction in terms of tool movement. The mean reaction times they recorded were 365 msec, which clearly indicates that it took more than 250 msec for participants irrespective of their groups and their respective training to decide direction of endoscope movement. They also noted that the spatial transformation would become more difficult, thereby increasing reaction time if the participant used a 30° or a 45° endoscope. This series of experiments used a 30° endoscope, and required the participant to estimate the direction based on instruction provided, as compared to the display of a visually-definite point in space used by Zheng et al. (2003) in their study. These added complexities ascertain the increase in average reaction times for all groups.

After the training phase, participants of all the four groups were tested on the same task, with same group of instructions. As mentioned above, average reaction times for all the four groups were similar; however, final accuracy attained for the task was much higher for the three graphic groups. A similar study conducted on testing reaction times of surgeons concluded that reaction time did not necessarily predict surgical skill (Shah et al., 2003). The study compared average reaction times of medical students with surgeons. Their study concluded that efficiency and performing of necessary steps with precise appropriate movements was more important for a surgeon as compared to speed. Thus, although the average time to decide direction of movement was similar across the four groups, accuracy of movement was much higher for the three graphic groups. It can thus be concluded that although graphics did not influence the time for decision



making process, they did influence the overall spatial understanding of trainer box space for their respective participants.

## **5.2 Proximity Sensor**

The proximity sensor HSDL 9100 was used in this study to provide proximity of objects in front of an endoscope. The idea was to provide this proximity in the form of distance along with other graphics to the participants so that they could avoid collisions, which can avert medical emergencies in an actual OR environment.

The sensor was selected for multiple reasons, among which the important ones were size and principle of working. As mentioned before, the IR does not get affected by the LED-lit environment of the trainer box and thus it would not distract the participant like a laser would. Similarly, this sensor was small enough to be placed directly on the endoscope tip, and hence used to provide proximity of objects in front of endoscope in order to avoid collisions.

The sensor assembly worked accurately for standard color sheets irrespective of the illumination conditions. As the FOVs of both the sensor and camera of this endoscope were equal, faithful indication of proximity was expected. However, the sensor did not work accurately for objects that were actually placed within the trainer box. There are potentially multiple reasons for the shortcomings of using this sensor in this training setup. First, objects placed and tested in the trainer box were cylindrical in shape, such as the central gray tree trunk and the branches used for placing white-colored target cylinders. The trunk had holes in it for attaching of the branches of task tree. Hence, even when the sensor assembly was tested for accuracy, it gave multiple output readings for the same trunk placed at a random static distance from the assembly. Some of the output readings were due to IR reflection by the external surface of the trunk near the sensor assembly, while some output readings were from the trunk's internal

surface that was away from the sensors. The darker color of the trunk and the amount of illumination within the trunk due to its location within the trainer box would have resulted in darker patch for center of the trunk, thereby changing the overall grayscale of the image obtained. This in turn affected the interpolation results, inducing an error in the proximity measurement.

Another factor of variation was the shape and material of construction of all the trainer box objects. The algorithm worked correctly for standard color sheets, which proved that color variations for large plain-surfaced objects did not affect performance of the sensor and provided accurate proximity. The color sheets were made of the same material, thus not affecting or introducing an error in reflectivity due to variations in material of construction. However, the trainer box objects were made of different materials, were small in size and cylindrical in shape, had perforations in them (tree trunk) and thin edges (white target cylinder rims) for requirements of the setup. The algorithm worked correctly for the flat standard color sheets, however, there is a possibility that it would not work for multiple colors on a single sheet.

A restricting ring was added so as to capture more IR reflection only from the object in front, and not the angular reflections from objects present in the periphery. However, the inherent issues of lighting and grayscale calculations seem to have affected the results. Current technical limitations thus hampered proximity sensing of the actual objects placed within the trainer box. Further intensive testing would be required for sensing proximity of objects made of different materials, different shapes or the standard color sheets (made of same material) placed at various angles other than perpendicular and with a collage of colors.

## CHAPTER 6 CONCLUSION AND FUTURE WORK

Simulator training improves camera navigation skills and learning of surgical steps of the trainees. Improvements in performance of trainees in terms of movements, accuracy, and total time to perform a procedure, retention of skills have been concluded by various researches (Jones, 2007; Guruswamy et al., 2009; Debes et al., 2010). Research has also shown that learning and retaining of skills acquired on both VT and VR systems are transferable to the actual OR environment (Grantcharov et al, 2004; Hamilton et al., 2002; Hyltander et al, 2002; Stefanidis et al., 2005; Stefanidis et al., 2006). Simulators designed until now have concentrated on teaching actual steps of surgery and part tasks to develop psychomotor and spatial abilities of trainees. Various parameters such as path length, velocity, time, accuracy etc. are provided as feedback to the trainee for improvement. However, these systems do not help trainees learn by providing them information about the position, direction and rotation of endoscope tip to help them interpret the camera output.

A training method using graphics was developed and tested for effectiveness in learning camera navigation for a minimally invasive surgery training task. Critical information related to the endoscope was provided using real-time graphics so as to improve the spatial understanding of the trainer box environment of the participants. Various training and testing parameters were analyzed and significant improvement in understanding of directions was seen for participants trained with graphics. Training with graphics also improved the ability to search and explore new / unknown operative space in lesser time. This would reduce training time for surgeons and help them develop a better understanding of the conceptual relationship between endoscope, port of entry and video scene on monitor. More number of participants would be needed to evaluate the effect of individual graphics in improvement of understanding of directions of the trainees. Also,

gradual fading of graphics can be implemented during the training phase so that the trainees are not over-dependent on graphics when operating in real OR environment.

Another idea was to provide information about proximity to objects on the graphics screen, which would help participants in reducing collisions with the endoscope. Although the proximity sensor setup gave accurate and encouraging results for standard color sheets, it was not implemented along with graphics as the results were not accurate for actual objects.

Potentially, a more technologically advanced and robust sensor could be used for sensing and providing proximity of objects within the trainer box to the participants. If the same HSDL-9100 sensor is used, further testing should be carried out using better collimators such as miniature lenses / prisms, or a completely different or slightly concave (curved-inside) assembly of these sensors. Different methods of restricting the FOV of sensors can be tried, or a better and alternate program using shape recognition can be written for object identification, to cancel the effects of shadows, illumination and angle of object from affecting the results.

## LITERATURE CITED

- Aggarwal R, Ward J, Balasundaram I, Sains P, Athanasiou T, Darzi A. Proving the Effectiveness of Virtual Reality Simulation for Training in Laparoscopic Surgery. *Annals of Surgery*, 2007; 246(5): 771-9
- Ahlberg G, Enochsson L, Gallagher A, Hedman L, Hogman C, McClusky D III, Ramel S, Smith C, Arvidsson D. Proficiency-based virtual reality training significantly reduces the error rate for residents during their first 10 laparoscopic cholecystectomies. *American Journal of Surgery*, 2007; 193(6): 797-804
- Akinbiyi T. Intelligent Instruments and Visual Force Feedback in Laparoscopic Minimally Invasive Surgery. M.S Thesis, Department of Mechanical Engineering, The Johns Hopkins University, 2005
- Anastakis D, Regehr G, Reznick R, Cusimano M, Murnaghan J, Brown M, Hutchison C. Assessment of technical skills transfer from the bench training model to the human model. *American Journal of Surgery*, 1999; 177: 167-170
- Arora S, Sevdalis N, Nestel D, Woloshynowych M, Darzi A, Kneebone R. The impact of stress on surgical performance: A systematic review of the literature. *Surgery*, 2010; 147(3): 318-30
- Avgerinos D, Goodell K, Waxberg S, Cao G, Schwaitzberg S. Comparison of the sensitivity of physical and virtual laparoscopic surgical training simulators to the user's level of experience. *Surgical Endoscopy*, 2005; 19:1211-15
- Berguer R. Ergonomics in the Operating Room. *American Journal of Surgery*, 1996; 171: 385-86
- Blum M, Powers T, Sundaresan S. Bronchoscopy simulator effectively prepares junior residents to competently perform basic clinical bronchoscopy. *The Annals of Thoracic Surgery*, 2004; 78(1): 287-91
- Breedveld P. Observation, Manipulation, and Eye-Hand Coordination Problems in Minimally Invasive Surgery. Conference on human decision making and manual control, 1997; 219-31
- Breedveld P, Wentink M. Eye-hand coordination in laparoscopy - an overview of experiments and supporting aids. *Minimally invasive therapy & allied technologies: MITAT: official journal of the Society for Minimally Invasive Therapy*, 2001; 10(3): 155-62
- Carter F, Schijven M, Aggarwal R, Grantcharov T, Francis N, Hanna G, Jakimowicz J. Consensus guidelines for validation of virtual reality surgical simulators. *Surgical Endoscopy*, 2005; 19(12):1523-32
- Castro F. Class I infrared eye blinking detector. *Sensors and Actuators A: Physical*, 2008; 148:388-394
- Cavusoglu M, Williams W, Tendick F, Sastry S. Robotics for Telesurgery: Second Generation Berkeley/UCSF Laparoscopic Telesurgical Workstation and Looking Towards the Future Applications. *Industrial Robot: An International Journal*, 2003; 30(1):22-29

- Chmarra M, Grimbergen C, Dankelman J. TrEndo, a device for tracking minimally invasive surgical instruments in training setups. *Sensors and Actuators A: Physical*, 2006; 126(2):328-34
- Coolican H. *Introduction to Research Methods in Psychology*. Third Edition. Exploring Psychology Study and Revision Guide for AS Level AQA A. © Oxford University Press, 2010; Pages 37-59. [Available online at [http://fds.oup.com/www.oup.com/pdf/oxed/secondary/psychology/explore\\_ch\\_3.pdf](http://fds.oup.com/www.oup.com/pdf/oxed/secondary/psychology/explore_ch_3.pdf) retrieved on June 25, 2012]
- Dankelman J. Surgical Simulator Design and Development. *World Journal of Surgery*, 2008; 32(2):149-55
- Debes A, Aggarwal R, Balasundaram I, Jacobsen M. A tale of two trainers: virtual reality versus a video trainer for acquisition of basic laparoscopic skills. *The American Journal of Surgery*, 2010; 199:840-45
- den Boer K, Straatsburg I, Schellinger A, de Wit L, Dankelman J, Gouma D. Quantitative analysis of the functionality and efficiency of three surgical dissection techniques: a time-motion analysis. *Journal of Laparoendoscopic & Advanced Surgical Techniques*, 1999; 9(5): 389-95
- DeLucia, P, Hoskins M, Griswold J. Laparoscopic Surgery: Are Multiple Viewing Perspectives Better than One? *Proceedings of the Human Factors and Ergonomics Society, 48th Annual Meeting, Santa Monica, CA: Human Factors and Ergonomics Society, 2004; 1-4*
- Derefeldt G, Menu J-P, Swartling T. Cognitive aspects of color. *Proceedings of the SPIE Human Vision, Visual Processing, and Digital Display, VI, 1995; 2411:16-24*
- Derefeldt G, Skinnars Ö, Alfredson J, Eriksson L, Andersson P, Westlund J, Berggrund U, Holmberg J, Santesson R. Improvement of tactical situation awareness with color-coded horizontal-situation displays in combat aircraft. *Elsevier, 1999; 20(4):171-84*
- Dunkin B, Adrales G, Apelgren K, Mellinger J. Surgical simulation: a current review. *Surgical Endoscopy*, 2007; 21:357-66
- Dušková M, et al. *Introduction to the Surgery : Textbook for Students of Third Faculty of Medicine Charles University in Prague*. 1st edition. Praha : Univerzita Karlova v Praze, 3. lékařská fakulta, Klinika plastické chirurgie, 2009. [Available online at <http://www.lf3.cuni.cz/miranda2/export/sites/www.lf3.cuni.cz/cs/pracoviste/plasticka-chirurgie/skripta/introduction-surgery.pdf> retrieved on July 01, 2012]
- Escolà A, Planas S, Rosell J, Pomar J, Camp F, Solanelles F, Gracia F, Llorens J, Gil E. Performance of an Ultrasonic Ranging Sensor in Apple Tree Canopies. *Sensors (Basel)*, 2011; 11(3): 2459-2477
- Eun D, Bhandari A, Boris R, Rogers C, Bhandari M, Menon M. Concurrent upper and lower urinary tract robotic surgery: strategies for success. *BJU International*, 2007;100(5):1121-5
- Eyal R, Tendick F. Spatial Ability and Learning the Use of an Angled Laparoscope in a Virtual Environment. *Studies in health technology and informatics*, 2001;81:146-52

- Feisner E. Colour: How to Use Colour in Art and Design. Laurence King Publishing, 2006; Pages 39-44
- Fine E, Ionita C, Lohr L. The history of the development of the cerebellar examination. *Seminars in neurology*, 2002; 22(4):375-84
- Fried G, Derossis A, Bothwell J, Sigman H. Comparison of laparoscopic performance in vivo with performance measured in a laparoscopic simulator. *Surgical Endoscopy*, 1999; 13(11):1077-81
- Fried G, Feldman L, Klassen D. Laparoscopic Cholecystectomy. *ACS Surgery: Principles and Practice*, 2002; WebMD Inc.: Pages 1-21. [Available online at <http://sabanet.unisabana.edu.co/medicina/semestre10/cirugiaI/Colelap.pdf> retrieved on June 25, 2012]
- Gallagher A, Cates C. Virtual reality training for the operating room and cardiac catheterisation laboratory. *The Lancet*, 2004; 364(9444):1538-40
- Gallagher A, Lederman A, McGlade K, Satava R, Smith C. Discriminative validity of the Minimally Invasive Surgical Trainer in Virtual Reality (MIST-VR) using criteria levels based on expert performance. *Surgical Endoscopy*, 2004; 18(4):660-5
- Gallagher A, Ritter E, Champion H, Higgins G, Fried M, Moses G, Smith C, Satava R. Virtual Reality Simulation for the Operating Room: Proficiency-Based Training as a Paradigm Shift in Surgical Skills Training. *Annals of Surgery*, 2005; 241(2):364-72
- Gallagher A, Satava R. Virtual reality as a metric for the assessment of laparoscopic psychomotor skills. *Surgical Endoscopy*, 2002; 16:1746-52
- Geryane M, Hanna G, Cuschieri A. Time-motion analysis of operation theater time use during laparoscopic cholecystectomy by surgical specialist residents. *Surgical Endoscopy*, 2004; 18(11): 1597-1600
- Gibson J. *The Perception of the Visual World*. ed. Westport, Conn: Greenwood Press; 1974: pp 235
- Grantcharov T, Kristiansen V, Bendix J, Bardram L, Rosenberg J, Funch-Jensen P. Randomized clinical trial of virtual reality simulation for laparoscopic skills training. *The British Journal of Surgery*, 2004; 91(2): 146-50
- Groeger M, Arbter K, Hirzinger G. Motion Tracking for Minimally Invasive Robotic Surgery. *Medical Robotics*. Pages 117-148. [Available online at [http://www.intechopen.com/books/medical\\_robotics/motion\\_tracking\\_for\\_minimally\\_invasive\\_robotic\\_surgery](http://www.intechopen.com/books/medical_robotics/motion_tracking_for_minimally_invasive_robotic_surgery) retrieved on June 28, 2012]
- Güntner P, Pfister T, Büttner L, Czarske J. Laser Doppler distance sensor using phase evaluation. *Optics Express*, 2009; 17(4): 2611-22
- Guruswamy K, Aggarwal R, Palanivelu L, Davidson B. Virtual reality training for surgical trainees in laparoscopic surgery. *Cochrane Database of Systematic Reviews*, 2009; 1

- Haluck R, Webster R, Snyder A, Melkonian M, Mohler B, Dise M, Lefever A. A Virtual Reality Surgical Trainer for Navigation in Laparoscopic Surgery. *Studies in health technology and informatics*, 2001; 81:171-6
- Hamilton E, Scott D, Fleming J, Rege R, Laycock R, Bergen P, Tesfay S, Jones D. Comparison of video trainer and virtual reality training systems on acquisition of laparoscopic skills. *Surgical Endoscopy*, 2002; 16(3): 406-11
- Heaton J, Kowaleski J, Bermejo R, Zeigler H, Ahlgren D, Hadlock T. A System for Studying Facial Nerve Function in Rats through Simultaneous Bilateral Monitoring of Eyelid and Whisker Movements. *Journal of Neuroscience Methods*, 2008; 171(2): 197-206
- Helander M, Landauer T, Prabhu P. *Handbook of Human-Computer Interaction*. Second, completely revised edition. © 1997 Elsevier Science B.V. ; ISBN 0444818626, 9780444818621; Marcus A, Chapter 19 – Graphical User Interfaces; Pages 423-440
- Hernández Á, Ureña J, Mazo M, García J, Jiménez A, Álvarez F. Reduction of blind zone in ultrasonic transmitter/receiver transducers. *Sensors and Actuators A: Physical*, 2007; 133(1): 96-103
- Hiemstra E. *Acquiring Minimally Invasive Surgical Skills*. Doctoral thesis, Leiden University, 2012
- Hyltander A, Liljegren E, Rhodin P, Lönroth H. The transfer of basic skills learned in a laparoscopic simulator to the operating room. *Surgical Endoscopy*, 2002; 16(9):1324-8
- Johnstone S. Multi-sensor method of producing a material independent inductive distance measuring device. *Boundary Elements XXVII, WIT Transactions on Modelling and Simulation*, 2005; 39: 717-726. [Available online at [www.witpress.com](http://www.witpress.com), ISSN 1743-355X]
- Jones D. Video Trainers, Simulation and Virtual Reality: A New Paradigm for Surgical Training. *Asian journal of surgery Asian Surgical Association*, 2007; 30(1):6-12
- Jones H, Ohlssen D, Spiegelhalter D. Use of the false discovery rate when comparing multiple health care providers. *Journal of Clinical Epidemiology*, 2008;61(3):232-40
- Jordan J, Gallagher A, McGuigan J, McClure N. Virtual reality training leads to faster adaptation to the novel psychomotor restrictions encountered by laparoscopic surgeons. *Surgical Endoscopy*, 2001; 15(10): 1080-4
- Keehner M, Wong D, Tendick F. Effects of Viewing Angle, Spatial Ability, and Sight of Own Hand on Accuracy of Movements Performed Under Simulated Laparoscopic Conditions. *Proceedings of the Human Factors and Ergonomics Society Annual Meeting*, 2004; 48(15):1695-99
- Kelsey C. Detection of visual information. In: *The Perception of Visual Information*, W Hendee and P. Wells, Eds. New York: Springer-Verlag, 1993; 30-51



- Kolkman W, van de Put M, Wolterbeek R, Trimbos J, Jansen F. Laparoscopic skills simulator: construct validity and establishment of performance standards for residency training. *Gynecological Surgery*, 2008; 5(2):109-14
- Korndorffer J, Dunne J, Sierra R, Stefanidis D, Touchard C, Scott D. Simulator Training for Laparoscopic Suturing Using Performance Goals Translates to the Operating Room. *Journal of the American College of Surgeons*, 2005; 201(1):23-9
- Korndorffer J, Hayes D, Dunne J, Sierra R, Touchard C, Markert R, Scott D. Development and transferability of a cost-effective laparoscopic camera navigation simulator. *Surgical Endoscopy*, 2005; 19(2): 161-7
- Kosslyn S. Graphics and Human Information Processing: A Review of Five Books. *Journal of the American Statistical Association*, 1985; 80(391): 499-512
- Lansdowne J, Mehler S, Boure L. Minimally invasive abdominal and thoracic surgery: principles and instrumentation. *Compendium (Yardley, PA)*, 2012; 34(5): E1-9
- Lapore C. Medicaid Modernization About Minimally Invasive Procedures a Case Study. Medicaid Health Plans of America Conference, 2011 [Available online at [http://www.mhpa.org/\\_upload/MinimallyinvasiveProcedureCaseStudies-ChrisLapore.pdf](http://www.mhpa.org/_upload/MinimallyinvasiveProcedureCaseStudies-ChrisLapore.pdf) retrieved on May 13, 2012]
- Larsen C, Oestergaard J, Ottesen B, Soerensen J. The efficacy of Virtual Reality Simulation Training in Laparoscopy: A Systematic Review of Randomized Trials. *Acta Obstetrica et Gynecologica Scandinavica*, 2012; "Accepted Article" doi: 10.1111/j.1600-0412.2012.01482.x
- Li R, Jensen J, Bowersox J. Microvascular anastomoses performed in rats using a microsurgical telemanipulator. *Computer Aided Surgery*, 2000; 5:326-32
- Lomanto D, Cheah WK. *Manual of Laparoscopic Surgery*. First Edition, 2004; 21-35
- Lowry R. Subchapter 14a. The Kruskal-Wallis Test for 3 or More Independent Samples. (Subchapter to a free, online statistics text book: Concepts and applications of inferential statistics, © Richard Lowry, 1999-2012), 2000; Pages 1-7. [Available online at <http://faculty.vassar.edu/lowry/PDF/c14a.pdf> retrieved on June 25, 2012]
- Maithel S, Sierra R, Korndorffer J, Neumann P, Dawson S, Callery M, Jones D, Scott D. Construct and face validity of MIST-VR, Endotower, and CELTS. *Surgical Endoscopy*, 2006; 20(1):104-12
- Mehta S, Juneja I, Udani D. Role of diagnostic laparoscopy in management of acute abdomen. *The Internet Journal of Surgery*, 2009; 20(1)
- Merrienboer J, Clark R, Croock M. Blueprints for Complex Learning: The 4C/ID-Model. *Educational Technology Research and Development*, 2002; 50(2):39-64
- Miall R, Christensen L, Cain O, Stanley J. Disruption of state estimation in the human lateral cerebellum. *PloS Biology*, 2007; 5(11):e316

- Molinas C, Win G, Ritter O, Keckstein J, Miserez M, Campo R. Feasibility and construct validity of a novel laparoscopic skills testing and training model. *Gynecological Surgery*, 2008; 5(4): 281-90
- Moulton C, Dubrowski A, Macrae H, Graham B, Grober E, Reznick R. Teaching Surgical Skills: What Kind of Practice Makes Perfect? *Annals of Surgery*, 2006; 244(3):400-9
- Munz Y, Kumar B, Moorthy K, Bann S, Darzi A. Laparoscopic virtual reality and box trainers. Is one superior to the other?. *Surgical Endoscopy*, 2004; 18(3):485-94
- Ng W, Sze S, Hui S. Port placement for laparoscopic appendectomy with the best cosmesis and ergonomics. *Surgical Endoscopy*, 2003; 17(1):166-7
- Nicolaou M, Atallah L, James A, Leong J, Darzi A, Yang G. The Effect of Depth Perception on Visual-Motor Compensation in Minimally Invasive Surgery. *Springer*, 2006; 4091:156-63
- Nicolaou M, James A, Lo B, Darzi A, Yang G. Invisible shadow for navigation and planning in minimal invasive surgery. *Medical image computing and computer-assisted intervention*, 2005; 8(2):25-32
- Nishikawa A, Sekimoto M, Taniguchi K, Yamada Y, Miyoshi N, Takiguchi S, Doki Y, Mori M, Miyazaki F. Design and Control of a Compact Endoscope Manipulator: a Biologically Inspired Approach. *Advanced Strategies for Robot Manipulators*, 2010; Pages 365-80. [Available online at <http://www.intechopen.com/books/advanced-strategies-for-robot-manipulators/design-and-control-of-a-compact-endoscope-manipulator-a-biologically-inspired-approach> retrieved on June 28, 2012]
- Omote K, Feussner H, Ungeheuer A, Arbter K, Wei G, Siewert J, Hirzinger G. Self-Guided Robotic Camera Control for Laparoscopic Surgery Compared with Human Camera Control. *American Journal of Surgery*, 1999; 177(4): 321-4
- Pasalar S, Roitman A, Durfee W, Ebner T. Force field effects on cerebellar Purkinje cell discharge with implications for internal models. *Nature neuroscience*, 2006; 9(11):1404-11
- Pastoor S. Legibility and subjective preference for color combinations in text. *Human Factors*, 1990; 32(2):157-71
- Proctor R, Vu K. *Handbook Of Human Factors In Web Design*. Psychology Press, 2004; Pages 122-123
- Ramel S, Smith CD, Arvidsson D: Proficiency-based virtual reality training significantly reduces the error rate for residents during their first 10 laparoscopic cholecystectomies. *Am J Surg* 2007;193:797-804.
- Ritter E, Kindelan T, Michael C, Pimentel E, Bowyer M. Concurrent validity of augmented reality metrics applied to the fundamentals of laparoscopic surgery (FLS). *Surgical Endoscopy*, 2007; 21(8): 1441-5

Rivera C, Cao C. Toward Improved Communication in Laparoscopic Surgery : Accounting for multiple frames of reference and mental rotations. Proceedings of the 49th Annual Meeting of the Human Factors and Ergonomics Society, 2005; Pages 999-1003

Salvendy G. Handbook of Human Factors and Ergonomics (3rd Edition). John Wiley & Sons, 2006; Pages 1191-1221 [Available online at [http://www.knovel.com/web/portal/browse/display?\\_EXT\\_KNOVEL\\_DISPLAY\\_bookid=2488&VerticalID=0](http://www.knovel.com/web/portal/browse/display?_EXT_KNOVEL_DISPLAY_bookid=2488&VerticalID=0)]

Schendel M, Patterson R, Allison J. An electromagnetic cervical range-of-motion system and its sensitivity to environmental metal. Assistive technology: the official journal of RESNA, 1990; 2(1): 27-32

Schuller B, Scheuermann C, Can S, Feussner H, Rigoll G. Robust Speech Recognition for Human-Robot Interaction in Minimal Invasive Surgery. 4th Russian-Bavarian Conference on Bio-Medical Engineering, RBC-BME 2008, Pages 197-201 [Available online at [www.mmk.e-technik.tu-muenchen.de/publ/pdf/08/08sch12.pdf](http://www.mmk.e-technik.tu-muenchen.de/publ/pdf/08/08sch12.pdf) retrieved on June 28, 2012]

Scott D, Bergen P, Rege R, Laycock R, Tesfay S, Valentine R, Euhus D, Jeyarajah D, Thompson W, Jones D. Laparoscopic Training on Bench Models: Better and More Cost Effective than Operating Room Experience? Journal of the American College of Surgeons, 2000; 191(3):272-83

Shadmehr R, Krakauer J. A computational neuroanatomy for motor control. Experimental brain research, 2008; 185(3): 359-81

Shadmehr R, Smith M, Krakauer J. Error Correction, Sensory Prediction, and Adaptation in Motor Control. Annual Review of Neuroscience, 2010; 33:89-108

Shah J, Buckley D, Frisby J, Darzi A. Reaction time does not predict surgical skill. The British Journal of Surgery, 2003; 90(10):1285-6

Shallaly El, Cuschieri A. Optimum view distance for laparoscopic surgery. Surgical Endoscopy, 2006; 20(12): 1879-82

Shanafelt T, Balch C, Bechamps G, Russell T, Dyrbye L, Satele D, Collicott P, Novotny P, Sloan J, Freischlag J. Burnout and medical errors among American surgeons. Annals of Surgery, 2010; 251(6): 995-1000

Stefanidis D, Haluck R, Pham T, Dunne J, Reinke T, Markley S, Korndorffer J, Arellano P, Jones D, Scott D. Construct and face validity and task workload for laparoscopic camera navigation: virtual reality versus videotrainer systems at the SAGES Learning Center. Surgical Endoscopy, 2007; 21(7): 1158-64

Stefanidis D, Korndorffer J, Markley S, Sierra R, Scott D. Proficiency maintenance: impact of ongoing simulator training on laparoscopic skill retention. Journal of the American College of Surgeons, 2006; 202(4): 599-603

Stefanidis D, Korndorffer J, Sierra R, Touchard C, Dunne J, Scott D. Skill retention following proficiency-based laparoscopic simulator training. Surgery, 2005; 138(2):165-70

- Stefanidis D, Scott D, Korndorffer J. Do metrics matter? Time versus motion tracking for performance assessment of proficiency-based laparoscopic skills training. *Simulation in Healthcare: The Journal of the Society for Simulation in Healthcare*, 2009; 4(2):104-8
- Sweller J, Merrienboer J, Paas F. Cognitive Architecture and Instructional Design. *Educational Psychology Review*, 1998; 10(3):251-96
- Taffinder N, Smith S, Huber J, Russell R, Darzi A. The effect of a second-generation 3D endoscope on the laparoscopic precision of novices and experienced surgeons. *Surgical Endoscopy*, 1999; 13(11):1087-92
- Tendick F, Jennings R, Tharp G, Stark L. Sensing and manipulation problems in endoscopic surgery: Experiment, analysis, and observation. *Presence*, 1993; 2: 66-81
- Tseng Y, Diedrichsen J, Krakauer J, Shadmehr R, Bastian A. Sensory Prediction Errors Drive Cerebellum-Dependent Adaptation of Reaching. *Journal of Neurophysiology*, 2007; 98(1): 54-62
- Uecker D, Lee C, Wang Y, Wang Y. Automated Instrument Tracking in Robotically-Assisted Laparoscopic Surgery. *Journal of Image Guided Surgery*, 1995; 1(6): 308-25
- Vasudevan D. Determination of Effective Training methods to learn a Laparoscopic Camera Navigation Tasks under Stressful Environments. <http://hdl.handle.net/10156/3701>, 2012
- Verdaasdonk E, Stassen L, Monteny L, Dankelman J. Validation of a new basic virtual reality simulator for training of basic endoscopic skills: the SIMENDO. *Surgical Endoscopy*, 2006; 20(3): 511-8
- Verdaasdonk E, Stassen L, van Wijk R, Dankelman J. The influence of different training schedules on the learning of psychomotor skills for endoscopic surgery. *Surgical Endoscopy*, 2007; 21(2):214-9
- Wayand W. The History of Minimally Invasive Surgery. *Business Briefing, Global Surgery*, 2004; 37-38. [Available online at <http://www.touchbriefings.com/pdf/952/Wayand.pdf>]
- Wentink M, Breedveld P, Stassen L, Oei I, Wieringa P. A clearly visible endoscopic instrument shaft on the monitor facilitates hand-eye coordination. *Surgical Endoscopy*, 2002; 16(11):1533-7
- Wentink M, Stassen L, Alwayn I, Hosman R, Stassen H. Rasmussen's model of human behavior in laparoscopy training. *Surgical Endoscopy*, 2003; 17:1241-46
- Wetzel C, Kneebone R, Woloshynowych M, Nestel D, Moorthy K, Kidd J, Darzi A. The effects of stress on surgical performance. *American Journal of Surgery*, 2006; 191(1): 5-10
- Whelan R, Fleshman J, Fowler D. The SAGES Manual Perioperative Care in Minimally Invasive Surgery. Springer, 2006; Page 456
- Wimmer R, Kranz M, Boring S, Schmidt A. A Capacitive Sensing Toolkit for Pervasive Activity Detection and Recognition. *Proceedings of the Fifth IEEE International Conference on Pervasive Computing and Communications*, 2007; 171-180

Wogalter M, DeJoy D, Laughery K. Warnings and Risk Communication. CRC Press, 1999; Pages 116-138

Zheng B, Janmohamed Z, MacKenzie C. Reaction times and the decision-making process in endoscopic surgery. Surgical Endoscopy, 2003; 17(9): 1475-80

## APPENDIX

	Page
A. Statistical analysis for number of training task trees attempted.....	106
B. Statistical analysis for total training time.....	107
C. Statistical analysis for number of targets found during training phase.....	108
D. Statistical analysis of RMS error of mental-map of training task trees on paper.....	109
E. Statistical analysis for number of instructions with endpoint within 0° - 30° error margin.....	110
F. Statistical analysis for number of instructions within 0° - 30° error margin 250 msec after giving instruction.....	111
G. Statistical analysis for time taken for deciding direction of movement for instructions with endpoint within 0° - 30° error margin.....	112
H. Program for generating graphics used during training phase.....	113
I. Program for removal of zeros from <i>MotionMonitor</i> data.....	122
J. Program for time slot numbering in Excel spreadsheets.....	123
K. Bitmap image of Legend inserted for vertical height bar in graphics window.....	125

APPENDIX A (Statistical analysis for number of training task trees required)

**One Way Analysis of Variance (ANOVA): Number of training task trees required**

Normality Test (Shapiro-Wilk): Failed ( $P < 0.050$ )

**Kruskal-Wallis One Way Analysis of Variance on Ranks**

Group	N	Min	Median	Max	Mean Rank	Sum Rank
NG	9	2	5	6	27.39	246.5
Line	9	2	2	6	14.94	134.5
Shading	9	2	2	4	16.17	145.5
Line + Shading	9	2	2	3	15.5	139.5

**Chi-Square DF Prob > Chi-Square**

12.26 3 0.007

At the 0.008 level, the populations are significantly different.

All Pairwise Multiple Comparison Procedures (Mann-Whitney Test)

Comparison	U	Z	Asymp. Prob >  U
NG vs Line	65.5	2.39	0.02
NG vs Shading	67	2.47	0.01
NG vs L + S	69	2.66	0.008
Line vs Shading	37	-0.41	0.68
Line vs L + S	44	0.41	0.68
Shading vs L + S	42.5	0.18	0.86

APPENDIX B (Statistical analysis for total training time)

**One Way Analysis of Variance (ANOVA): Total training time**

Normality Test (Shapiro-Wilk): Failed ( $P < 0.050$ )

**Kruskal-Wallis One Way Analysis of Variance on Ranks**

Group	N	Min	Median	Max	Mean Rank	Sum Rank
NG	9	40.25	115	143.5	28.61	257.5
Line	9	24.25	33.25	149.5	14.28	128.5
Shading	9	33	40.33	100	17.89	161
Line + Shading	9	15.75	38	66.75	13.22	119

**Chi-Square DF Prob > Chi-Square**

12.03 3 0.007

At the 0.008 level, the populations are significantly different.

All Pairwise Multiple Comparison Procedures (Mann-Whitney Test)

Comparison	U	Z	Asymp. Prob >  U
NG vs Line	67	2.30	0.02
NG vs Shading	70.5	2.61	0.009
NG vs L + S	75	3.00	0.003
Line vs Shading	29	-0.97	0.33
Line vs L + S	40.5	0	1
Shading vs L + S	53.5	1.10	0.27



APPENDIX C (Statistical analysis for number of targets found per tree during training phase)

**One Way Analysis of Variance (ANOVA): Number of targets found per tree during training phase**

Normality Test (Shapiro-Wilk): Failed ( $P < 0.050$ )

**Kruskal-Wallis One Way Analysis of Variance on Ranks**

<b>Group</b>	<b>N</b>	<b>Min</b>	<b>Median</b>	<b>Max</b>	<b>Mean Rank</b>	<b>Sum Rank</b>
NG	9	4.67	5.5	8	10.28	92.5
Line	9	4.5	8	8	21.56	194
Shading	9	5.5	7.5	8	19.39	174.5
Line + Shading	9	6.67	8	8	22.78	205

**Chi-Square DF Prob > Chi-Square**

8.93 3 0.03

At the 0.008 level, the populations are not significantly different.

All Pairwise Multiple Comparison Procedures (Mann-Whitney Test)

<b>Comparison</b>	<b>U</b>	<b>Z</b>	<b>Asymp. Prob &gt;  U </b>
NG vs Line	19	-1.94	0.05
NG vs Shading	16.5	-2.12	0.03
NG vs L + S	12	-2.6	0.01
Line vs Shading	47.5	0.63	0.53
Line vs L + S	41.5	0.05	0.96
Shading vs L + S	31.5	-0.83	0.41

APPENDIX D (Statistical analysis of RMS error of mental-map of training task trees on paper)

**One Way Analysis of Variance (ANOVA): RMS error of mental-map of training task trees on paper**

Normality Test (Shapiro-Wilk): Failed ( $P < 0.050$ )

**Kruskal-Wallis One Way Analysis of Variance on Ranks**

<b>Group</b>	<b>N</b>	<b>Min</b>	<b>Median</b>	<b>Max</b>	<b>Mean Rank</b>	<b>Sum Rank</b>
NG	9	10.39	12.46	26.15	31.11	280
Line	9	7.18	8.21	12.27	12.44	112
Shading	9	7.03	9.76	10.34	17.67	159
Line + Shading	9	7.06	8.74	11.69	12.78	115

**Chi-Square DF Prob > Chi-Square**

18.58 3 0.0003

At the 0.008 level, the populations are significantly different.

All Pairwise Multiple Comparison Procedures (Mann-Whitney Test)

<b>Comparison</b>	<b>U</b>	<b>Z</b>	<b>Asymp. Prob &gt;  U </b>
NG vs Line	77	3.18	0.002
NG vs Shading	81	3.53	0.0004
NG vs L + S	77	3.18	0.002
Line vs Shading	23	-1.50	0.13
Line vs L + S	41	0	1
Shading vs L + S	56	1.33	0.19

APPENDIX E (Statistical analysis for number of instructions with endpoint within 0° - 30° error margin)

**One Way Analysis of Variance (ANOVA): Number of instructions with endpoint within 0°**

**- 30° error margin**

Normality Test (Shapiro-Wilk): Failed (P < 0.050)

**Kruskal-Wallis One Way Analysis of Variance on Ranks**

Group	N	Min	Median	Max	Mean Rank	Sum Rank
NG	9	5	5	8	5	45
Line	9	13	23	27	22.67	204
Shading	9	14	22	26	21.44	193
Line + Shading	9	11	24	28	24.89	224

**Chi-Square DF Prob > Chi-Square**

20.37 3 0.0001

At the 0.004 level, the populations are significantly different.

All Pairwise Multiple Comparison Procedures (Mann-Whitney Test)

Comparison	U	Z	Asymp. Prob >  U
NG vs Line	0	-3.58	0.0003
NG vs Shading	0	-3.58	0.0004
NG vs L + S	0	-3.57	0.0004
Line vs Shading	45	0.36	0.72
Line vs L + S	48	0.62	0.53
Shading vs L + S	31	-0.80	0.42

APPENDIX F (Statistical analysis for number of instructions within 0° - 30° error margin 250 msec after giving instruction)

**One Way Analysis of Variance (ANOVA): Number of instructions with endpoint within 0°**

**- 30° error margin 250 msec after giving instruction**

Normality Test (Shapiro-Wilk): Passed (P < 0.050)

**One Way Analysis of Variance on Ranks**

Group	N	Mean	Standard Deviation	SE of Mean
NG	9	4.11	1.62	0.54
Line	9	4.11	1.45	0.48
Shading	9	5.56	1.74	0.58
Line + Shading	9	5.52	1.56	0.52

	DF	Sum of Squares	Mean Square	F value	Prob > F
Model	3	15.19	5.06	1.99	0.14
Error	32	81.56	2.54		
Total	35	96.75			

At the 0.004 level, the populations are not significantly different.

All Pairwise Multiple Comparison Procedures (Student's Two sample t-test)

Comparison	Prob >  t
NG vs Line	1
NG vs Shading	0.09
NG vs L + S	0.16
Line vs Shading	0.07
Line vs L + S	0.14
Shading vs L + S	0.68

APPENDIX G (Statistical analysis for time taken for deciding direction of movement for instructions with endpoint within 0° - 30° error margin)

**One Way Analysis of Variance (ANOVA): Time taken for deciding direction of movement for instructions with endpoint within 0° - 30° error margin**

Normality Test (Shapiro-Wilk): Passed (P < 0.050)

**One Way Analysis of Variance on Ranks**

Group	N	Mean	Standard Deviation	SE of Mean
NG	9	287.19	51.35	17.12
Line	9	294.38	98.35	32.78
Shading	9	278.46	81.55	27.19
Line + Shading	9	246.94	72.82	24.27

	DF	Sum of Squares	Mean Square	F value	Prob > F
Model	3	11802.81	3934.27	0.65	0.59
Error	32	194106.76	6065.84		
Total	35	205909.57			

At the 0.008 level, the populations are not significantly different.

All Pairwise Multiple Comparison Procedures (Student's Two sample t-test)

Comparison	Prob >  t
NG vs Line	0.85
NG vs Shading	0.79
NG vs L + S	0.19
Line vs Shading	0.71
Line vs L + S	0.26
Shading vs L + S	0.40

## APPENDIX H (Program for generating graphics used during training phase)

```
%% % ===== MODULEWISE ARRANGEMENT OF ALL GRAPHICS
FOR INDIVIDUAL OR COMBINED SELECTION =====
% =====
% © COPYRIGHT Ketan Vikas Vidwans - Virginia Commonwealth University, May 11, 2011
% Code for creating generating Figure window equal to Screen Size, establishing TCP/IP
connection with The Motion Monitor (TMM)
% in real-time, getting bytes of data, generating map, height bar, legend, position circle, line for
indicating direction of
% view and filling of circle based on rotation of endoscope.
% This program will work only on Matlab installed on The Motion Monitor.
% Special dll's required to export data using TCP/IP to Matlab on any other desktop.
% Data exported from TMM is imported in Matlab installed on TMM itself to reduce time-lag
and generate real-time graphics.
% Comment code lines for individual program slots to enable different combinations of graphics.
% =====
% ===== Program initialization, closing all other windows and clearing all previously created
variables =====
close all; % Closing all open windows prior to program
execution
close all hidden;
clear all; % Clearing all variables prior to program execution
clc; % Clearing workspace prior to program execution

SS = get(0,'ScreenSize');
% Getting screen size to create video size accordingly
set(figure(1),'Position',[0 10 ((SS(3))*1/2) ((SS(4))*1/2)];
% Creating new figure according to screen size for flexibility over monitors
% =====
% Start of code for Creating Map, Position Indicator (circle), Direction of View (line), Top
Indication Marker (filling)
sizeofmat = 22;
% Variable name - Size of Matrix
rad = 10;
% Radius of position indicator circle
theta = 0;
% Angle of landmark 2 with respect to landmark 0 (center of lens)
plotted_value = 0;
flag = 0;
flag2 = 0;
flag3 = 0;
commandWindow = uint8(zeros(779,986,3));
% Setting figure to zeros, creating a blank figure, over which all graphics would be generated
upon
linematrix = uint8(zeros(sizeofmat,sizeofmat,3));
```

```

% Setting figure to zeros, creating a blank figure
linematrix1 = uint8(zeros(sizeofmat,sizeofmat,3));
% Setting figure to zeros, creating a blank figure
fillcirmatrix = uint8(zeros(sizeofmat,sizeofmat,3));
% Setting figure to zeros, creating a blank figure
cirbormatrix = uint8(zeros(sizeofmat,sizeofmat,3));
% Setting figure to zeros, creating a blank figure
finalfillup = uint8(zeros(sizeofmat,sizeofmat,3));
% Setting figure to zeros, creating a blank figure
d = uint8(zeros(sizeofmat,sizeofmat,3));
% Setting figure to zeros, creating a blank figure
blackfillmat = uint8(zeros(552,649,3));
% Setting figure to zeros, creating a blank figure
halfwbmat = uint8(zeros(sizeofmat,sizeofmat,3));
% Setting figure to zeros, creating a blank figure
left_map = 330; right_map = 980; top_map = 009; bottom_map = 562; % Values used
for creating a map on upper right side of figure
left_bar = 755; right_bar = 794; top_bar = 569; bottom_bar = 778; % Values used for
creating vertical bar
total_x = 0.455; % Total length of trainer box
total_y = 0.360; % Total width of trainer box
total_z = 0.255; % Total height of trainer box
% ===== FOR FUTURE USE - TO ADD COLORS =====
% colorofliner = 000; % Initializing RED color combinations to be filled in vertical bar
for height
% coloroflineg = 000; % Initializing GREEN color combinations to be filled in vertical
bar for height
% coloroflineb = 000; % Initializing BLUE color combinations to be filled in vertical
bar for height
% =====
% ===== Commands for creating map and vertical bar, filling them with white and then black to
show borders =====
commandWindow((top_map-4):(bottom_map+4),(left_map-5):(right_map+5),:) = 255; %
Map white filling
commandWindow((top_map+1):(bottom_map-1),(left_map+1):(right_map-1),:) = 1; %
Map black filling
commandWindow((top_map-8):(bottom_map+217),(left_map-329):(left_map-7),:) = 204; %
Filling rest of figure with gray color
% ===== FOR FUTURE USE - TO ADD COLORS, JUST ASSIGN VALUES FROM 0-255
FOR DIFFERENT COLORS =====
% commandWindow(top_bar:bottom_bar,left_bar:right_bar,1) = 255; % Vertical
bar YELLOW filling
% commandWindow(top_bar:bottom_bar,left_bar:right_bar,2) = 255; % Vertical
bar YELLOW filling
% commandWindow(top_bar:bottom_bar,left_bar:right_bar,3) = 000; % Vertical
bar YELLOW filling

```

```

% =====
commandWindow(top_bar:bottom_bar,left_bar:right_bar,:) = 255;          % Vertical bar
WHITE filling
commandWindow((top_bar+1):(bottom_bar-1),(left_bar+1):(right_bar-1),:) = 1;    % Vertical
bar BLACK filling
commandWindow((top_bar+055):(top_bar+055),(left_bar-10):(right_bar+10),:) = 255;    %
White lines for indicating level mark of Legend
commandWindow((top_bar+105):(top_bar+105),(left_bar-10):(right_bar+10),:) = 255;    %
White lines for indicating level mark of Legend
commandWindow((top_bar+155):(top_bar+155),(left_bar-10):(right_bar+10),:) = 255;    %
White lines for indicating level mark of Legend
% ===== End of code for Creating Map and Vertical Bar =====
calx = (right_map-left_map)/total_x;
% Calculating pixels for filling in respective graphics
caly = (bottom_map-top_map)/total_y;
% Calculating pixels for filling in respective graphics
calz = (bottom_bar-top_bar)/total_z;
% Calculating pixels for filling in respective graphics
height_in_rect_left = left_bar + 1;
% Inner rectangle left edge for Vertical Z bar
height_in_rect_right = right_bar - 1;
% Inner rectangle right edge for Vertical Z bar
height_in_rect_top = top_bar + 1;
% Inner rectangle top edge for Vertical Z bar
height_in_rect_bottom = bottom_bar - 1;
% Inner rectangle bottom edge for Vertical Z bar
% Generating upper-half black, lower-half white as indicator of base orientation of endoscope in
next line
halfwbmat((sizeofmat/2):sizeofmat,1:sizeofmat,:) = 255;
% imshow(halfwbmat)
% Generating circle of radius "rad" and storing it in Circle-Border-Matrix (cirbormatrix)
for ang=theta:1:360
    x_circle = round(rad*cos(ang));
    y_circle = round(rad*sin(ang));

cirbormatrix(((sizeofmat/2)+y_circle):((sizeofmat/2)+y_circle),((sizeofmat/2)+x_circle):((sizeof
mat/2)+x_circle),:) = 255;
end
% imshow(cirbormatrix)
% Generating filled circle of radius "rad" and storing it in Filled-Circle-Matrix (fillcirmatrix)
for ang=theta:1:360
    for radius=0.1:0.1:rad
        x_circle = round(radius*cos(ang));
        y_circle = round(radius*sin(ang));
fillcirmatrix(((sizeofmat/2)+y_circle):((sizeofmat/2)+y_circle),((sizeofmat/2)+x_circle):((sizeof
mat/2)+x_circle),:) = 255;

```



```

    end
end
% imshow(fillcirmatrix)
%% % ===== Opening TCP/IP Port for XYZ transfer of all four landmarks marked on
endoscope =====
t = tcpip('127.0.0.1', 2000);      % Creating TCP/IP object, default IP address of TMM
set(t,'InputBufferSize', 64000); % 96 is size(double)*12 values (X,Y,Z) being exported from
TMM, keeping a large buffer
fopen(t);                        % Connecting TCP/IP object to server for receiving values
%=====
%% Main Loop for getting XYZ values of all four landmarks marked on endoscope tip,
calculations and manipulating marker in map and height
%=====
while (1<2)
% ===== Start of complete code for generating all possible graphics =====
% ===== Loop for TCP/IP values to be received from Motion Monitor =====
    byt = t.BytesAvailable;
    if byt < 96
        byt = 96;
    end
    val = floor((floor(byt/96)*96)/8);
    [b,count] = fread(t,val,'double');
    bstart = val-11;
    a = b((bstart:(bstart+11))); % Getting all 12 bytes of data
    c = swapbytes(a());
% Swapping bytes to get actual XYZ values in array "c"
    x0 = floor(c(1)*calx);
% Receiving X0-value in meters as c(1) and calculating pixel offset for marker
    y0 = floor(c(2)*caly);
% Receiving Y0-value in meters as c(2) and calculating pixel offset for marker
    z0 = abs(floor(c(3)*calz));
% Receiving Z0-value in meters as c(3) and calculating pixel offset for height bar
    x1 = floor(c(4)*calx);
% Receiving X1-value in meters as c(4) and calculating pixel offset for marker
    y1 = floor(c(5)*caly);
% Receiving Y1-value in meters as c(5) and calculating pixel offset for marker
    z1 = abs(floor(c(6)*calz)); % Receiving Z1-value in meters as c(6)
    x2 = floor(c(7)*calx);
% Receiving X2-value in meters as c(7) and calculating pixel offset for filling of marker
    y2 = floor(c(8)*caly);
% Receiving Y2-value in meters as c(8) and calculating pixel offset for filling of marker
    z2 = abs(floor(c(9)*calz)); % Receiving Z2-value in meters as c(9)
    x3 = floor(c(10)*calx);
% Receiving X3-value in meters as c(10) and calculating pixel offset for filling of marker
    y3 = floor(c(11)*caly);
% Receiving Y3-value in meters as c(11) and calculating pixel offset for filling of marker

```

```

z3 = abs(floor(c(12)*calz)); % Receiving Z3-value in meters as c(12)
% ===== Do not need Z1,Z2,Z3 in any version of graphics, hence no calculations performed ==
% ===== End of Loop for TCP/IP values from Motion Monitor=====
if c~=0
% Proceed only if data in array "c" is non-zero, else, display graphics from previous time frame
if c(1) >= 0.436 % Limiting circle to right edge of map
x0 = 640;
elseif c(1) <= 0.012 % Limiting circle to left edge of map
x0 = 010;
end
if c(2) >= 0.352 % Limiting circle to top edge of map
y0 = 543;
elseif c(2) <= 0.027 % Limiting circle to bottom edge of map
y0 = 010;
end
% =====
% ===== Start of PROGRAM 1 (Generating map and displaying circle for Position in map only)
=====
% Displaying graphics by a pause of 0.00001 seconds
commandWindow((top_map+1):(bottom_map-1),(left_map+1):(right_map-1),:) =
blackfillmat; % Map black filling
pause(0.00001);

% Next single line command is for DRAWING the circular marker - drawing CIRBORMATRIX
in COMMANDWINDOW Map
commandWindow((bottom_map-y0-(sizeofmat/2)+1):(bottom_map-
y0+(sizeofmat/2)),(left_map+x0-(sizeofmat/2)+1):(left_map+x0+(sizeofmat/2)),:) =
cirbormatrix;
% ===== End of PROGRAM 1 =====
% Commenting code present in slots of PROGRAM 2 and PROGRAM 3 would generate only
the circle within the map,
% thus giving only position information to user.
% =====
% ===== Start of PROGRAM 3 Part 1 (Calculations and displaying graphics for current
iteration of loop only) =====
% Superimposing filling on circle from Program 1 above starts here
=====
% ===== Start of code for DRAWING previous filling of circle indicating orientation of
landmark 2 wrt landmark 0 =====
xx0 = round(c(1)*10000);
yy0 = round(c(2)*10000);
xx3 = round(c(10)*10000);
yy3 = round(c(11)*10000);
ang = (atan2((yy3-yy0),(xx3-xx0)))*180/pi;
bbb = imrotate(halfwbmat,ang,'crop');
d = bitand(bbb,fillcirmatrix);

```

```

    finalfillup = bitor(d,cirbormatrix);
    commandWindow((bottom_map-y0-(sizeofmat/2)):(bottom_map-y0+(sizeofmat/2)-
1),(left_map+x0-(sizeofmat/2)+1):(left_map+x0+(sizeofmat/2)),:) = finalfillup;
% ===== End of code for DRAWING previous filling in circle indicating orientation of
landmark 2 wrt landmark 0 =====
% ===== End of PROGRAM 3 Part 1 - Superimposing filling on circle from Program 1 Circle
ends here =====
% Commenting code present in slots of PROGRAM 3 Part 1 and Part 2 would generate only the
circle within the map,
% NOT FILLING OF CIRCLE thus NOT giving Rotation of endoscope information to user.
% =====
% ===== Start of PROGRAM 2 (Line added on circle from Program 1 above) =====
% Start of code for drawing line from landmark 0 to landmark 1 for indicating direction of lens,
and hence view =====
    if z0==z2
% Drawing a point in center to indicate endoscope pointing straight downwards
        commandWindow((bottom_map-y0-1):(bottom_map-y0+1),(left_map+x0-
1):(left_map+x0+1),:) = 255;
        elseif x0==x1
            if y0<y1 % flag = '201';
                commandWindow((bottom_map+(y1-y0)-y1):(bottom_map+(y1-y0)-
y0),(left_map+x0):(left_map+x1),:) = 255;
            elseif y0>y1 % flag = '202';
                commandWindow((bottom_map-(y0-y1)-y0):(bottom_map-(y0-y1)-
y1),(left_map+x0):(left_map+x1),:) = 255;
            end
            elseif x0<x1 %flag2 = '20'
                X01 = [x0 x1];
% For tip of endoscope line - landmark 0 to landmark 1
                Y01 = [(y0+(y0-y1)) (y1+(y0-y1))];
% For tip of endoscope line - landmark 0 to landmark 1
                xi01 = x0:1:x1;
% For tip of endoscope line - landmark 0 to landmark 1
                yi01 = interp1(X01,Y01,xi01,'linear');
% Linear interpolation for joining landmark 0 and 1
                formatted_yi01 = floor(yi01);
% Rounding up interpolated y-values for landmark 0 to landmark 1
                xi01 = (left_map+(x0-(x1-x0))):1:(left_map+x0);
                for i=1:1:length(yi01)
                    if xi01(i)<left_map
% Setting restrictions for line drawn between landmarks 0 and 1 so that it does not go outside left
edge of map
                        xi01(i) = left_map;
                    elseif (bottom_map-formatted_yi01(i))<top_map
% Setting restrictions for line drawn between landmarks 0 and 1 so that it does not go outside top
edge of map

```

```

        formatted_yi01(i) = (top_map-1);
    elseif (bottom_map-formatted_yi01(i))>bottom_map
% Setting restrictions for line drawn between landmarks 0 and 1 so that it does not go outside
bottom edge of map
        formatted_yi01(i) = 1;% 1;
    end
    commandWindow((bottom_map-formatted_yi01(i)),(xi01(i)),:) = 255;
    commandWindow((bottom_map-formatted_yi01(i)),(xi01(i)+1),:) = 255;
    commandWindow((bottom_map-formatted_yi01(i)),(xi01(i)-1),:) = 255;
    commandWindow((bottom_map-formatted_yi01(i)),(xi01(i)+2),:) = 255;
    commandWindow((bottom_map-formatted_yi01(i)),(xi01(i)-2),:) = 255;
    end
elseif x0>x1
%     flag2 = '21'
        X01 = [x1 x0];
% For tip of endoscope line - landmark 0 to landmark 1
        Y01 = [(y1+(y0-y1)) (y0+(y0-y1))];
% For tip of endoscope line - landmark 0 to landmark 1
        xi01 = x1:1:x0;
% For tip of endoscope line - landmark 0 to landmark 1
        yi01 = interp1(X01,Y01,xi01,'linear');
% Linear interpolation for joining landmark 0 and 1
        formatted_yi01 = floor(yi01);
% Rounding up interpolated y-values for landmark 0 to landmark 1
        xi01 = (left_map+x0):1:(left_map+(x0+(x0-x1)));
        for i=1:1:length(yi01)
            if xi01(i)>right_map
% Setting restrictions for line drawn between landmarks 0 and 1 so that it does not go outside
right edge of map
                xi01(i) = right_map;
            elseif (bottom_map-formatted_yi01(i))<top_map
% Setting restrictions for line drawn between landmarks 0 and 1 so that it does not go outside top
edge of map
                formatted_yi01(i) = (top_map-1);
            elseif (bottom_map-formatted_yi01(i))>bottom_map
% Setting restrictions for line drawn between landmarks 0 and 1 so that it does not go outside
bottom edge of map
                formatted_yi01(i) = 1;
            end
            commandWindow((bottom_map-formatted_yi01(i)),(xi01(i)),:) = 255;
            commandWindow((bottom_map-formatted_yi01(i)),(xi01(i)+1),:) = 255;
            commandWindow((bottom_map-formatted_yi01(i)),(xi01(i)-1),:) = 255;
            commandWindow((bottom_map-formatted_yi01(i)),(xi01(i)+2),:) = 255;
            commandWindow((bottom_map-formatted_yi01(i)),(xi01(i)-2),:) = 255;
        end
    end
end
end

```

```

% ===== End of PROGRAM 2 - Line added over Program 1
=====
% ===== End of code for drawing line from landmark 0 to landmark 1 for indicating direction
of lens =====
% Commenting code present in slot of PROGRAM 2 would generate only the circle within the
map,
% NOT THE LINE thus NOT giving direction of view of endoscope information to user.
% =====
% ===== Start of code for filling Height (Z) vertical bar
=====
    if abs(c(3))>=total_z
        commandWindow(top_bar:bottom_bar,left_bar:right_bar,:) = 255;          % Full
filled Z vertical bar for full height
    elseif abs(c(3))<=0.019
        commandWindow(top_bar:bottom_bar,left_bar:right_bar,:) = 255;          % Vertical
bar WHITE filling
        commandWindow((top_bar+1):(bottom_bar-1),(left_bar+1):(right_bar-1),:) = 1;    %
Vertical bar BLACK filling
    else
        commandWindow((height_in_rect_bottom-z0):bottom_bar,left_bar:right_bar,:) = 255;
% Logic for vertical Z-bar WHITE filling
        commandWindow(height_in_rect_top:(height_in_rect_bottom-z0-
1),height_in_rect_left:height_in_rect_right,:) = 1; % Logic for vertical Z-bar BLACK filling for
rest of the portion
    end
% ===== End of code for filling Height (Z) vertical bar =====
% Next single command is displaying legend for vertical bar indicating height in trainer box - Z
axis
    commandWindow((bottom_bar-1-209):(bottom_bar-
1),(right_bar+11):(right_bar+11+103),:) = imread('C:\Documents and Settings\Diane
Pawluk\Desktop\Ketan_MM_Files_Aug_02_2010\Vertical_Legend_104x210.bmp');
    image(commandWindow); % Displaying all generated graphics in the figure window for
current time frame
    axis off;          % Keeping axes tick marks for figure "off"
% =====
% ===== Start of PROGRAM 3 Part 2 - Superimposing filling on circle from Program 1 Circle
starts here =====
% ===== Code for ERASING previous filling in circle indicating orientation of landmark 2 wrt
landmark 0 starts here =====
    linematrix = uint8(zeros(sizeofmat,sizeofmat,3));
% Setting figure to zeros, creating a blank figure
    linematrix1 = uint8(zeros(sizeofmat,sizeofmat,3));
% Setting figure to zeros, creating a blank figure
    finalfillup = uint8(zeros(sizeofmat,sizeofmat,3));
% Setting figure to zeros, creating a blank figure
    d = uint8(zeros(sizeofmat,sizeofmat,3));

```

```

% Setting figure to zeros, creating a blank figure
% ===== Code for ERASING previous filling in circle indicating orientation of landmark 2 wrt
landmark 0 ends here =====
% ===== PROGRAM 3 Part 2 - Superimposing filling on circle from Program 1 Circle ends
here =====
% =====
end
% =====
% ===== End of complete code for generating all possible graphics =====
end                                     % End of entire While Loop
%% % ===== Final Clean-up of all variables and objects created and used in the program
=====
fclose(t);    % Closing TCP/IP object
delete(t);    % Deleting TCP/IP object
close all;    % Closing all open windows after program execution
clear all;    % Clearing all variables after program execution
clc;          % Clearing workspace prior after program execution
% =====

```

APPENDIX I (Program for removal of zeros from *MotionMonitor* data)

```

%% % =====DETECTING ZEROS IN DATA AND DELETING THOSE ROWS =====
% =====
% © COPYRIGHT Ketan Vikas Vidwans - Virginia Commonwealth University, July 22, 2011
% Code for detecting zeros present in data received from The Motion Monitor (TMM).
% This program detects all the rows containing zeros, and deletes four rows prior to the first row
of zero of each set of rows
% containing zeros, and four rows after the last row of zero of each set of rows containing zeros.
% This program may not delete the last set of rows of zeros, it may have to be done manually in
certain cases.
% This program also uses peak detection algorithm, which is freely available code/function on
MatlabCentral.
% =====
% ==Program initialization, closing all other windows and clearing all previously created
variables =====
close all; clear all; clc;
format short;
Dtemp = xlsread('H:\Ketan Files\Testing Files\Gunjan\Gunjan_1.xls');
D=Dtemp(7:end,2:4); % Reading all data except the header
generated by TMM
D=[(1:length(D))' D];
clear Dtemp;
disp(D(1:50,:));
% ===== Detecting the Zeros =====
srZero=D(D(:,2)==0);
% ===== Start of zeros =====
[~, mintab] = peakdet(D(:,2), 0.001, D(:,1));
% ===== End of Zeros =====
dV=diff(srZero)>1;
dV(end+1)=0;
diffVector=srZero(dV);
% Making a Zero Vector Indi
DM=D;
for h=1:length(mintab)
    DM(mintab(h,1)-4:mintab(h,1),2:4)=0;
end;
DM(mintab(end,1):mintab(end,1)+4)=0;
for h=1:length(diffVector)
    DM(diffVector(h,1):diffVector(h,1)+4,2:4)=0;
end;
disp([D(1:500,1:2) DM(1:500,1:2)]);
% ===== Removing the zero vectors =====
srNonzero=DM(DM(:,2)>0);
dNZ=[DM(srNonzero,2) DM(srNonzero,3) DM(srNonzero,4)];
save Gunjan 'dNZ';

```

APPENDIX J (Program for time slot numbering in Excel spreadsheets)

```

%% %% ==NUMBERING TIME SLOTS IN EXCEL SHEETS OF TARGETS OF TESTING
TREE ONLY ===
% =====
% © COPYRIGHT Ketan Vikas Vidwans - Virginia Commonwealth University, March 01, 2012
% Code for numbering multiple time slots of movement of endoscope during Testing Tree.
% Before executing the program, fill in column beside trigger (column 15) with zeros till one
frame before double trigger.
% For time frames of double trigger, mention the target number. Mention zeros from double
trigger at end of file and fill
% the rest of frames with zero will End of File.
% =====
% ===== Program initialization, closing all other windows and clearing all previously created
variables =====
close all; clear all;clc;
data = xlsread('H:\Ketan Files\Testing Files\Gunjan\Gunjan_9.xls','Sheet1');
% The variable "num" is kept common for all targets, execute only the one for numbering the
slots of the target number you wish to allocate
num = [111; 112; 113; 114; 116; 115; 122; 123; 124; 126; 125; 132; 133; 134; 136; 135; 142;
143; 144; 146; 145; 152; 153; 154; 156; 155; 162; 163; 164; 166; 165];
num = [211; 212; 213; 214; 216; 215; 222; 223; 224; 226; 225; 232; 233; 234; 236; 235; 242;
243; 244; 246; 245; 252; 253; 254; 256; 255; 262; 263; 264; 266; 265];
num = [311; 312; 313; 314; 316; 315; 322; 323; 324; 326; 325; 332; 333; 334; 336; 335; 342;
343; 344; 346; 345; 352; 353; 354; 356; 355; 362; 363; 364; 366; 365];
num = [411; 412; 413; 414; 416; 415; 422; 423; 424; 426; 425; 432; 433; 434; 436; 435; 442;
443; 444; 446; 445; 452; 453; 454; 456; 455; 462; 463; 464; 466; 465];
num = [511; 512; 513; 514; 516; 515; 522; 523; 524; 526; 525; 532; 533; 534; 536; 535; 542;
543; 544; 546; 545; 552; 553; 554; 556; 555; 562; 563; 564; 566; 565];
num = [711; 712; 713; 714; 716; 715; 722; 723; 724; 726; 725; 732; 733; 734; 736; 735; 742;
743; 744; 746; 745; 752; 753; 754; 756; 755; 762; 763; 764; 766; 765];
num = [911; 912; 913; 914; 916; 915; 922; 923; 924; 926; 925; 932; 933; 934; 936; 935; 942;
943; 944; 946; 945; 952; 953; 954; 956; 955; 962; 963; 964; 966; 965];
i = 1;
j = 1;
k = 1;
% ===== Calculating number of cells to be filled with time slot numbers =====
for i = 1:1:length(data(:,1))
    if (isnan(data(i,15)))
        if(data(i,14) ~= '')
            j = j + 1;
        end
    end
end
end
t = j - 1    % Number of cells to be numbered
% =====

```

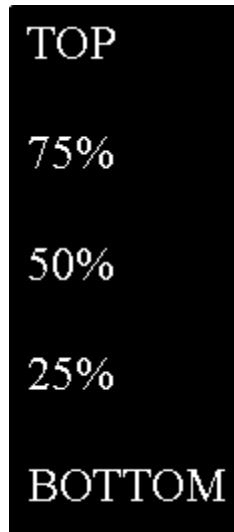


```

% == Mention Excel sheet cell number as "start" from where slot numbering shall begin ==
start = 1499;% Time slot numbering shall begin from this cell number of Excel
finish = start + t - 1% Time slot numbering shall end at this cell number of Excel
j = 1;
k = 1;
flag = 1;
% === Code for filling time slot number from array "num" for that particular target
number=====
for i = start:1:finish
    if(data(i,14)>2 && data(i+1,14)>2)
        flag = 1;
        tt(k,1) = num(j,1);
        k = k + 1;
    elseif(data(i,14)>2 && data(i+1,14)<2)
        flag = 2;
        tt(k,1) = num(j,1);
        k = k + 1;
    elseif(data(i,14)<2 && data(i+1,14)<2)
        flag = 3;
        tt(k,1) = num(j+1,1);
        k = k + 1;
    elseif(data(i,14)<2 && data(i+1,14)>2)
        flag = 4;
        j = j + 1;
        tt(k,1) = num(j,1);
        k = k + 1;
    end
end
% Mention "start" and "finish" variable values in last element of next line to fill Excel sheet with
time slot numbers
xlswrite('H:\Ketan Files\Testing Files\Gunjan\Gunjan_9.xls',tt,'Sheet1','O1499:O16941');
% =====

```

APPENDIX K (Bitmap image of Legend inserted for vertical height bar in graphics window)



## VITA

Ketan Vikas Vidwans was born on October 03, 1983 in Nagpur, Maharashtra, India. He completed High School from Saraswati Education Society's (SES) High School and Junior College in 2001. He received his Bachelor of Instrumentation Engineering from Vivekanand Education Society's Institute of Technology (VESIT), Mumbai, India in 2005. He completed a Post-Graduate Diploma in Embedded Systems from ECIT – Electronics Corporation of India Limited (Computer Education Division), Mumbai, India in 2006. He worked in Johnson & Johnson Ltd. Medical R&D Center, Mumbai, India from 2006-2008. He began his graduate studies in Biomedical Engineering at Virginia Commonwealth University in Fall 2008. During his time at VCU, his work was focused on human factors analysis during minimally invasive surgery. He is very keen to enhance and apply his knowledge in the field of Minimally Invasive Surgery.